International Scientific-Technical and Production Journal

The Paton WELDING JOURNAL

February
2006
2

English translation of the monthly «Avtomaticheskaya Svarka» (Automatic Welding) journal published in Russian since 1948

Founders: *E.O. Paton Electric Welding Institute of the NAS of Ukraine*
International Association «Welding»

Publisher: *International Association «Welding»*

Address:
E.O. Paton Electric Welding Institute,
International Association «Welding»,
11, Bozhenko str., 03680, Kyiv, Ukraine
Tel.: (38044) 287 67 57
Fax: (38044) 528 04 86
E-mail: journal@paton.kiev.ua
http://www.nas.gov.ua/pwj

State Registration Certificate
KV 4790 of 09.01.2001

Subscriptions:
$324, 12 issues per year,
postage and packaging included.
Back issues available.

CONTENTS

LASER-MICROPLASMA ALLOYING AND COATING OF STEEL

V.D. SHELYAGIN, V.Yu. KHASKIN and **Yu.N. PEREVERZEV**
E.O. Paton Electric Welding Institute, NASU, Kiev, Ukraine

The hybrid process is suggested for laser-microplasma alloying and coating. The process is free from drawbacks of laser cladding and microplasma spraying. Main parameters, characteristic structure of the transition zone and distribution of microhardness were determined.

Keywords: laser cladding, microplasma spraying, powder materials, adhesion strength, surface preparation, combined coating, microplasmatron, microcracks, process parameters, structures

One of the application areas of laser technology is its combination with existing industrial technologies, e.g. the use of laser radiation for thermal spraying of coatings. Laser heat treatment is applied to consolidate and glaze sprayed layers [1]. Combination of laser surface heating with plasma coating, where the laser radiation focusing spot coincides with the coating formation zone, has received acceptance lately [2]. The latter technology is called laser assisted atmospheric plasma spraying (LAAPS) [2, 3]. The process provides a dense layer with increased adhesion strength. Companies LERMPS-IPS and IREPA-Laser developed and patented the PROTAL technology, which provides the effect of surface preparation and eliminates the need of jet-abrasive blasting owing to incomplete overlapping of the plasma spraying zone by the laser heated zone [4]. The present article gives results of experiments on application of laser radiation combined with a microplasma jet for deposition of coatings.

Thermal spraying methods have wide commercial application for deposition of decorative and wear- and corrosion-resistant surface layers [5]. One of the promising methods in this respect is microplasma coating [6], which is characterised by the following advantages: low heat effect on a workpiece (part), comparatively low power of plasmatrons (up to 2–3 kW), increased material utilisation factor compared with plasma coating, small size of a spraying spot (2–5 mm), and low level of noise.

The microplasma spraying equipment and technology were developed by the E.O. Paton Electric Welding Institute [7]. The equipment is characterised by high mobility, comparatively low weight, small dimensions, and it is simple in operation. The set of equipment comprises a microplasmatron generating a thin laminar argon plasma jet (2–5 mm), and a feeder providing a proportioned feed of powders to the plasma jet. Coatings produced by this method impart wear-resistant properties to the workpiece surfaces. However, they may have pores and low strength of adhesion to the substrate (20–40 MPa). Preliminary surface preparation is required to deposit the coatings.

The required quality of a coating is achieved through improving its continuity and providing the absence of pores and cracks. It is desirable that a narrow transition zone be present to increase strength of adhesion to the substrate [8]. To raise productivity of the process and widen the range of products, it is necessary to reduce the quantity of auxiliary technological operations. The latter include preliminary machining of the surface, associated with formation of a developed surface geometry to ensure adhesion between the coating and substrate. Most often the surface preparation involves sand or grit blasting [5].

One of the methods that meet the above requirements to a sufficient degree is laser powder cladding [9]. It has a number of benefits associated not only with a high adhesion strength of the deposited layers, satisfactory control of geometry and thickness (within a range of 0.1–6.0 mm) and local thermal effect on a workpiece, but also with the absence of the necessity to apply preliminary surface preparation. The main drawback of laser cladding in the case of using self-fluxing alloys is the presence of microcracks in the deposited layer, if its hardness is higher than *HRC* 35–40 [10–11].

The most efficient method for avoiding cracks is preliminary (concurrent) heating of a workpiece and additive material, as well as decreasing of height of the deposited layer to values at which residual stresses are not in excess of tensile strength [12]. In practice, height of the deposited layer is related to minimisation of allowance for finishing machining. The optimal deposited layer is produced by controlling the cross section profile of cladding (or alloying) strips, this affecting the character of convective mass transfer in the molten pool [13]. For example, in deposition of coatings 0.1–0.5 mm high, the allowance for finishing polishing should be 0.05–0.25 mm, which means that the coating roughness profile should be no more than 0.05–0.10 mm. The best roughness profile produced by now is 0.15–0.30 mm. The problem of minimisation of roughness of a coating deposited on steels and avoidance of cracks in it was solved by to combining the microplasma spraying and laser cladding methods.

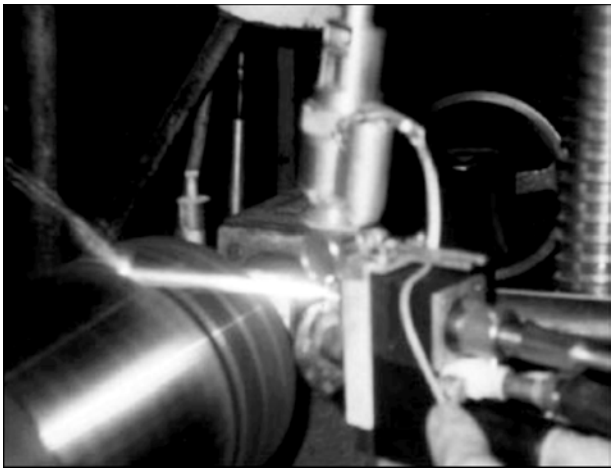

Figure 1. Laser-microplasma coating and alloying of cylindrical parts

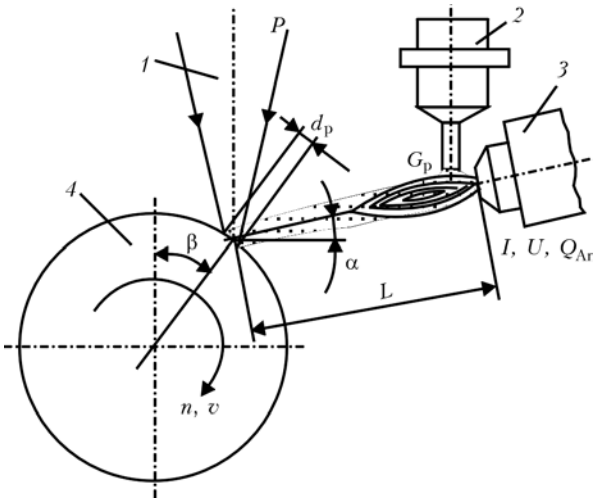

Figure 2. Schematic of the process of laser-microplasma coating (alloying) (for explanations see the test)

We used a combined method of laser-microplasma coating as a version of LAAPS, where the spray powder is fed to the microplasma jet that heats and accelerates it, while transporting to the laser radiation affected zone (Figure 1). Laser radiation heats the workpiece metal to temperatures close to the melting point, or forms a thin skin-layer of the melt on its surface. As a result, a coating 0.1–0.5 mm thick is deposited in one pass on metal of the workpiece surface. Properties of the coating depend upon the selected process parameters, and can vary from properties of the layers deposited by microplasma spraying to properties of the layers deposited by laser cladding. If laser radiation power density and process speed allow melting of the base metal to a depth of 0.1–1.0 mm, this method can be used for laser-microplasma alloying. In this case, an additive material transported by the microplasma jet is mixed in the molten pool with the workpiece material as a result of convective mass transfer [13].

Figure 2 shows schematic of the process of laser-microplasma coating (alloying) of parts having a rotation axis. According to this schematic, sample *4* is rotated about its axis, and laser beam *1* with microplasmatron *3* is moved along it. Main parameters of this process can be subdivided into four groups. The first group related to laser radiation includes radiation power density W_r and angle β, determining the point of introduction of laser radiation to a cylindrical sample with respect to its vertical axis. The second group related to the microplasmatron includes current I, voltage U, flow rates of plasma and shielding (argon) gases, Q_{pl} and Q_{sh}, respectively, distance L from the microplasmatron nozzle to the laser radiation affected zone, and angle α of incidence of the microplasma jet onto the sample surface. The third group of parameters related to the additive material feeder includes mass flow rate G_p of a powder material, material utilisation factor, particle size, chemical composition, and point of introduction to the plasma jet relative to the anode spot. And the last group related to a sample includes linear velocity v of movement of the sample, and strip overlapping coefficient K_o.

Height h of the deposited layer (or depth of alloying) and its roughness depend upon the combination of these parameters. Experiments were conducted to determine the above process parameters. Technological laser LT 104 with a power of up to 10 kW [14] and microplasma equipment described in [7] were used in the experiments. The sample materials were steels St3ps (semi-killed), 20 and 38KhN3MFA, and additive materials were powders PG-AN9 (particle size 50–160 μm) of the Ni–Cr–B–Si system, PG-N1 (particle size 50–160 μm) of the Ni–Fe–B–Si system, and chromium (particle size 0–40 μm).

Dependencies shown in Figure 3 were derived in the course of the experiments. It should be noted that angles α and β have a low effect on height h of the deposited layer. Thus, variations of angle β within 5–30° and angle α within 5–50° did not show relative deviations of the h value exceeding the measurement

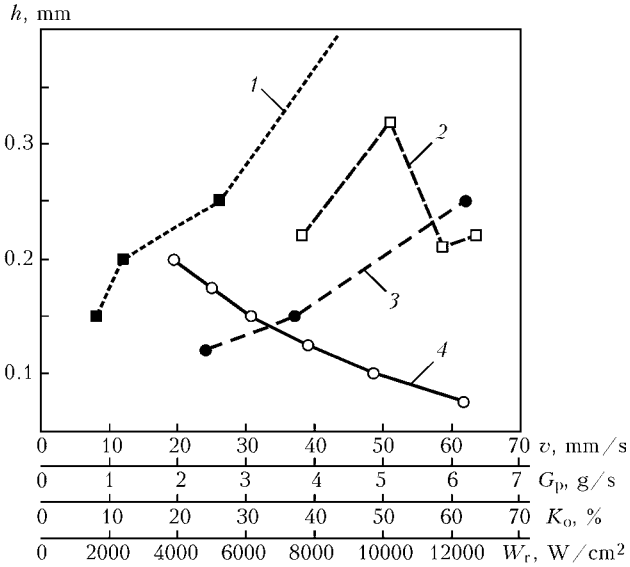

Figure 3. Dependences of height h of the deposited layer upon parameters of combined deposition of coatings of powders PG-AN9 and PG-N1, produced under the following conditions: 1 — W_r = = 10.19 kW / cm², v = 30.6 mm / s, K_o = 24 %; *2* — v = 30.6 mm / s, G_p = 0.26 g / s, K_o = 62 %; *3* — W_r = 10.19 kW / cm², v = = 30.6 mm / s, G_p = 0.26 g / s; *4* — W_r = 10.19 kW / cm², G_p = = 0.26 g / s, K_o = 37 %

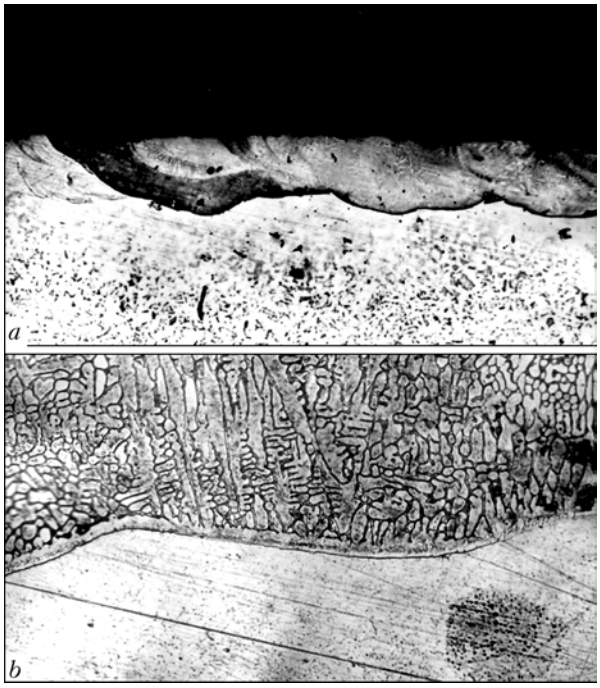

Figure 4. Microstructure of the coating of alloy PG-N1 deposited by the combined method on steel 20: *a* — ×63; *b* — ×1000

error. The process parameters related to the microplasmatron were kept unchanged in the experiments. The experiments allowed a conclusion that four parameters, the effect of which on layer height *h* is shown in Figure 3, are the most significant ones in the combined coating process.

As noted above, to increase strength of adhesion between the coating and substrate, it is necessary to have a transition zone, i.e. coatings produced by the combined method should be similar in structure to coatings produced by laser cladding. Metallography shows that laser-microplasma coatings have a dendritic structure. However, dendrites are 3–5 times smaller in size than in laser cladding (Figure 4), while in HAZ they are not revealed at all, which is attributable to a high speed of movement of the sample, short (0.05–0.25 s) time of existence of the molten pool, and 2–3 times lower radiation power density, compared with laser cladding. Hardness of the coating is related to chemical composition of an additive material. However, it can be 20–30 % lower than initial hardness of a cladding powder. This may be associated with partial burning out of boron and silicon in the plasma jet during melting and transportation of the powder to a workpiece.

In the case of combined alloying of steels, depending upon their content of carbon, partial or complete formation of bainite or martensite may take place in the remelted strips, as well as their alloying with the additive material. The longer the time of existence of the molten pool, the higher is the content of alloying elements in the surface layer. Typical structure of the hybrid alloying strips on a cylindrical sample, having a spiral path with overlapping, is shown in Figure 5. In the case of alloying without overlapping, the strips penetrate into the base metal, as shown in Figure 6, *a*. Distribution of microhardness through depth of the strips in the latter case is shown in Figure 6, *b*. HAZ is formed around the alloying strips because of a much higher radiation power density. The HAZ size is directly proportional to depth of the strips, depends upon the power density and sample movement speed, as well as the sensitivity of steel to formation of

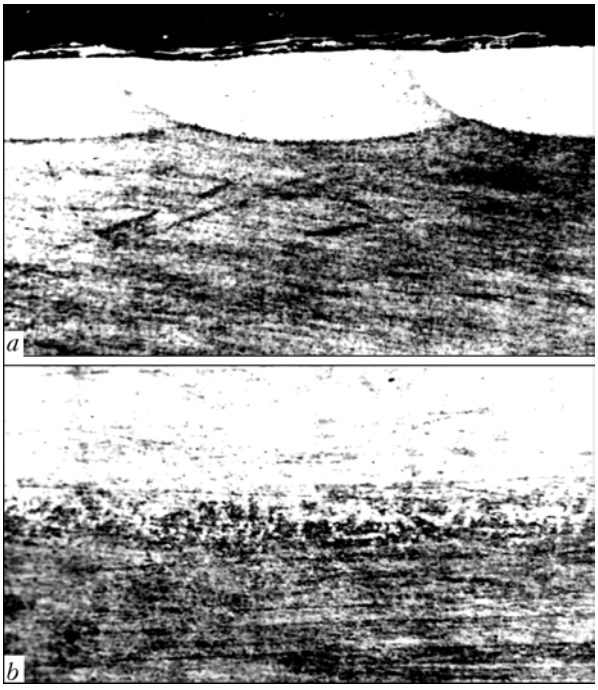

Figure 5. Microstructure of the chromium layer deposited by the combined method on steel 38KhN3MFA (the process was carried out with overlapping of strips at K_o = 24 %): *a* — strip structure (×50); *b* — transition zone (×500)

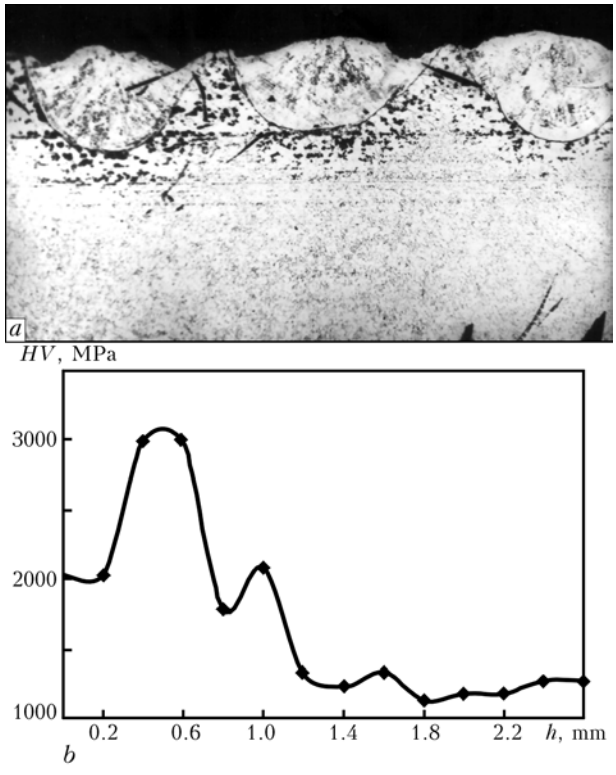

Figure 6. Structure of the chromium alloying strips on steel St3ps without overlapping (*a* — ×32), and distribution of microhardness through depth *h* in the central part of the strips (*b*)

quenching structures. Some weakening (loss of hardness) takes place in the upper part of the alloying strips. This phenomenon is associated with overheating of the sub-surface layers. Also, it occurs in the coatings deposited by the combined method, which, however, is not a drawback, as the weakened layer is removed in finishing machining.

An example of practical application of the developed coating method is reconditioning of railroad car axle journals.

CONCLUSIONS

1. Considered is the combined process of deposition of thin (0.05–0.50 mm) wear- and corrosion-resistant coatings of the Ni–Cr–B–Si and Ni–Fe–B–Si systems on low-carbon steels. The process combines advantages of laser cladding and microplasma spraying. A related process, i.e. laser-microplasma alloying, is suggested.

2. The coating process increases strength of adhesion between the coating and substrate and eliminates microcracks in the deposited layers. Also, it avoids the need to apply jet-abrasive blasting for surface preparation.

3. Main parameters of the coating and alloying processes were determined. The most significant of these parameters were identified under the experimental conditions. Metallographic examinations were conducted, showing the presence of the transition zone and absence of HAZ in clading, as well as presence of HAZ in alloying. In both cases a loss of hardness occurs in the upper layers of coatings (alloying strips), which is not critical, as size of these layers is comparable with allowance for finishing machining.

4. The highest effect on height of coatings deposited in one pass is exerted by the mass flow rate of powder and strip overlapping coefficient. The sample movement speed and laser radiation power density have the lowest effect. Variations of the angle between the laser radiation and microplasma jet axes have almost no effect on the coating height.

1. Grigoriants, A.G. (1989) *Principles of laser treatment of materials*. Moscow: Mashinostroenie.
2. Sasaki, S., Shimura, H., Kawakami, Y. et al. (1995) Laser assisted plasma spray coating method for surface modification of tribo-materials. In: *Proc. of ITSC'95* (Kobe, Japan, May 1995). Vol. 1.
3. Zreris, R., Nowotny, S., Berger, L.-M. et al. (2003) Characterization of coatings deposited by laser-assisted atmospheric plasma spraying. In: *Proc. of ITSC'03* (Orlando, USA, 2003).
4. Coddet, C., Montaron, G., Marchione, T. et al. (1998) Surface preparation and thermal spray in a single step: the PROTAL process. In: *Proc. of 15th ITSC* (Nice, France, 1998). Vol. 2.
5. Borisov, Yu.S., Kharlamov, Yu.A., Sidorenko, S.L. et al. (1987) *Thermal spraying using powder materials*. Refer. Book. Kiev: Naukova Dumka.
6. Bogachek, V.L., Tsybina, L.N. (1988) Quality of coatings deposited by microplasma spraying. *Avtomatich. Svarka*, **8**, 58–60.
7. Borisov, Yu.S., Pereverzev, Yu.N., Vojnarovich, S.G. et al. (1999) Deposition of narrow-strip coatings by microplasma spraying method. *Ibid*., **6**, 53–55.
8. Khaskin, V.Yu., Velichko, O.A. (1994) Bond strength between laser clad layer and substrate metal. *Ibid*., **7/8**, 51–52.
9. Velichko, O.A., Avramchenko, P.F., Molchan, I.V. et al. (1990) Laser cladding of cylindrical parts by powder materials. *Ibid*., **1**, 59–65.
10. Grezev, A.N., Safonov, A.N. (1986) Cracking and microstructure of chrome-nickel alloys clad by laser. *Svarochn. Proizvodstvo*, **3**, 6–8.
11. Morozov, V.P., Misyurov, A.I., Grigoriants, A.G. et al. (1987) Analysis of conditions of crack formation in laser cladding of Ni–Cr–B–Si system powders. *Ibid*., **5**, 32–35.
12. Kovalenko, V., Haskin, V. (1995) Selection of self-fluxing powder materials for laser cladding. *Informatyzatsiya ta Novi Tekhnologii*, **1**, 36–39.
13. Majorov, V.S., Matrosov, M.P. (1989) Influence of surface active materials on hydrodynamics of laser alloying of metals. *Kvant. Elektronika*, **4**, 806–810.
14. Garashchuk, V.P., Shelyagin, V.D., Nazarenko, O.K. et al. (1997) Technological 10 kW CO_2-laser LT 104. *Avtomatich. Svarka*, **1**, 36–39.

EVALUATION OF REMAINING LIFE OF WELDED JOINTS OF PIPELINES FOR THERMAL POWER PLANTS

V.V. DMITRIK[1], **A.K. TSARYUK**[2], **A.A. BUGAETS**[2] and **E.D. GRINCHENKO**[3]
[1]Ukrainian Engineering Pedagogical Academy, Kharkov, Ukraine
[2]E.O. Paton Electric Welding Institute, NASU, Kiev, Ukraine
[3]OJSC «Turboatom», Kharkov, Ukraine

Structure and properties of welded joints in heat-resistant steel 15Kh1M1F after long-time operation are described. An estimate of damageability of the joints and a negative forecast of further operation are given.

Keywords: welded joints, heat-resistant steels, steam supply line, pores, operating life, damaging, structure, creep

Currently major part (up to 90 %) of equipment and pipelines of thermal power plants and heat electric generation plants exhausted their service life (100,000 h) and economic (up to 50 %) life (150,000 h) [1]. Therefore, provision of their operational capacity and reliability proves to be an important and urgent problem.

For determining a remaining life of welded joints of steam lines in addition to the methods of calculation by the rated stresses since recently one widely uses a method of evaluation by the structural factor with metal microdamaging as its main index and metal microstructure as a facultative one.

Damages in the welded joints are one of the main factors affecting a decrease of the operating life of pipelines of power units of thermal power plants. Life of the welded joints in pipes amounts, as a rule, to 0.6-0.8 of the parent metal life [2]. Damages in welded joints of steam line pipes develop by different mechanisms. The main type of damage of welded joints resulted from long-tern operation of steam lines of heat-resistant Cr–Mo–V steel (operating time is more than 150,000 h) is creep microcracks [3], which nucleate and propagate mainly in the site of incomplete recrystallization of the HAZ metal, which is heated in welding in the intercritical temperature range A_{c_3}–A_{c_1}. In this case several stages may be distinguished in the process of damage development [2, 4–7]:

- preparatory (initial) when changes in the microstructure do not result in the initiation of microdamages;
- incubation when creep micropores 0.05–0.90 μm in size form (identified only by electronic microscope);
- initiation of microdamages as creep pores 1–3 μm in size and larger (formation of a chain of pores, their merge and formation of microcracks are observed; a considerable degradation of the metal microstructure is observed in this site).

The aim of this work is to evaluate a remaining life of the welded joints in pipes of live steam lines (630 × 25 mm) and of reheat pipes (325 × 60 mm) of 15Kh1M1F steel at the Zaporozhie Thermal Power Plant after their operation during more than 180,000 h. In this case a method of evaluation by the structural factor on the basis of studies of microstructure and properties of the metal of welded joints of steam line pipes of the indicated steel grade was employed.

Chemical composition of the parent and deposited metal of welded joints of steel 15Kh1M1F is presented in Table 1.

Designed useful life specifying permissible stresses in the norms of creep strength calculation was determined on the basis of the ultimate long-term strength for 100,000 h with the safety factor 1.5 [4]. Time before failure of the studied welded joints with the indicated safety factor in most cases considerably exceeded the designed useful life. Results of studies of microstructure and properties of the metal of welded joints in pipes of live steam lines, reheat pipes and pipes in the boiler being operational for more than 180,000 h at the temperature 545 °C showed a possibility to extend their service life above the term provided in the specifications [8]. However, prevention of the immediate failure, which may be very dangerous and quite probable, requires sufficiently accurate and concrete forecasting of the remaining life of the welded joints in the pipes of steam lines.

Content of chemical elements of welded joints of steel 15Kh1M1F pipes, wt.%

Object of study	C	Si	Mn	Cr	Mo	V	P	S
Parent metal	0.13	0.26	0.77	1.26	0.99	26.0	0.021	0.020
Weld	0.01	0.27	1.13	1.04	0.61	0.16	0.024	0.022

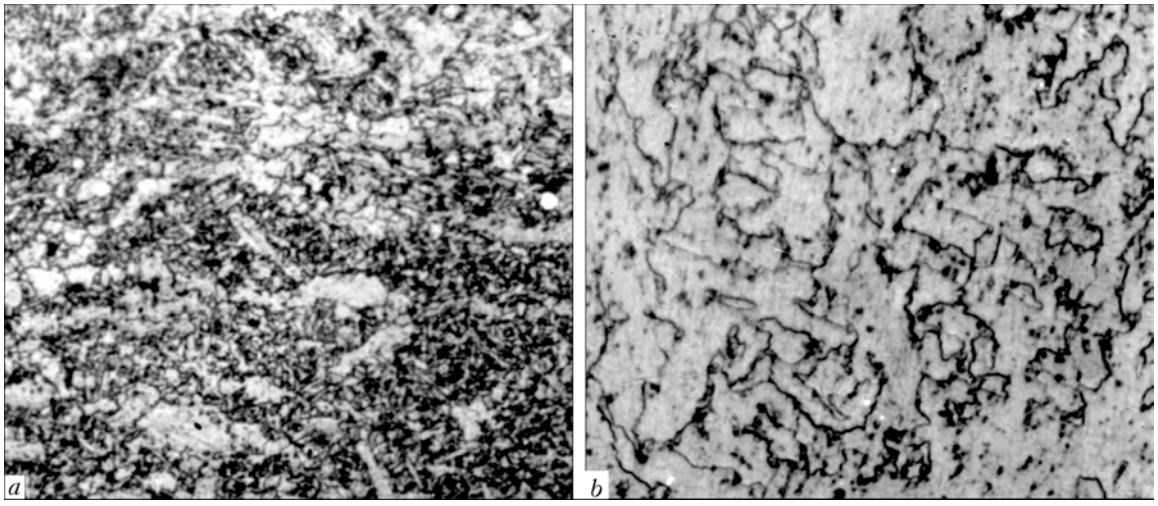

Figure 1. Microstructure of weld metal in the welded joint of live steam lines (198,000 h of operating time): *a* — ×100; *b* — ×750

Individual diagnostics of the steam line pipe metal was carried out by the methods used to study its microstructure. These methods consider a correlation between the structure and properties of the metal of welded joints, which permitted obtaining sufficiently accurate data for evaluation of their remaining life depending on the degree of damage [9, 10].

Damaging specified by technological factor was 80 % in the site of incomplete recrystallization, 8 % at the site of fusion and 12 % in the weld metal in the structure of 30 welded joints in pipes of the steam lines of thermal power plant of Ukraine (single-type or approaching it) whose operating time was more than 190,000 h.

The presented data approach those obtained in work [2]. Some difference between them can be attributed to a different operating time of welded joints. It is noteworthy that the frequent number of starts and stops has a significant effect on their damaging after 150,000 h of operating time. Damaging in conditions of low temperature creep proceeds mainly by a mechanism of pore formation [5].

Damaging intensity in the weld metal increases after 190,000 h of operating time of pipe welded joints performed by manual arc welding with coated electrodes according to the standard technology.

Microstructure of weld metal (Figure 1) presents ferrite-carbide mixture. Specific ferrite grains have an elongated shape. Chains 0.1–0.3 mm long are formed of equiaxial and elongated grains oriented towards heat removal in welding. Size of equiaxial grains of weld metal corresponds to 9 points according to GOST 5639–82. Carbide precipitates are located by boundaries of the grains more frequently than by their body. No migration of grain boundaries from carbide precipitates including from coagulating $M_{23}C_6$ is observed. Pores in some cases enlarged are detected near coagulating carbides in the grain boundary (Figure 2). It is noteworthy that intensity of coagulation of separate carbide precipitates located by the boundaries of the weld metal grains is higher than in the parent metal. The availability of pores was detected by light and electron microscopy. Specimens were etched by the advanced method [5] and also in the solution of H_2SO_4 (20 ml) in 100 ml of the distilled water heated to the temperature 75 °C [11].

Nuclear micropores 0.05–2 μm in size of mainly spherical and ellipsoidal shape detected by the elec-

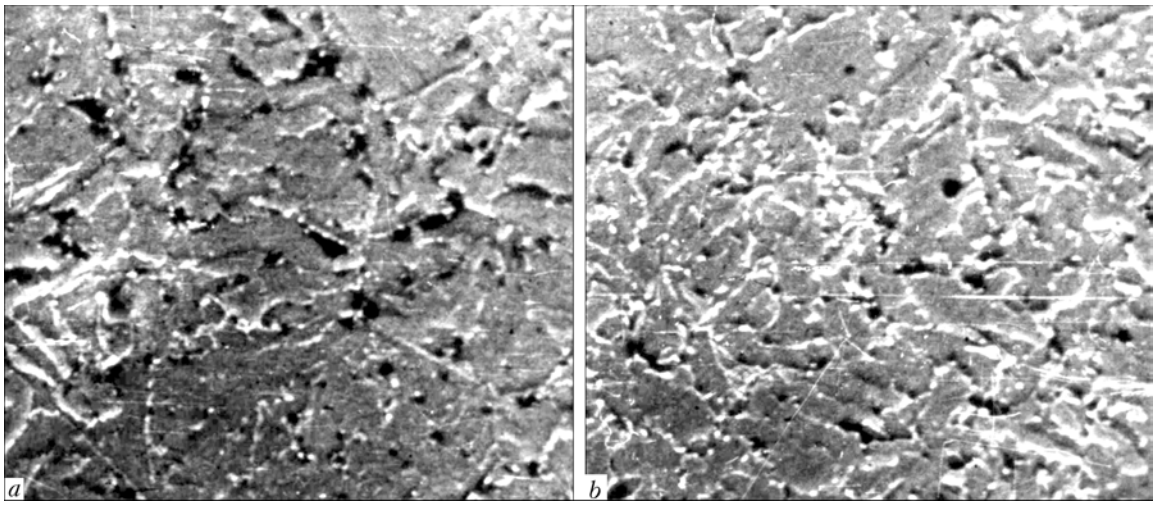

Figure 2. Microstructure of welded joints of steam line pipes with damages: *a* — weld metal; *b* — site of incomplete HAZ recrystallization (×2500)

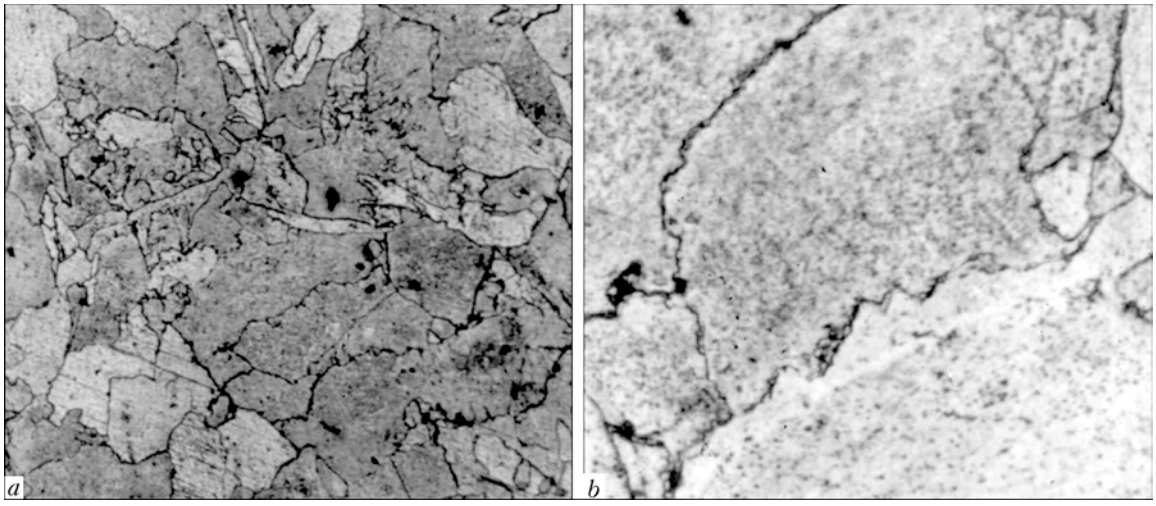

Figure 3. Microstructure of parent metal of 15Kh1M1F steel welded joint: *a* — ×100; *b* — ×750

tron microscopy were formed in the weld metal microstructure together with pores 2–7 μm in size detected by the metallographic analysis and by replicas using the optical microscopy method (Figure 2). In this case the indicated pores in the form of microcracks were mainly concentrated in the grain boundaries and were in the direct contact with the carbide precipitates $M_{23}C_6$ as well as with non-metallic inclusions. Pores were combined into chains forming microcrack nuclei by the grain boundaries.

Microstructure of the parent metal presented a ferrite-carbide mixture with grain size of 4 points (Figure 3). Relatively fine carbides (0.7–1.2 μm) are sufficiently uniformly distributed in the grain body. Enlarged (1.2–2.1 μm) carbide precipitates $M_{23}C_6$ were mainly formed by the grain boundaries. The parent metal was characterized by the pores of mainly spherical or ellipsoidal shape 0.05–1.50 μm in size located more uniformly than in the weld metal. Microcracks by the grain boundaries formed considerably rarely and their average density was about 300–400 pcs / mm^2, which was by 40–50 % lower than in the weld metal.

Microstructure of the site of incomplete recrystallization (Figure 4) is characterized by a variety of grains: along with fine grains (5–10 μm) there are also large grains (50–70 μm) being present. Globular pearlite is mainly present as a new product of austenite decomposition. Average density of pores (see Figure 2, *b*) is by about 10–15 % larger than in the weld metal, however the size of pores is smaller, their distribution is more uniform and the shape is more spherical (see Figure 2).

Failure by the weld metal under conditions of working stresses and temperatures is of intergranular nature, since the pore coalescence by the boundaries of the elongated grains is simplified. Failure resistance here is specified both by stability of the strengthening phases and by an increased level of their fluctuation by the grain boundaries provided by the relevant welding heating. Metal damaging with operating time of more than 190,000 h depends on the shape of grains determined by a correlation of their length L to width l, i.e. on the grain heterogeneity coefficient [12]. It is established that grains of the weld metal structure, where $L > l$, are formed in welding by increased (standard) conditions. With correlation $L / l = 1$ equiaxial grains are formed, while at $L / l = 1.5$–1.9 the damaging intensity of weld metal in conditions of low temperature creep increases by 20–30 % on the

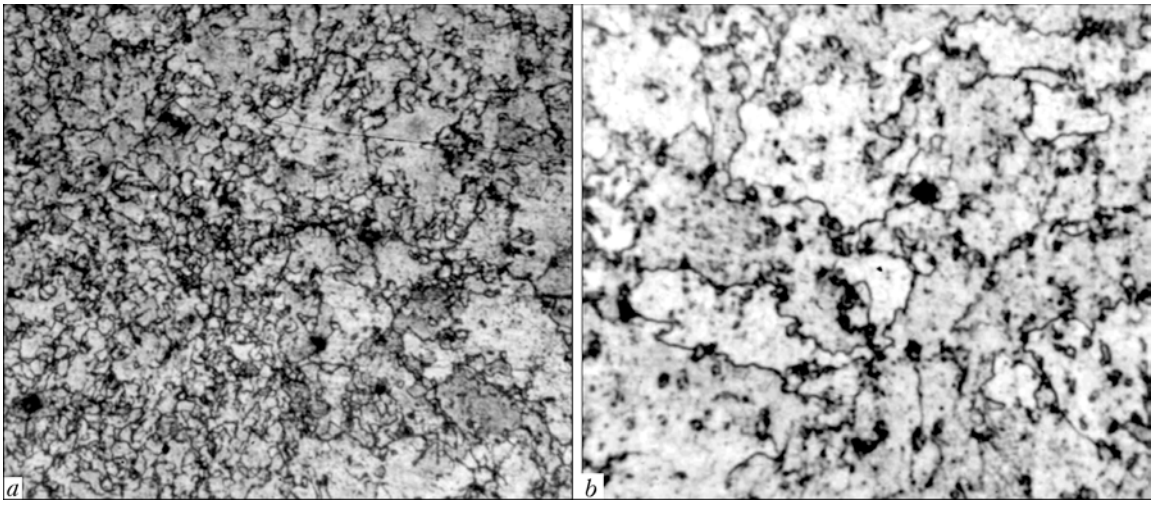

Figure 4. Microstructure of site of incomplete recrystallization of welded joint: *a* — ×100; *b* — ×750

average, which is confirmed by the number of pores per 1 mm^2 and by their concentration (see Figure 2).

Simulation of the welding heating [13, 14] was the basis for development of the recommendations on selection of the welding conditions for heat-resistant steels, which provide formation of the fine-grain weld metal structure composed of equiaxial disoriented grains. Besides, it is established that a size of non-metallic inclusions in the weld metal corresponding to point 2 according to GOST 1178–70 after 190,000 h of operating time facilitates formation of creep pores, therefore, there is a necessity to decrease the number of such inclusions [15].

Short-term mechanical properties of specimens cut from the metal of live steam supply line pipes after 196,000 h of operating (Figure 5) are lower than initial ones, which is in good agreement with the data from works [2, 8]: σ_t = 421 MPa; σ_y = 280 MPa; δ = 15.8 %; ψ = 71.6 %; KCU = 59 J / cm^2 (KCU of specimens of 325 × 60 mm in size cut out from the steam line by the fusion site (Figure 6) is at the level of 69 kJ / cm^2).

A procedure described in [6] was used for evaluation of the remaining life of the studied welded joints of steam lines. According to this procedure the following criteria are proposed: a critical damaging with pores f_{cr} when an urgent replacement of pipeline elements is required, ultimately permissible damaging with pores f_{ult} when the planned replacement of the damaged components is required for the time period not more than $\tau_{add} = \tau(f_{cr}) - \tau(f_{ult})$. Critical and ultimately permissible damaging was determined regarding structural condition of the metal. For calculation of time of the remaining work of the studied welded joint up to its critical damaging it is necessary to calculate time allowance coefficient K_τ:

$$K_\tau = \frac{0.85\tau_{cr}}{\tau} - 1.$$

In this case a time of remaining work before critical longevity is $\tau_{add} = \tau K\tau$. In compliance with the indicated conditions a scale for calculation of the time allowance coefficient before critical damaging [6] is:

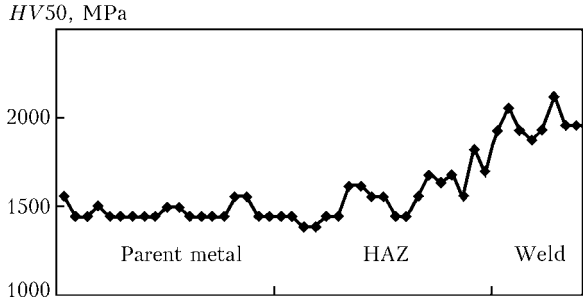

Figure 5. Distribution of microhardness HV in welded joint metal

f, %	0.08	0.10	0.15	0.20	0.25	0.30	0.35	0.40
τ / τ_{cr}	0.50	0.55	0.65	0.72	0.78	0.82	0.85	0.88
K_τ	0.70	0.50	0.30	0.18	0.09	0.05	0	0

The presented scale may be used for calculation of residual longevity by the metal damaging with pores.

In this specific case evaluation of the resource for steam line of steel 15Kh1M1F allowed establishing formation of pores more than 1 mm in size, pore chains and microcrack nuclei in the weld metal, HAZ and parent metal. In this situation the calculated damaging f was more than 35 %. Then the remaining life of the steam line components may be determined as

$$\tau_{add} = \tau K_\tau = 190000 K_\tau.$$

In compliance with the indicate calculation scale with damaging f = 0.35 %, K_τ = 0, i.e. the remaining life τ_{add} is completely exhausted. Therefore, the studied components of the steam line of steel 15Kh1M1F cannot be operational any longer and are subject to urgent replacement.

CONCLUSIONS

1. Structure and properties of steel 15Kh1M1F welded joints of pipes in live steam lines with operating time of more than 190,000 h were studied. After completion of this operating time the welded joints of pipes receive damages (pores, pore chains, microcracks) in the weld metal, site of incomplete HAZ recrystallization and in the parent metal. In this case calculated damaging of the metal of welded joint is more than 0.35 %.

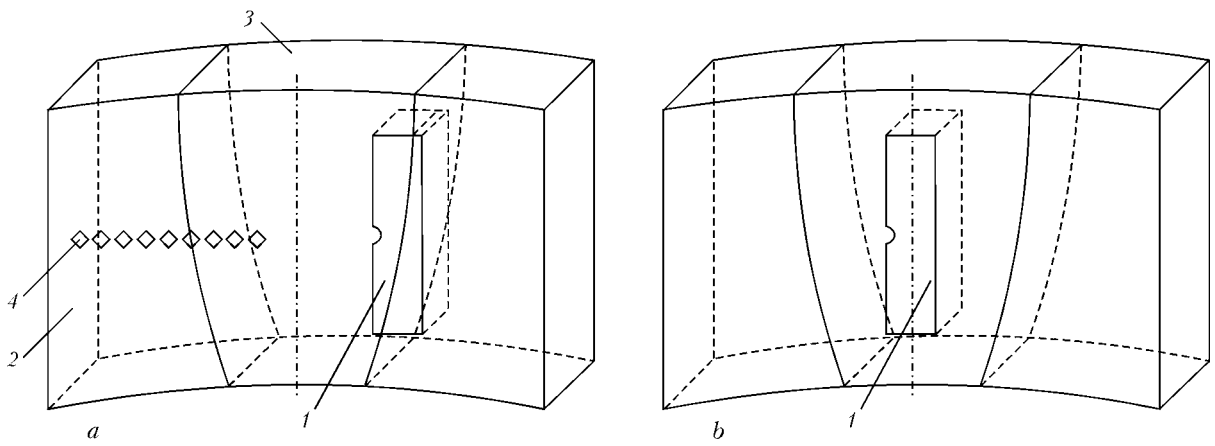

Figure 6. Scheme of cutting out specimens for impact bending tests (KCU) from metal of steam line welded joint in the fusion site (*a*), and weld metal (*b*): *1*— Mesnager specimen; *2* — parent metal; *3* — weld; *4* — site of microhardness measurement

2. The obtained results allowed determining that the studied steam line welded joints cannot be admitted for further operation and should be urgently replaced.

1. Sheberstov, A.N. (2004) State-of-the-art of thermal power plants in Ukraine, prospects of their renovation and improvement. *Energetika i Elektrifikatsiya*, **12**, 478.
2. Khromchenko, F.A. (2002) *Life of welded joints of steam lines*. Moscow: Mashinostroenie.
3. Gofman, Yu.M. (2000) Long-term strength as a criterion of service reliability of steam line metal. *Teploenergetika*, **4**, 58–59.
4. Tyurin, P.Ya., Gulyaev, V.N. (1972) About increase of service life of heat-and-power engineering equipment elements under conditions of metal creep. *Ibid*., **6**, 2–4.
5. Anokhov, A.E., Alekhova, I.A. (1982) Damage accumulation in welded joints of steam lines of steel 12Kh1MF in creep process. *Svarochn. Proizvodstvo*, **9**, 34–35.
6. Berezina, T.G. (1986) Structural method of determination of residual life of steam line parts being in long-term service. *Teploenergetika*, **3**, 53–56.
7. Rozenberg, V.M. (1967) *Creep of metal*. Moscow: Metallurgiya.
8. *RD 34.17.421–92:* Standard manual on control and extension of metal service life of main elements of boilers, turbines and pipelines of thermal power plants. Moscow: ORGRES CPO.
9. Antikajn, P.A. (1996) Maintenance of reliable service of boilers, vessels and pipelines after the design service life is over. *Teploenergetika*, **12**, 2–7.
10. Zemzin, V.N., Shron, R.Z. (1988) Ways of improvement of service reliability and increase of life of heat-and-power engineering equipment welded joints. *Ibid*., **7**, 2–5.
11. (1972) *Metallography of iron*. Part 2: Structure of steels with atlas of micrographs. Ed. by F.N. Tavadze. Moscow: Metallurgiya.
12. Portnoj, B.K., Babich, B.N. (1974) *Dispersion-strengthened materials*. Moscow: Metallurgiya.
13. Dmitrik, V.V., Kalinichenko, V.I. (2003) Modeling of arc welding process. *Izvestiya Vuzov. Mashinostroenie*, **4**, 59–64.
14. Dmitrik, V.V. (2000) Modeling of structure of welded joints from low-alloyed heat-resistant Cr–Mo–V pearlitic steels. *The Paton Welding J.*, **4**, 26–29.
15. Tsaryuk, A.K. (1999) Peculiarities of effect of phosphorus on size of non-metallic inclusions and properties of heat-resistant steel welded joints. *Avtomatich. Svarka*, **4**, 26–30.

CALCULATION OF THE KINETICS OF DIFFUSION PHASE TRANSFORMATIONS IN LOW-ALLOYED STEELS IN BEAM WELDING

U. DILTHEY[1], **A.V. GUMENYUK**[1] and **G.A. TURICHIN**[2]
[1]Rheinisch-Westfaellische HTS, Aachen, Germany
[2]St.-Petersburg State Polytechnic University, St.-Petersburg, Russia

Parametric description of TTT- and CCT-diagrams has been developed on the basis of the results of growth of cementite inclusions and redistribution of carbon in the ferritic phase under non-equilibrium conditions for welding of steels at high cooling rates. The model has been developed to estimate the effect of initial structure of a material and parameters of the thermal cycles on the transformation diagrams.

Keywords: arc welding, low-alloyed steel, thermal cycles, diffusion, phase transformation kinetics

Level of mechanical properties of the metal of the weld and HAZ is the determinant factor in development of welded structures, selection of welding consumables and welding process parameters. Analysis of structural transformations proceeding in steel in welding is usually performed using diagrams, obtained experimentally and correlating the metal microstructure with the thermal cycle parameters. Unlike the diagrams of isothermal decomposition of austenite (CCT) [1] used at heat treatment, diagrams of anisothermal decomposition (TTT) are used in welding [2]. Current approaches to theoretical description of transformation diagrams are based on their parametric description and thermodynamics principles [3].

At high cooling rates typical for electron beam, laser and plasma welding, phase transformations in the HAZ have several features. In this case, it is practically impossible to produce equilibrium ferritic-pearlitic structures, and HAZ metal properties are determined by the ratio of bainite and martensite components. According to [4], austenite decomposition in welding starts from a diffusionless transformation of the crystalline lattice of γ–α phases in small regions located at grain boundaries. Cementite inclusions formed here become larger due to carbon diffusion from the α-phase. Further cooling leads to martensite formation from residual austenite.

Several models are known, which describe austenite decomposition proceeding at heat treatment [5] and at welding [6]. Description of transformation kinetics is based on the theory of second phase initiation [7], and use of Avrami equation for calculation of transformation degree at exponential dependence of new phase growth rate on Gibbs potential difference of the new and initial phases. A non-stationary nature of the diffusion processes is not taken into account. Classical theory [8, 9] of diffusion-controlled growth is usually used to determine the inclusion dimensions. In [10] stationary kinetics is applied instead of non-equilibrium kinetics to describe the growth of ferrite grains. Approach combining chemical transformation kinetics with a non-stationary concept of diffusion processes, was developed [11] to describe the phase transformations, proceeding in Al–Mg alloys. To make a valid prediction of the HAZ metal microstructure in beam welding, it is necessary to take into account the relative influence of the kinetics of chemical reaction of cementite formation and non-stationary carbon diffusion in the solid solution, surrounding the growing non-metallic inclusions.

Problem definition. Ratio of non-metallic inclusion volume and their surface area is determined by their shape. At the start of structural transformations, size a of the cementite inclusion is much smaller than the diffusion layer thickness. This may be caused by point sink for carbon, the concentration field around which is spherically symmetrical. Non-equilibrium growth of the cementite inclusion in the solid solution is described by the equation of kinetics of the chemical reaction with cementite formation [11]:

$$\frac{da}{dt} = K_1(T)C - K_2(T), \qquad (1)$$

where t is time; $K_1(T)$ and $K_2(T)$ are the constants of velocities of the direct and reverse reactions, respectively; C is the concentration of diffusible carbon on the inclusion surface; T is the temperature.

Constants of reaction rates are described by Arrenius formulas

$$K_{1,2}(T) = K_{1,2}^{(0)} \exp(U_{f,s}/kT),$$

where $K_1^{(0)}$ and $K_2^{(0)}$ are the frequency factors; U_f and U_s is the activation energy of the direct and reverse reaction, respectively [12].

Surface concentration of diffusible carbon is found from expression (1) by solving the diffusion problem. In view of the smallness of Peclet number, the convective term associated with the motion of inclusion boundary, may be neglected:

$$\frac{\partial C}{\partial t} = D\Delta C = D\frac{1}{r^2}\frac{\partial}{\partial r}\left(r^2\frac{\partial C}{\partial r}\right). \qquad (2)$$

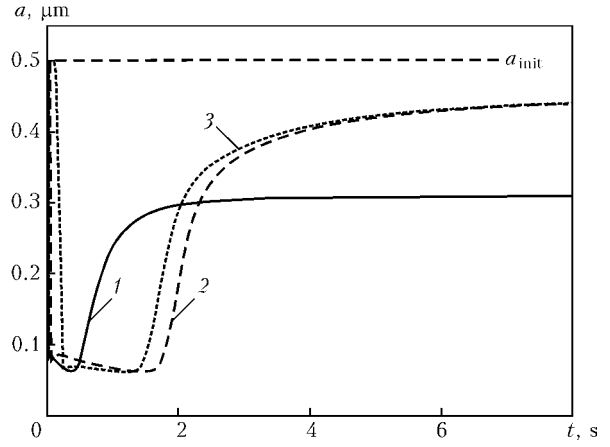

Figure 1. Increase of dimension a of cementite inclusions in low-alloyed steel at different thermal cycles: *1* — T_{max} = 1350 °C, v_w = = 10 mm / s; *2* — T_{max} = 1350 °C, v_w = 5 mm / s; *3* — T_{max} = 900 °C, v_w = 5 mm / s

Boundary condition on the inclusion surface (r = = a) depends on the continuity of the impurity flow:

$$-D \frac{\partial C}{\partial r}\Big|_{r=a} = K_1(T)C\Big|_{r=a} - K_2(T). \qquad (3)$$

Carbon concentration at a distance from inclusions is determined by its initial concentration C_0:

$$C|_{r\to\infty} \to C_0. \qquad (4)$$

This problem, described by equations (1) and (2), belongs to problems of reaction–diffusion type.

Solution of problem of inclusion size increase. Standard methods of mathematical physics were used to solve this problem [13]. Carbon concentration in the solid solution at the surface of the growing inclusion is described by the expression

$$C = C_0 - \frac{1}{\sqrt{\pi}} \int_0^t \frac{a(\tau)}{a(t)} \frac{K_1C_0 - K_2}{\sqrt{D(t-\tau)}} \times$$
$$\times \left[1 - \left(\frac{K_1}{D} - \frac{1}{a}\right)\sqrt{\pi D(t-\tau)}\, e^{(K_1/D - 1/a)^2 D(t-\tau)} \times \right. \qquad (5)$$
$$\left. \times \left(1 - \mathrm{erf}\left[\left(\frac{K_1}{D} - \frac{1}{a}\right)\sqrt{D(t-\tau)}\right]\right)\right] d\tau,$$

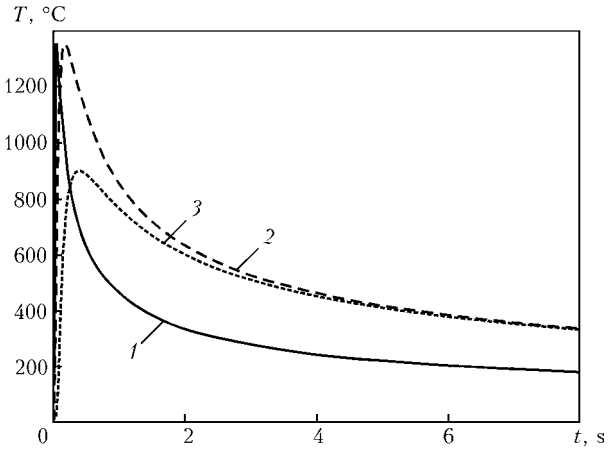

Figure 2. Curves of thermal cycles obtained in different HAZ points at different speed of EBW: *1–3* — same as in Figure 1

where K_1, K_2 and D are the $T(\tau)$ functions; a is the function of t.

Equations (1) and (5) form a system, the solution of which allows establishing the dependence of inclusion size and carbon concentration at its surface on time. Proceeding from [11], a simplified solution for surface concentration, can be presented as

$$C = C_0 - \frac{1.56}{D\sqrt{\pi}} \frac{(K_1C_0 - K_2)}{\left(\frac{K_1}{D} - \frac{1}{a}\right)}.$$

Dynamics of growth of the inclusion size is determined by their relative influence. Taking [11] into account, expression (1) can be rewritten as

$$\frac{da}{dt} = K_1 \left(C_0 - nC' \frac{4}{3}\pi a^3 - \frac{1.56}{\sqrt{D\pi}} \frac{(K_1C_0 - K_2)}{\left(\frac{K_1}{D} - \frac{1}{a}\right)} \right) - K_2,$$

where C' is the carbon concentration in cementite (at Fe_3C $C' \cong 0.25$).

Euler method was used to solve the equation of inclusion size increase. Figure 1 gives an example of calculation. As the resultant solution for the steady-state inclusion size reached after completion of the heating-cooling cycle, a_{lim}, is part of the equation, the «shooting» method was used, i.e. a preliminary a_{lim} value was selected, at which the same final a value would be ensured. Thermal cycles were calculated, using an EBSIM system [14] (Figure 2).

Calculated values of inclusion size mostly coincide with the experimental values. Calculations showed that the inclusion size is approximately the same over the entire HAZ, but it becomes much smaller with increase of welding speed. Change of carbon concentration at the inclusion surface and in the solid solution is shown in Figures 3 and 4, from which the influence of kinetic effects on microstructure formation can be seen. Calculated value of carbon concentration in the solid solution essentially exceeds the solubility limit (about 0.1 %), and carbon concentration at the inclusion surface is much smaller than in the solid solution.

Plotting and analysis of transformation diagrams. Solution of a non-stationary diffusion problem

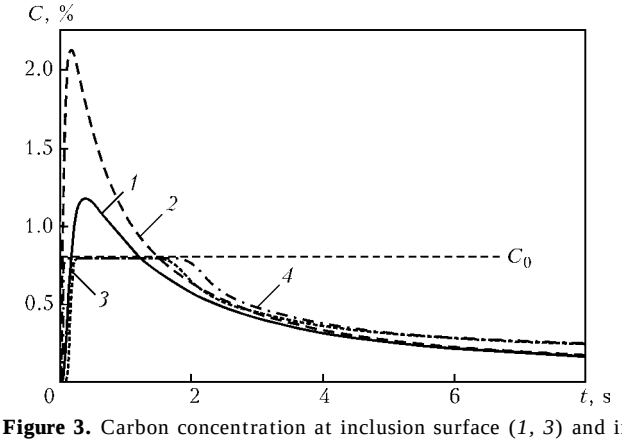

Figure 3. Carbon concentration at inclusion surface (*1, 3*) and in α-Fe solid solution (*2, 4*) in different regions of HAZ metal at v_w = = 5 mm / s: *1, 2* — T_{max} = 1350 °C; *3, 4* — T_{max} = 900 °C

should be used for an expression describing the CCT and TTT diagrams. After integration of (5) using the saddle-point technique, equation of inclusion growth becomes

$$\frac{da}{dt} = (K_1C_0 - K_2) \times$$
$$\times \left[1 + \frac{2}{\sqrt{\pi}} \frac{K_1}{D} \left[\sqrt{Dt}\left(1 - \frac{a_1}{p}\sqrt{\pi}\right) - \frac{a_1}{p^2}\sqrt{\pi}\frac{A}{\frac{1}{a} - \frac{K_1}{D}}\right] + \right. \quad (6)$$
$$\left. + \frac{dT}{dt}\frac{2K_1}{\sqrt{\pi}}\frac{\frac{d}{dT}(K_1C_0 - K_2)}{K_1C_0 - K_2} 0.1t\left[\sqrt{Dt}\left(\frac{1}{a} - \frac{K_1}{D}\right)\right]\right],$$

using approximation of error function $\mathrm{erf}(x) \approx \approx 1 - a_1/(1 + p\,x)e^{-x^2}$. Here $a_1 = 0.348$; $p = 0.47$; $A = \ln\left(1 + p\sqrt{Dt}\left(\frac{1}{a} - \frac{K_1}{D}\right)\right)$.

Transformation start corresponds to the condition of $da / dt = 0$. In the equilibrium case, this condition is satisfied by fulfillment of the obvious equality

$$K_1(T)C - K_2(T) = 0. \quad (7)$$

Under non-equilibrium conditions the transformation temperature differs from its equilibrium value so that condition (7) cannot be satisfied. Then condition $da / dt = 0$ can be satisfied only in the case, if the expression placed in brackets in (6), is equal to zero.

This condition correlates the temperature and time of transformation start, i.e. provides a mathematical description of C-shaped curve of phase transformation. Assuming $dT / dt = 0$, we obtain an equation of the TTT curve. If $dT / dt \neq 0$, we come to the equation of CCT curve.

In the explicit form, the equation of the transformation diagram, describing the decomposition of Fe–C solid solution can be written as

$$\ln t = 2\ln\left|1.48A\frac{1}{\frac{D_0}{K_1^{(0)}a}\exp\left(\frac{U_f - U_D}{kT}\right) - 1}\right| +$$
$$+ 2\ln\left|2.84\frac{\sqrt{D_0}}{K_1^{(0)}}\exp\left(\frac{U_f - U_D/2}{kT}\right)\right| -$$
$$- \frac{dT}{dt} 2.58\sqrt{D_0}K_1^{(0)} e^{\frac{U_f + U_D/2}{kT}} \frac{U_f}{kT^2} \times$$
$$\times \left(1 + \frac{K_2^{(0)}}{K_1^{(0)}C_0}\left(1 - \frac{U_s}{U_f}\right)e^{\frac{U_f - U_s}{kT}}\right) \times \quad (8)$$
$$\times \left|\frac{1}{a} - \frac{K_1^{(0)}}{D_0} e^{\frac{U_p + U_f}{kT}}\right| \times$$
$$\times \left(\frac{2a_1A}{p^2}\left(\frac{D_0}{K_1^{(0)}a}\exp\left(\frac{U_f - U_D}{kT}\right) - 1\right)^{-1} - 1\right)^2 \times$$
$$\times \left(\frac{\sqrt{D_0}}{K_1^{(0)}}\exp\left(\frac{U_f - U_D/2}{kT}\right)\right)^3.$$

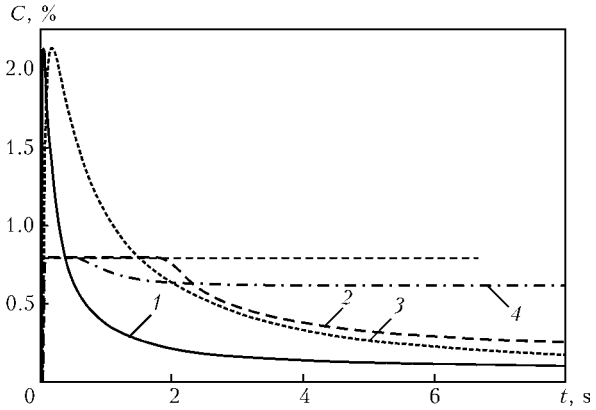

Figure 4. Carbon concentration at inclusion surface (*1*, *2*) and in α-Fe solid solution (*3*, *4*) at different welding speeds and T_{max} = = 1350 °C: *1*, *2* — v_w = 10 mm / s; *3*, *4* — v_w = 5 mm / s

Here, U_D is the activation energy of carbon diffusion in α-Fe.

Five independent conditions should be used for determination of such parameters as energy of reaction activation, frequency factors and initial inclusion size. The first of them corresponds to the reaction equilibrium constant being determined from Fe–C constitutional diagram; the second is the equality of the differences of activation energies of the direct and reverse reactions of cementite formation enthalpy. The third condition associates the value of the initial inclusion size with the maximum transformation temperature $1 / a(K_1(T) / D(T)) = 0$. The last two conditions are based on the correspondence between the calculated and experimental curves.

In welding of 5690QL steel the following parameters are used: $K_1^{(0)}$ = 45 m / s; $K_2^{(0)}$ = 2.2 m / s; U_f = = $1.12 \cdot 10^{-19}$ J / at; U_s = $1.60 \cdot 10^{-19}$ J / at; D_0 = = $2 \cdot 10^{-6}$ m^2 / s; U_d = $1.38 \cdot 10^{-19}$ J / at; a_{cr} = $1.1 \cdot 10^{-8}$ m; A = 3.35.

Coefficient of carbon diffusion in α-Fe is taken from study [15].

Two first terms in the right-hand part of expression (8) determine the curve of isothermal transformation, the third describes the curve distortion associated with the cooling rate. According to (8), cooling ($dT / dt <$ < 0) delays the transformation start, which corresponds to the shift of the transformation curve to the right. It should be noted that allowing for the cooling

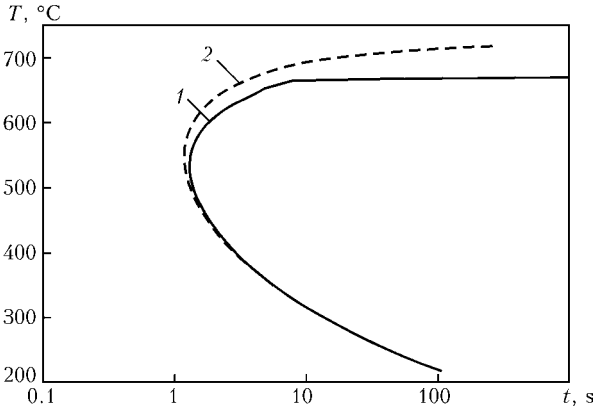

Figure 5. TTT (*1*) and CCT (*2*) diagrams produced for model low-alloyed steel with 0.2 % C

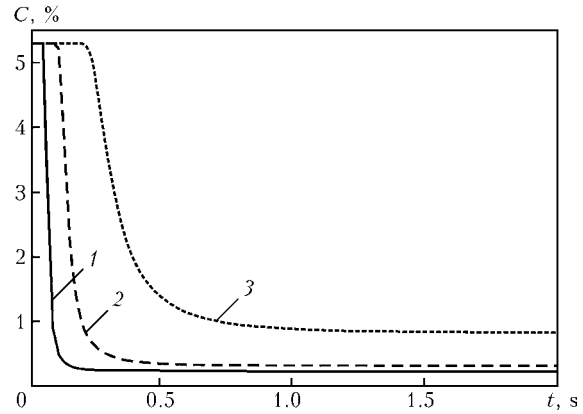

Figure 6. Change of carbon concentration in the center of «former» cementite inclusion of 0.8 μm decomposing under the impact of thermal cycle of welding in sample of model low-alloyed steel with 0.2 % C, depending on maximum heating temperature: *1* — T_{max} = = 880; *2* — 1080; *3* — 1330 °C

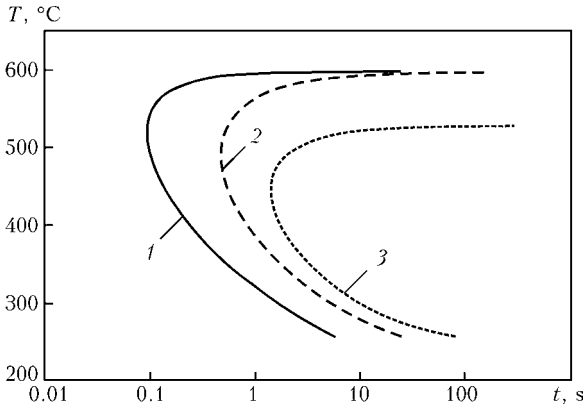

Figure 7. Influence of initial carbon concentration on the shift of transformation curves at the change of maximum heating temperature from 1350 to 880 °C: *1* — C_{init} = 0.2; *2* — 0.3; *3* — 0.8 %

rate leads not only to the shift (as is known from [6]), but also to distortion of the transformation curve.

The above procedure allows obtaining a branch of the transformation curve, corresponding to bainite formation, due to substitution of $dT / dt = f(T)$. Figure 5 shows an example illustrating the difference between the TTT and CCT diagrams calculated using the developed model.

The effect of shift and distortion of the shape of transformation curves, due to the features of the thermodynamic cycle and initial steel microstructure was observed during the experiment [16]. Alongside the heating and cooling rates, the initial dimensions of the inclusions, maximum heating temperature have a significant influence on the position and shape of C-shaped curves. This is due to the dependence of the time of transformation start and cementite growth rate during the time from the initial carbon concentration to the transformation start. Assuming that the transformations start in the sites of the highest concentration of carbon, it is necessary to determine the initial concentration value, based on solution of the problem of initial carbide dissolution:

$$\frac{\partial C}{\partial t} = D(T)\frac{\partial^2 C}{\partial x^2}, \quad C\Big|_{t=0} = \begin{cases} C_{cem};\ x \le a, \\ 0;\ x > a, \end{cases} \quad C|_{x \to \infty} = C_\infty,$$

where C_{cem} is the carbon concentration in cementite (25 %); C_∞ is the initial carbon concentration in the solid solution volume.

Maximum value of residual concentration, yielded by solution of this problem, can be written as

$$C = (C_{cem} - C_\infty)\left(1 - \exp\left(-\frac{a^2}{4\int\limits_0^t D(T(t))dt}\right)\right) + C_\infty. \quad (9)$$

Time dependence of residual carbon concentration after dissolution of the initial carbides for the calculated thermal cycles [14], corresponding to three different HAZ areas, is shown in Figure 6.

Transformation curves, corresponding to the above thermal cycles, are given in Figure 7. Position of the curves depends on the values of local initial carbon concentration, which in their turn are determined by the real thermal cycles of welding.

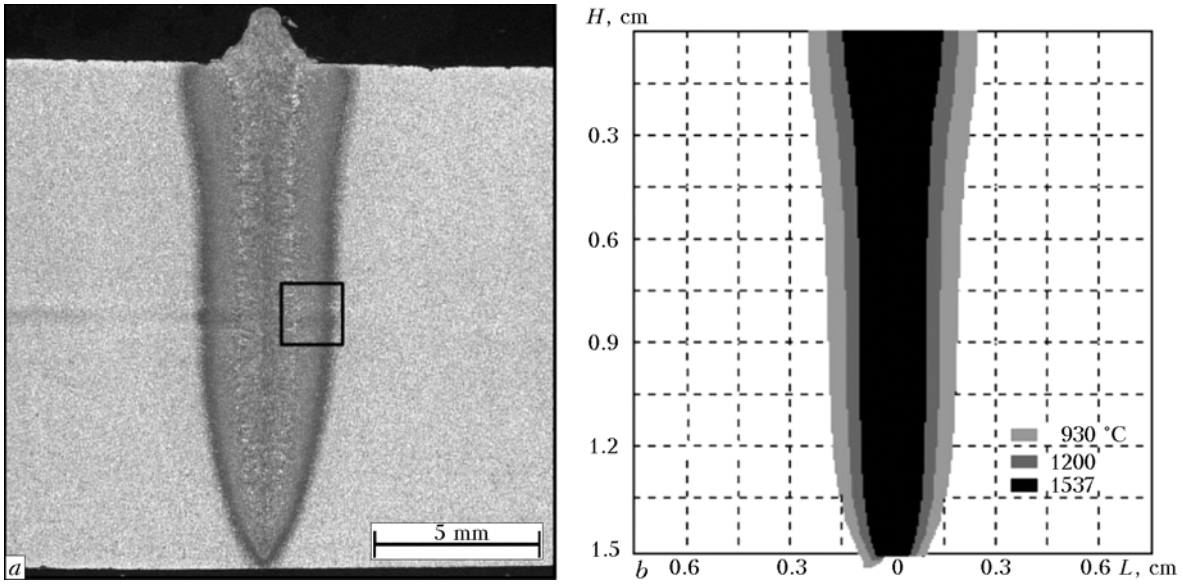

Figure 8. Macrosection of welded joint (*a*) produced experimentally, and simulation results (*b*): *L* — distance from weld axis

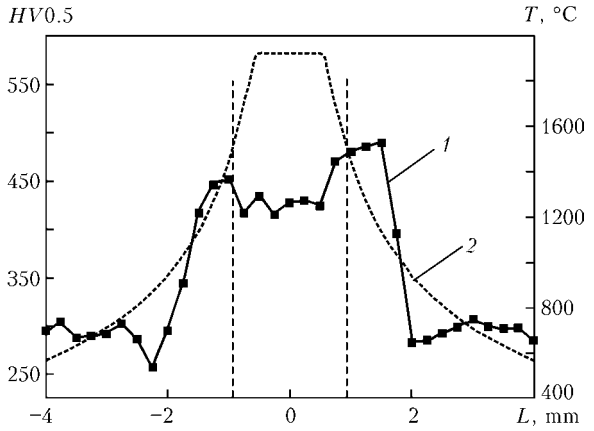

Figure 9. Distribution of microhardness *HV* (*1*) and maximum heating temperature (*2*) at greater distance *L*

Test EBW of 15 mm thick samples from S690QL steel was performed to check the above dependence. Samples were joined by butt welds at up to 20 mA beam current, accelerating voltage of 150 kV and beam focusing on the surface at 800 mm distance. Welding speed was equal to 5 mm / s, which corresponded to cooling time $t_{8/5}$ = 4 s in a middle HAZ region. It is established that this parameter only slightly depends on the distance from the fusion line. Measurement of microhardness of the weld and HAZ metals is indicative of a transition from the martensite to bainite microstructure at greater distance from the fusion line, this being confirmed by the results of metallographic analysis (Figures 8 and 9).

CCT curves of transformations under the conditions simulating the thermal cycle in beam welding were obtained at thermomechanical simulation in GLEEBLE 3500 unit by dylatometric and metallographic analysis of the samples. Figure 10 gives the transformation curves, corresponding to three different maximum heating temperatures. The observed tendency of the curve shift is confirmed experimentally. Some discrepancy between the experimental and calculated results is attributable to a more complex composition of the actual steel and influence of manganese, as well as other alloying elements (the latter was not considered in this study).

It follows from the above-said that the developed mathematical model based on solution of the problems of diffusion and kinetics of chemical reaction, allowing for the mutual influence of the inclusions, permits describing the processes of cementite growth and carbon redistribution in the α-phase. Calculated dimensions of cementite inclusions correspond to experimental values.

The developed model can be used to obtain a parametric description of TTT and CCT diagrams. The

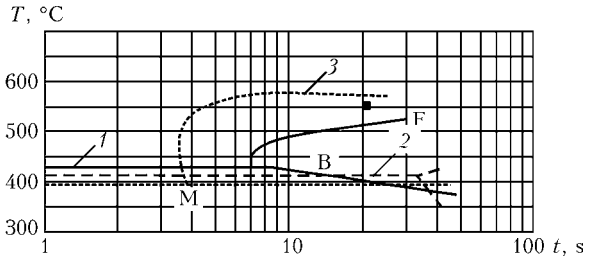

Figure 10. CCT diagrams derived for steel S690QL experimentally at T_{max} = 1350 (*1*), 1100 (*2*) and 950 (*3*) °C

proposed model based on a small number of physically interpretable parameters, allows for the influence of the initial material structure and welding thermal cycle parameters on the behaviour of transformation curves. Use of the developed method together with the transformation diagrams obtained experimentally, expands the possibilities of microstructural analysis and welded joint metal properties.

The authors are grateful to DFG and RFFI for financial support (Grant 04-02-04000-NNIO_a), as well as A. Scharff (SLV-Rostok) for the provided experimental data.

1. (1991) *Atlas of time-temperature diagrams for irons and steels*. Ed. Vander Voort G.F. Materials Park, USA. ASM Int.
2. Seyffarth, P., Meyer, B., Scharff, A. (1992) *Grosser Atlas Schweiss-ZTU-Schaubilder*. Duesseldorf: DVS.
3. Staley, J.T. (1987) Quench factor analysis of aluminium alloys. *Mater. Sci. and Technol.*, **3**, 923–934.
4. Dilthey, U., Trube, St. (1995) *Schweisstechnische Fertigungsverfahren*. Duesseldorf: VDI.
5. Matsuda, H., Bhadeshia, H.K., Avrami, D.H. (2003) Theory for transformation from non-uniform austenite grain structures. *Mater. Sci. and Technol.*, **19**, 1330–1334.
6. Grong, O. (1994) *Metallurgical modelling of welding*. Cambridge: IM.
7. Cahn, J.W. (1956) The kinetic of the grain boundary nucleation reactions. *Acta Metallurg.*, **4**, 449–459.
8. Lifshitz, I.M., Slyozov, V.V. (1961) The kinetics of precipitation from supersaturated solid solutions. *J. Phys. and Chem. Sol.*, **19**, 35–50.
9. Wagner, C. (1961) Theorie der Alterung von Niederschlagen durch Umloesen. *Z. Elektrochemie*, **65**, 581–591.
10. Lyubov, B.Ya (1969) *Kinetic theory of phase transformations*. Moscow: Metallurgiya.
11. Lopota, V., Turichin, G., Valdaitseva, E. et al. (2004) Theoretical investigation and modelling of intermetallic inclusions formation in laser treatment of Al–Mg alloys. *SPIE Proc.*, **5399**, 197–203.
12. Prokhorov, N.N. (1976) *Physical processes in metals during welding*. Vol. 1. Moscow: Metallurgiya.
13. Tikhonov, A.N., Samarsky, A.A. (1977) *Equations of mathematical physics*. Moscow: Nauka.
14. Dilthey, U., Bohm, St., Welters, T. et al. (1998) EBSIM — a simulation tool for electron beam welding. In: *Proc. of CISFEL'98* (Toulon, France, June 15–19, 1998). Paris: Institut de Soudure.
15. Umansky, Ya.S., Skakov, Yu.A. (1978) *Physics of metals*. Moscow: Atomizdat.
16. Adil, G.K., Bhole, S.D. (1992) HAZ hardness and microstructure predictions in arc welded steels. *Can. Met. Quart. J.*, **31**, 151–157.

STRUCTURE CHANGES IN HAZ METAL OF STEEL X60 WELDED JOINTS IN UNDERWATER WELDING

S.Yu. MAKSIMOV[1], **V.S. BUT**[1], **V.G. VASILIEV**[1], **S.M. ZAKHAROV**[2] and **N.V. ZAJTSEVA**[2]
[1]E.O. Paton Electric Welding Institute, NASU, Kiev, Ukraine
[2]G.V. Kurdyumov Institute for Physics of Metals, NASU, Kiev, Ukraine

Phase composition of the HAZ microstructure in welded joints of steel X60, made under the water, was evaluated proceeding from analysis of the diagram of anisothermal transformation of austenite and results of metallographic examination. It is established that at cooling rates characteristic of the conditions of underwater welding, in HAZ martensite structure inevitably develops, which determines brittle nature of a welded joint failure under the impact of external load.

Keywords: underwater welding, low alloy steels, HAZ metal, cooling rate, structure transformations, cold cracks

Low alloy steels of increased strength of X60 type are widely used in construction of pipeline systems due to the complex of their mechanical properties, acceptable corrosion resistance and good weldability [1]. However, despite actuality of using underwater welding in repair of metal structures, which operate under water, weldability of these steels in water environment practically is not studied.

For the purpose of determining possibility of using wet arc welding for imported steel of X60 grade diagram of its anisothermal transformation (CCT) was analyzed, and phase composition and structure of HAZ metal of welded joints made under water were studied using methods of optical and scanning electron microscopy analysis, X-ray structure analysis and durometry.

For performing metallographic studies in the laboratory water pool at the depth of 1 m deposition on plates of X60 steel of 14 mm thickness was carried out using flux-cored wire of ferrite type PPS-AN1 under the following conditions: I_w = 180–200 A, U_a = = 30–32 V, reverse polarity current.

Studies of microhardness showed that in HAZ metal in immediate proximity to the fusion line hardening of metal up to the level of *HV* 280 takes place, i.e. at least 1.5 times in comparison with the base metal in initial state. Coarse-grain martensite structure is observed (size of austenite grains is about 0.1 mm). In these areas of the structure rather big cracks were detected, which were located on the austenite grain boundaries. Character of arrangement of the cracks allows us to assume that their formation is connected with cessation of quick growth of martensite crystals inside austenite grains.

By means of moving away from the fusion line size of martensite grains reduces (similar to welding in the air) and coarse-grain martensite structure is sequentially changed for the structure of more disperse martensite, then bainite, and in HAZ periphery ---- for pearlite. Micro-cracks, which would be potential centers of catastrophic failure, practically are not observed in pearlite structure. By X-ray analysis exclusively lines of BCC-solid solution of iron are registered in HAZ metal, which confirm metallographic data on mainly martensite nature of transformation in steel X60 in welding under water.

Shock bending tests of specimens cut out across a weld in the form of templates without a notch were carried out for the purpose of determining character of a welded joint failure under action of the external load. Failure was initiated in the area of transition from the weld to the base metal. The specimens failed at vary low (6.7–11.6 J / cm^2) values of impact toughness. Such level unambiguously proves presence of failure centers ---- brittle martensite structures, microcracks, etc. formed in welding [2].

Trajectory of a crack development corresponds to the most weakened areas of HAZ metal. Failure is initiated in zone of transition from a deposited metal to the base one, whereby according to the fractogram the failure is of tough nature. Formed under action of external load tough cracks of 0.5–2.0 mm size may be efficient concentrators of stresses and initiate failure of other areas of HAZ metal. Areas, which relate to the main centers of subsequent catastrophic failure, are shown in Figure 1, *a*.

The second characteristic zone of a welded joint failure is a zone with coarse-grain martensite structure. It has exclusively brittle nature of fracture (Figure 1, *b*). Presence of nucleating microcracks in this zone, complex stressed state, and high number of defects in the structure significantly facilitate development of the main crack in it and origination of failure directly in zone of martensite crystals.

On HAZ boundaries and outside it brittle failure is sequentially changed for brittle-tough, and than for purely tough failure.

An important peculiarity of the fractograms is presence of specific microcracks, located at an angle to propagation of the main crack (Figure 1, *c*). Most frequently they occur in areas with bainite structure near HAZ boundaries.

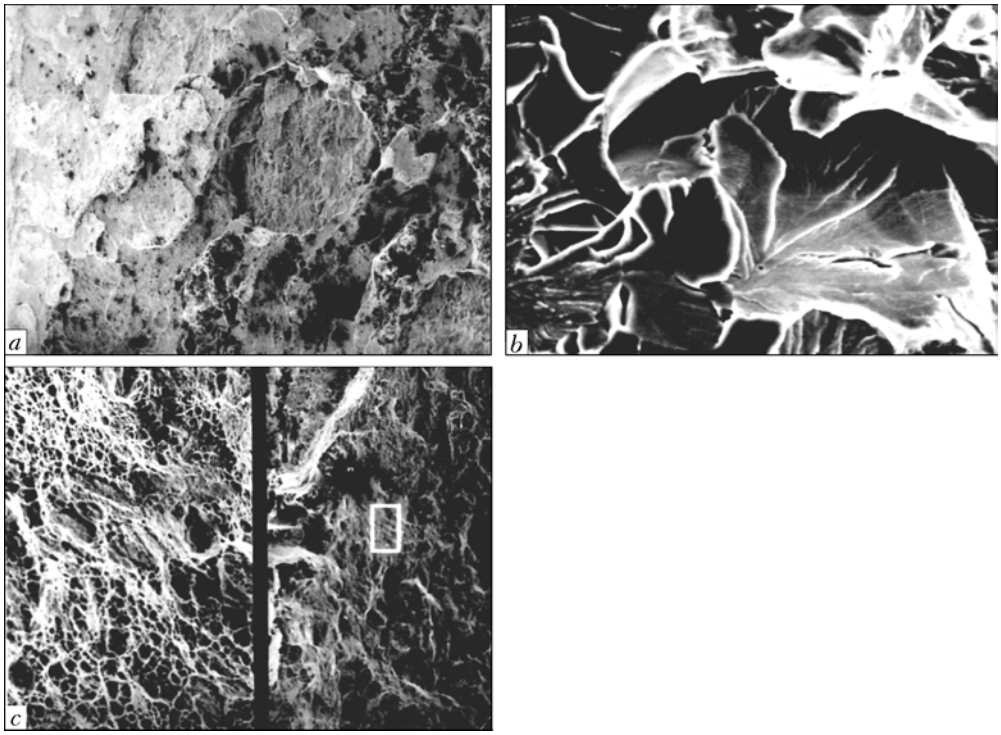

Figure 1. Fractogram of specimen fracture after impact bend tests: *a* — area of main crack origination (×300); *b* — brittle failure in area of coarse-grain martensite in HAZ metal (×3000); *c* — failure in area of bainite structure of HAZ metal (×300)

Metallographic study of the HAZ metal unambiguously proves that conditions of heating and cooling in underwater welding cause principal change of the structure and properties of welded joints in comparison with welding in the air. HAZ size reduces 2–3 times, its hardness increases, hardening structures and cracks are formed, i.e. degradation of the structure and controlled by it mechanical properties takes place. It is evident that degree of degradation of properties of various areas of a welded joint depends upon their phase composition, which is determined, first of all, by maximum temperature of heating and the rate of subsequent cooling, i.e. thermal cycle of welding.

In Figure 2 CCT diagram of steel X60 is shown depending upon cooling rate within the range of 100–0.3 °C / s, the temperature interval being 800–500 °C. Within studied range of cooling rates austenite transformation takes place in martensite, bainite, ferrite, and pearlitee areas. Peculiarity of the diagram is presence of a wide bainite area over the whole range of cooling rates. This proves inevitable formation of this structural component as the main one over a wide range of cooling rates. Even at such insignificant rates as 1.6–0.3 °Ñ / s share of bainite in the structure makes up 60–45 %.

Ferrite and pearlitee transformations are determined by rather narrow areas of the diagram, which proves comparatively low probability of formation of ferrite and pearlitee components under non-equilibrium conditions of HAZ metal structure formation. This fact is confirmed by relatively low share of mentioned components in the final structure: up to 10 % at $w_{8/5}$ = 36–14 °C / s and up to 20 % at $w_{8/5}$ = 5.0–2.7 °C / s. Only at cooling rates below 0.3 °C / s ferrite and pearlitee components occupy a significant volume in HAZ metal (almost half). Characteristic view of the microstructure at various cooling rates is shown in Figure 3.

According to conclusions of [3, 4], steel is considered predisposed to formation of cold cracks in arc welding if content of martensite component in HAZ metal structure exceeds 50 % and integral Vickers

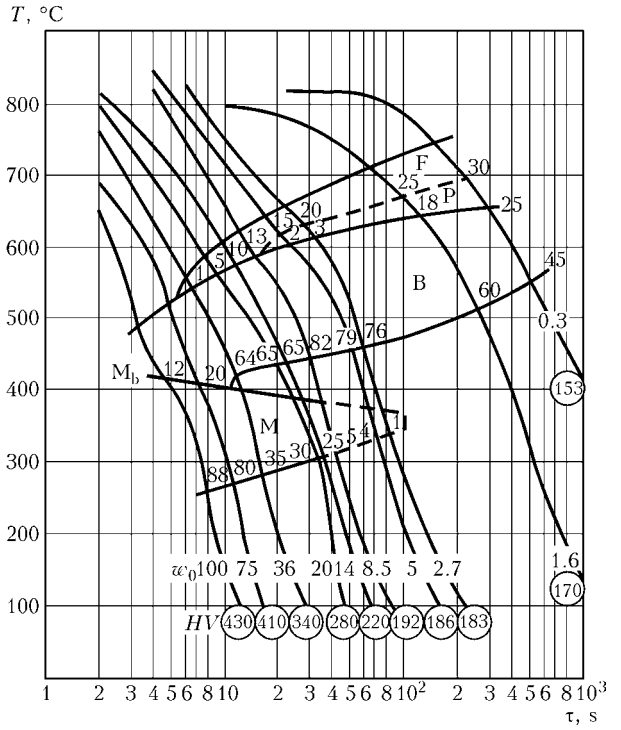

Figure 2. CCT diagram of X60 steel depending upon cooling rate of samples w_0 (°C / s): *HV* — hardness; M — martensite; M_b — beginning of martensite transformation; B — bainite; P — pearlitee; F — ferrite (figures show number of respective structural component)

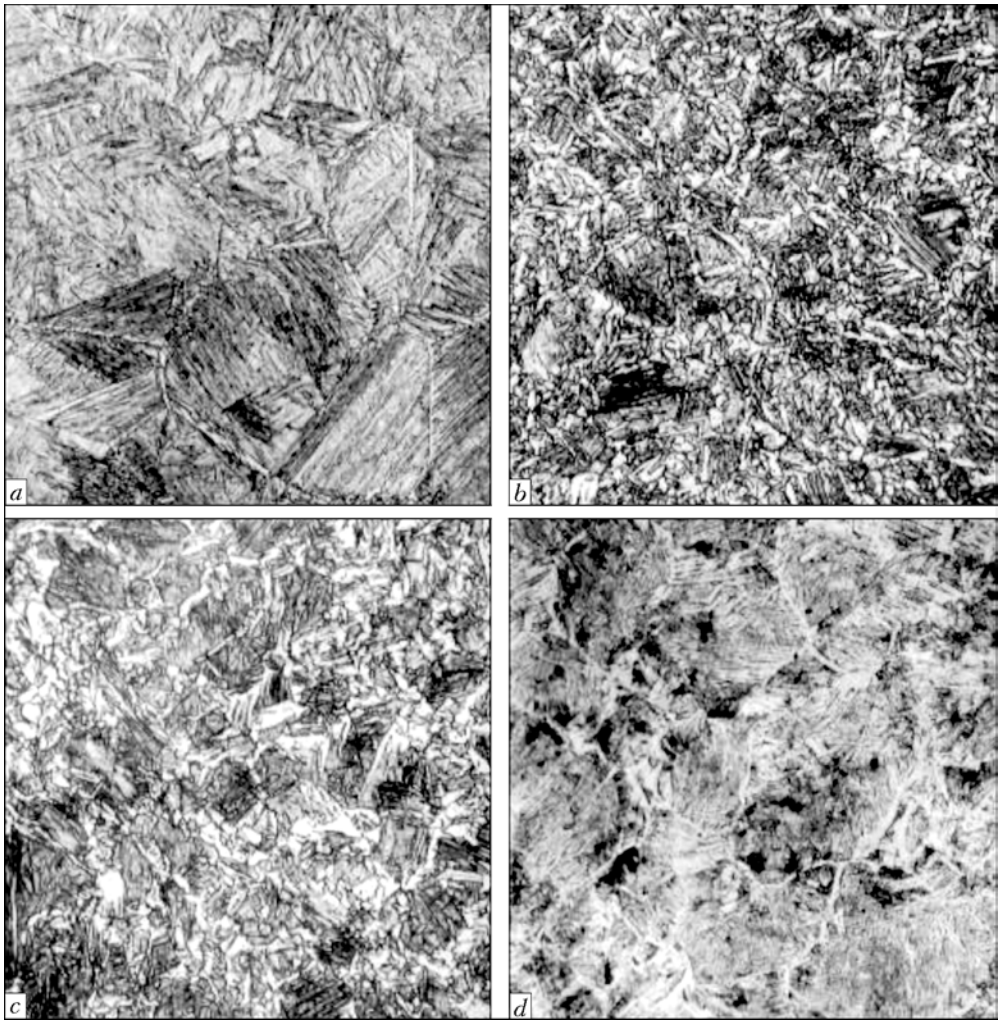

Figure 3. Microstructure of steel of type X60 depending upon cooling rate: *a* — 75; *b* — 20; *c* — 5; *d* — 1.6 °C / s (×320)

hardness in HAZ metal achieves *HV* 350. In Figure 4 dependence of the martensite component share and hardness upon cooling rate is shown within temperature range 800–500 °C obtained on the basis of analysis of the diagram shown in Figure 2. As one can see from the Figure, 50 % martensite form at $w_{8/5}$ > 49 °C / s and hardness is *HV* 350 at $w_{8/5}$ > 41 °C / s. So, one may consider that in welding of real items from steel X60 danger of formation of cold cracks is excluded if cooling rate of the HAZ metal does not exceed 41 °C / s. At cooling rate about 100 °C / s, which is characteristic of welding conditions under water [5], martensite content achieves 88 % and hardness is *HV* 430, which proves high probability of formation of cold cracks.

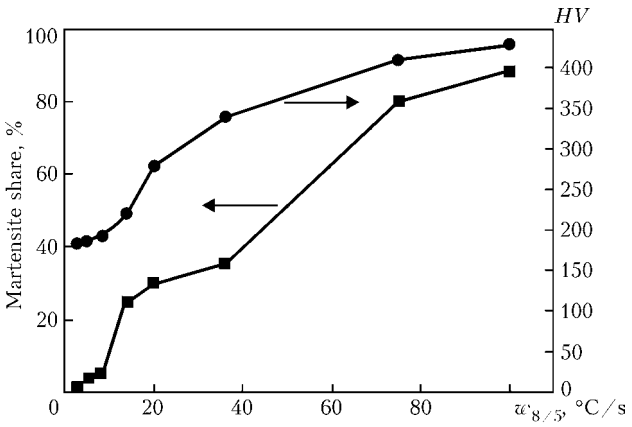

Figure 4. Influence of cooling rate on martensite share in HAZ metal of steel X60 and its hardness

Comparison of the results of performed analysis with metallographic studies allows drawing conclusion that real thermal cycle in underwater welding of steel X60 stipulates risk of crack formation in greater part of the HAZ metal. However, as it was noted above, greater part of nucleating cracks is observed on HAZ boundaries in the areas with bainite structure. It allows us to state that in addition to the thermal factor exists another factor, which affects formation of cracks in HAZ metal. Taking into account conditions of electric arc burning under water, such factor may be considered saturation of the HAZ metal with hydrogen and occurrence, as a result, of hydrogen brittleness [6].

Results of numerical studies of hydrogen redistribution in welded joints made under water [7] prove hydrogen concentration increase in HAZ metal near fusion line. As showed presented above results of metallographic studies, exactly in this zone occurs rather defective martensite structure, which contains significant amount of potential traps for hydrogen, which

diffuses here. Hydrogen, which diffuses into the HAZ metal, fills internal cavities in the metal and gets molar in them in presence of microcracks and other discontinuities and developed interfaces. In case of application of the external tensile load, internal pressure of hydrogen will be added to it and cause growth of a crack, provided stressed state, which corresponds to the conditions of failure according to Griffits theory [8], is formed. Another explanation of metal failure in case of its saturation with hydrogen is also possible, for example on the basis of a theory of plastic strain localization in areas with dissolved hydrogen and failure as a result of inhomogeneous deformation [9].

So, under conditions of wet underwater welding of prone to hardening low alloy steels probability of formation of cold cracks in HAZ metal is very high. Taking into account rather limited possibility of reducing cooling rates as a result of increasing heat input energy in welding, for solution of this problem it is necessary to reduce entry of hydrogen into HAZ metal, which is possible to achieve either by using special technological methods or electrode materials, which would ensure austenite structure of the weld metal.

1. Wegst, C.W. (1995) *Stahlschluessel*. Verlag Stahlschluessel Wegst GMbH.
2. Lukianov, V.F., Naprasnikov, V.V. (1983) Influence of fracture initiation type on crack propagation in welded joints. *Svarochn. Proizvodstvo*, **5**, 3–5.
3. Makarov, E.L. (1981) *Cold cracks in welding of alloy steels*. Moscow: Mashinostroenie.
4. Seferian, D. (1963) *Metallurgy of welding*. Moscow: Mashgiz.
5. Chigarev, V.V., Ustinov, A.V. (2000) Design-experimental estimation of the possibility of reduction of the HAZ metal cooling rate in wet underwater welding. *The Paton Welding J.*, **5**, 24–29.
6. Morozov, A.N. (1980) *Hydrogen and nitrogen in steel*. Moscow: Metallurgiya.
7. Makhnenko, V.I., Maksimov, S.Yu., Korolyova, T.V. (2004) Investigation of peculiarities of transport of hydrogen in underwater fusion welding of structural steels. *The Paton Welding J.*, **1**, 11–21.
8. Banmann, H., Behrens, U., Bethe, K. (1980) Analysis of hydrogen in solids. In: *Proc. of 7th Div. Conf. on Nucl. Phys. Meth. Mater. Res.* (Darmstadt, Sept. 23–26, 1980). Weisbaden.
9. Gavriljuk, V.G., Shivanjuk, V.N., Foct, J. (2003) Diagnostic experimental results on the hydrogen embrittlement of the austenitic steel. *Acta Material.*, **51**, 1293–1305.

EFFECT OF SCANDIUM ADDITIONS ON FINE STRUCTURE OF WELD METAL IN ALUMINIUM ALLOY 1460 WELDED JOINTS

L.I. MARKASHOVA, G.M. GRIGORENKO, A.Ya. ISHCHENKO, A.V. LOZOVSKAYA and **O.S. KUSHNARYOVA**
E.O. Paton Electric Welding Institute, NASU, Kiev, Ukraine

Peculiarities of structure-phase condition of metal of the welds and welded joints made on alloy 1460 by argon-arc welding using standard filler wire Sv1201 and experimental wire 1201 with an addition of scandium were studied by transmission electron microscopy. Main structural changes caused by adding scandium are characterised by grain refining, increase in volume density of dislocations, formation of fine inclusions containing scandium, and activation of solid solution decomposition processes.

Keywords: arc welding, aluminium alloy, scandium alloying, weld metal, fine structure, phase precipitates, eutectic, dislocation density

Almost all properties of any materials are known to be determined primarily by their structure-phase condition: chemical composition, presence of impurities, grain size and different types of phase precipitates. This information can be generated from examinations conducted at different structural and scale levels, i.e. grain, sub-grain and dislocation [1–3].

Unfortunately, not all of the required data on structure of materials can be generated using such widely available and express examination methods as optical metallography and scanning electron microscopy. Important structural parameters relating to the sub-grain and dislocation levels of examinations, which reflect the real picture of the condition of a material, can be revealed only by direct methods of analysis of fine foils using transmission electron microscopy. Moreover, locality of the method allows direct analysis of the presence and distribution of structural and phase changes in any zone of an object being examined, revealing of regions of internal stress concentrations, and determination of causes of their formation [4–7].

Such examinations are of special interest in terms of investigation of structural peculiarities of aluminium alloys with scandium additions, as these alloys are reportedly [8] characterised by a complex structure-phase composition and diversity of different types of phase precipitates. Some researchers [9] consider changes in size, morphology and distribution of the latter to be the decisive factor ensuring a number of the required properties of materials. Investigations of welded joints in this respect are particularly topical, as microstructure of the weld and HAZ metals becomes much more complex due to their non-equilibrium structure-phase condition.

The purpose of this study was to investigate peculiarities of structure-phase condition of metal in the bulk of grains and at the grain boundaries between eutectics, as well to reveal sizes and distributions of phases formed in different regions of the weld metal in argon-arc welding of alloy 1460 using standard Sv1201 and experimental 1201 + Sc filler wires.

Examined was the central zone of metal of the welded joints on aluminium alloy 1460 (Al–3 % Cu–2 % Li–0.08 % Sc), produced by using standard Sv1201 (Al–6.5 % Cu–0.25 % Zr–0.3 % Mn) and experimental 1201 (Al–6.5 % Cu–0.25 % Zr–0.3 % Mn) + 0.5 % Sc filler wires.

To examine structure of the weld metal, thin foils were prepared by preliminary mechanical grinding, electrolytic polishing in acetic-chloric electrolyte, followed by multiple ion thinning with ionised argon flows in a specially developed unit [10]. Examinations of the prepared foils were carried out using the JEOL transmission electron microscope JEM-200CX at an accelerated voltage of 200 kV.

Structure of the weld metal in the as-welded condition produced by argon-arc welding of alloy 1460 using filler wire Sv1201 (without scandium) is characterised, first of all, by a uniform distribution of dislocations at a minimum density of crystalline lattice defects, equal to $\rho \cong (2–5)\cdot 10^9$ cm^{-2}. In this case the individual extended dislocations, featuring the absence of local clusters and interactions, as well as individual slip systems (Figure 1, *a–d*), are formed.

As to phase precipitates in the weld metal, they can be conditionally subdivided in size *d* into two groups: coarse (from 1.3–1.5 to 3.0 μm) (Figure 1, *f*, *g*) and less coarse ($d \cong 1$ μm) (Figure 1, *e*). It can be seen from the Figure that relatively fine precipitates have a composite structure and consist of the Al–Li phase (inside the phase precipitates) bordered with the Al–Cu phase (Figure 1, *e*). Coarser precipitates are mostly conglomerates of phase constituents (blocks), having different sizes and compositions. In Figure 1, *f*, light blocks ($d \cong 0.15–0.30$ μm) correspond to the Al–Li phase, and blocks with a darker contrast correspond to the Al–Cu phase.

There are cases where such inclusions have a complex composite structure as well. However, they are

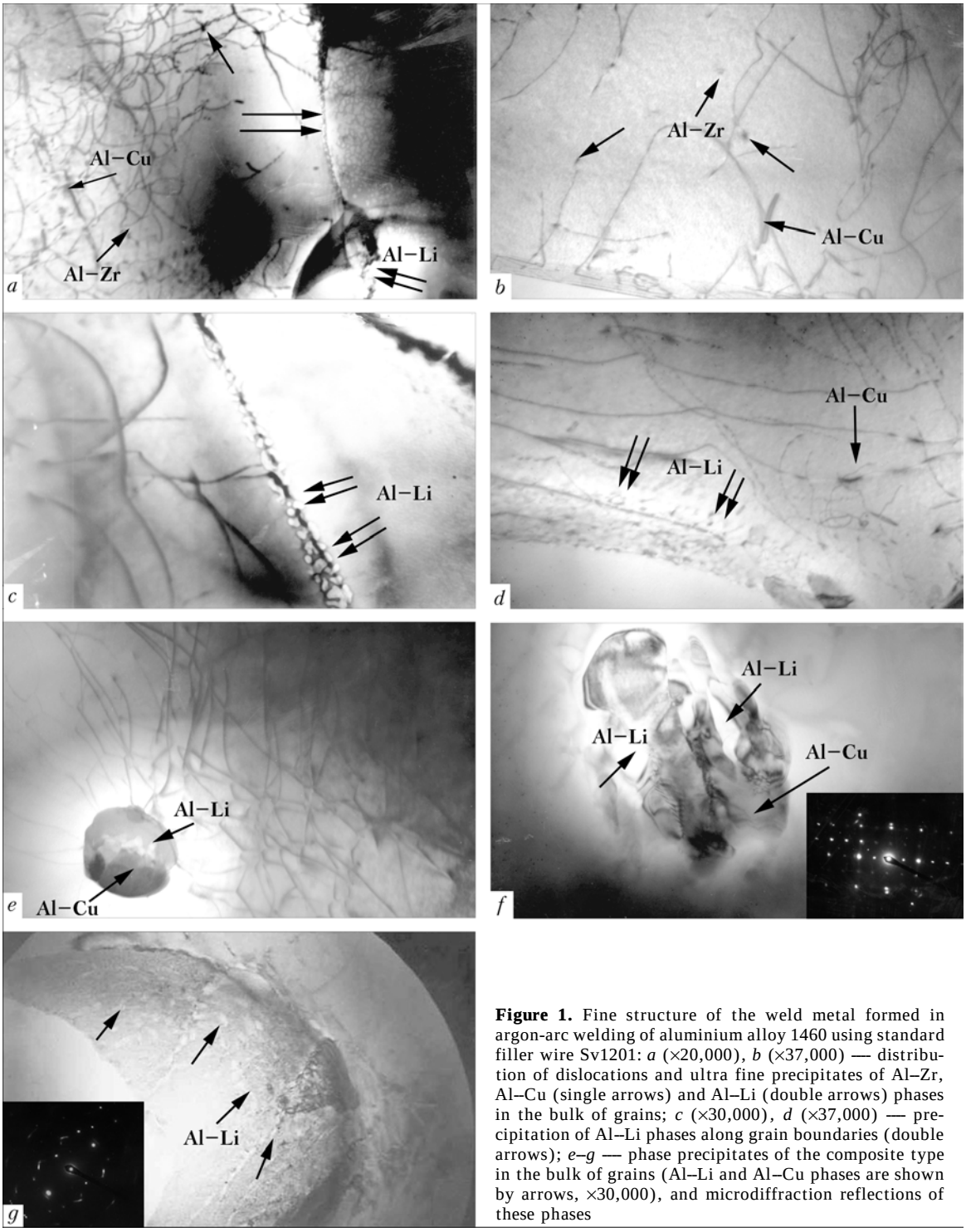

Figure 1. Fine structure of the weld metal formed in argon-arc welding of aluminium alloy 1460 using standard filler wire Sv1201: *a* (×20,000), *b* (×37,000) — distribution of dislocations and ultra fine precipitates of Al–Zr, Al–Cu (single arrows) and Al–Li (double arrows) phases in the bulk of grains; *c* (×30,000), *d* (×37,000) — precipitation of Al–Li phases along grain boundaries (double arrows); *e*–*g* — phase precipitates of the composite type in the bulk of grains (Al–Li and Al–Cu phases are shown by arrows, ×30,000), and microdiffraction reflections of these phases

saturated with very fine Al–Li phases ($d \cong 0.03$–0.07 μm) (Figure 1, *g*), rather than consist of the blocks.

The other group of the phases formed in the bulk of grains includes phases of an ultra fine size ($d \cong \cong 0.02$–0.03 μm). Some of them are characterised primarily by a globular shape and dark contrast (Figure 1, *a*, *b*). As a rule, they are not related to a specific location of dislocations. Zirconium phases are one of the examples of this type. Ultra fine rod-shaped phases 0.10–0.15 μm in size can also be seen. As a rule, they are formed at individual crystalline lattice defects and their clusters. In Figure 1, *a*, *b*, *d*, these phase precipitates have the form of thick dark strokes at individual dislocations. In addition, the Al–Li phases ($d \cong 0.01$–0.03 μm) can also be seen in the bulk of grains, having a lighter contrast (marked by double arrows in Figure 1, *a*) against a background of the matrix grains.

Grain boundaries, as well as sub-grain boundaries, are characterised primarily by an equilibrium dislocation structure (Figure 1, *a*, *c*, *d*). It should be noted, however, that the grain boundaries are regions of active local nucleation of a chain of lithium phases with

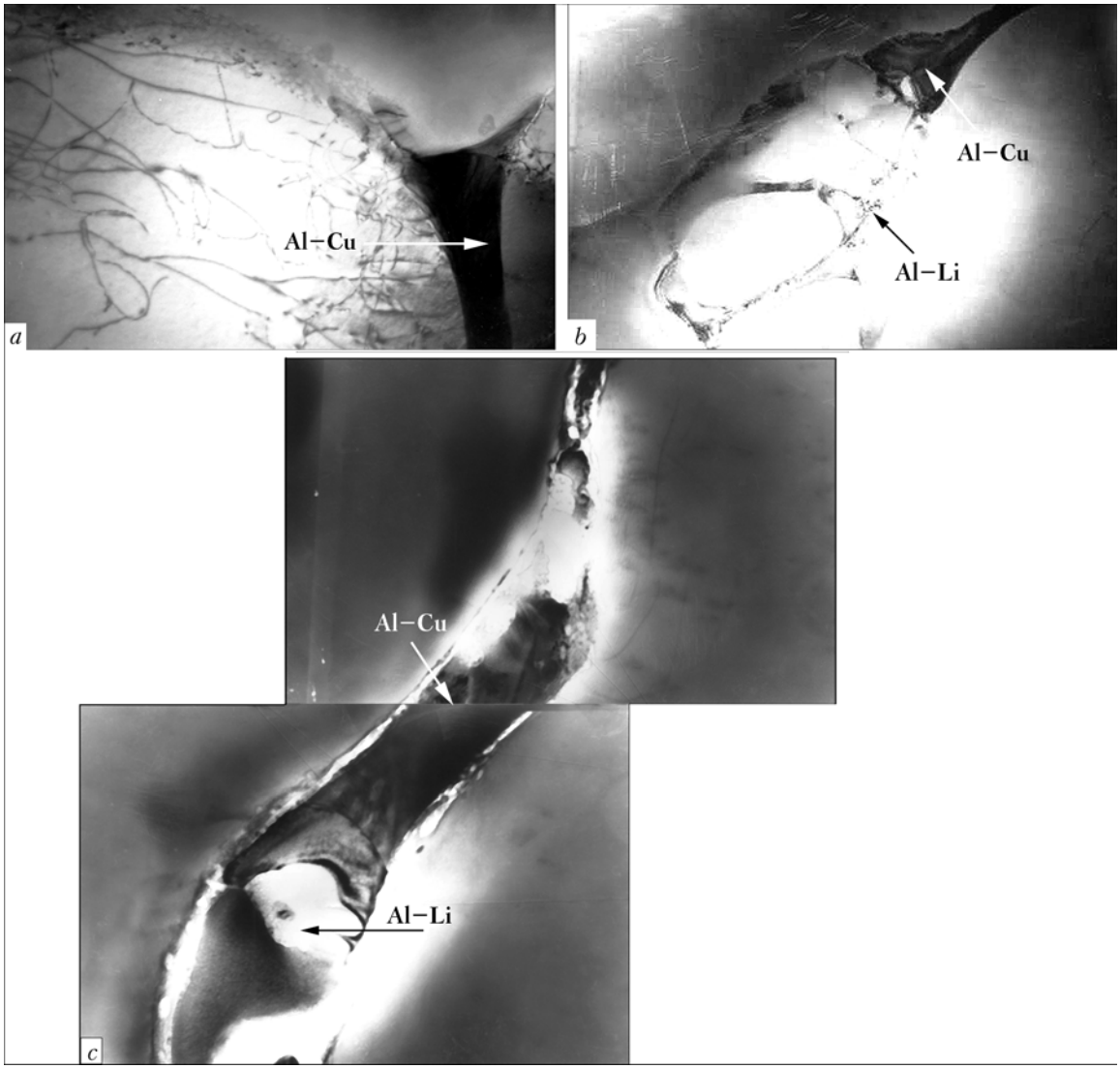

Figure 2. Microstructure of the weld metal produced by argon-arc welding using filler wire Sv1201 (arrows show phase constituents of grain-boundary eutectics): *a* (×30,000) — continuous formations of Al–Cu phases; *b* (×15,000), *c* (×30,000) — conglomerates of Al–Cu and Al–Li phases

$d \cong 0.03$–0.17 μm. Formation of rather wide ($d \cong 0.3$–0.4 μm) interlayers consisting of the lithium phase clusters (Figure 1, *c*) can be seen in some boundary zones in regions with a higher density of dislocations and dislocation loops.

Other characteristic structural elements of the weld metal containing no scandium are grain-boundary eutectic interlayers, the general view and more detailed image of which are shown in Figure 2. As seen from the Figure, the eutectic interlayers are either continuous formations of the Al–Cu phases (Figure 2, *a*) or conglomerates of the Al–Cu (having a dark contrast) and Al–Li (with characteristic light contrast) phases (Figure 2, *b, c*).

Analysis of phase components of the weld metal shows that coarse intragranular phase precipitates are a conglomerate of phases (see Figure 1, *e, f*), similar in composition and morphology to the eutectic precipitates formed along the grain boundaries. However, unlike the grain-boundary eutectics, the intragranular phases have an isolated shape and, as already noted, are located in the bulk of grains.

Microstructure of the weld metal on aluminium alloy 1460 produced by argon-arc welding using the filler wire with an addition of 0.5 % Sc, is characterised by the following. First of all, the weld metal features a high and irregular density of crystalline lattice defects, i.e. linear dislocations and dislocation loops. The dislocation density ranges from $6 \cdot 10^9$ to $(5$–$6) \cdot 10^{10}$ cm^{-2}. Active dislocation slip and interaction of dislocations, showing up as formation of dislocation walls and networks, as well as sub-structural elements of different types, cells, blocks and sub-grains (Figure 3, *a*–*c*), take place in this case. Considerable part of dislocation lines is decorated with segregations of chemical elements and fine phase formations.

Based on the type of microdiffraction reflections, at which slight satellite reflexes can be seen directly near the main reflexes (Figure 3, *c*), it can be concluded that the processes of formation of pre-phase precipitates, coherent with the matrix, occur in the weld metal. Phases with a globular (Al_3Zr) and rod-like (Al_2Cu) shape (Figure 3, *a, c*) are also formed. Chains of the Al–Li phases (Figure 3, *d*) and inter-

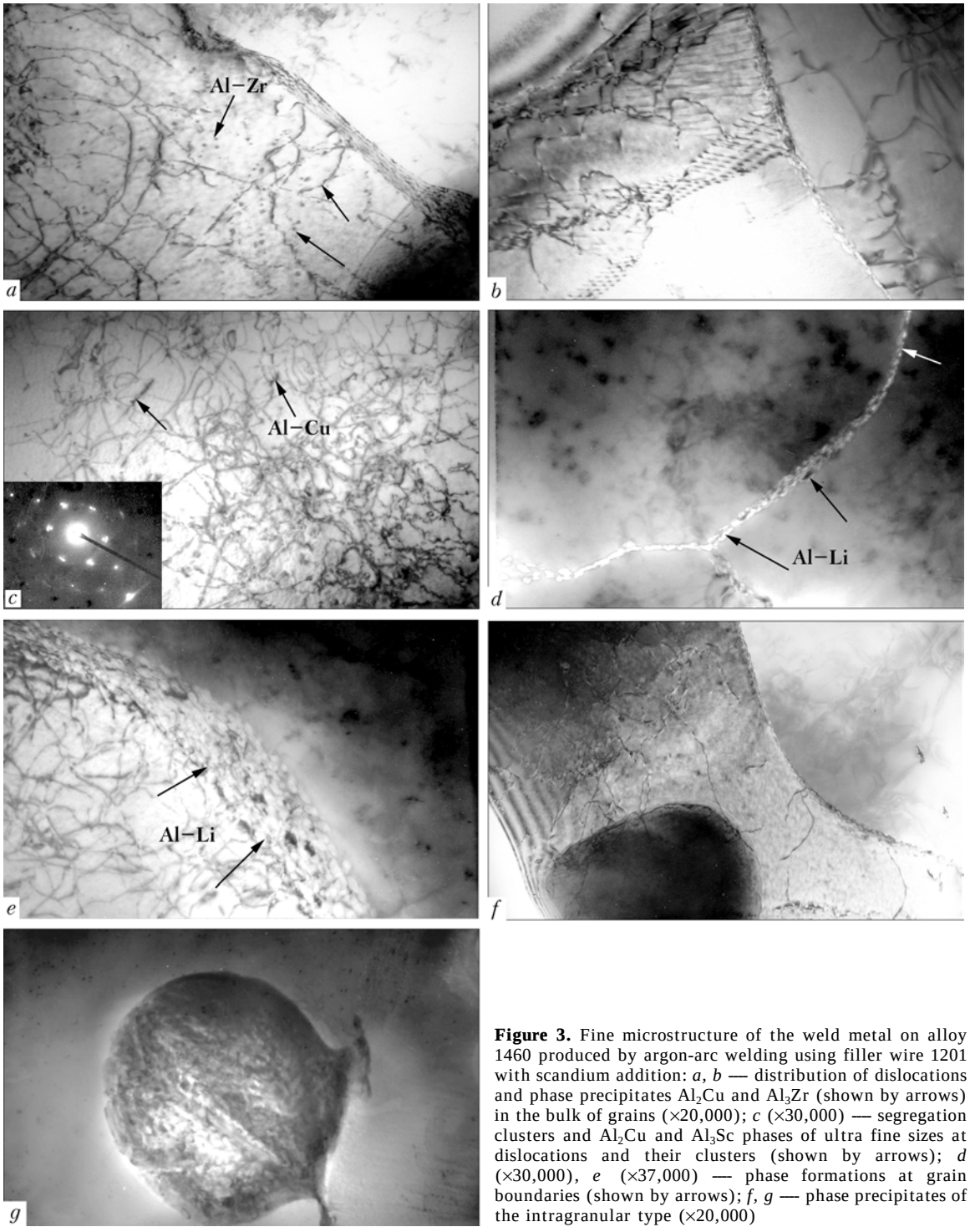

Figure 3. Fine microstructure of the weld metal on alloy 1460 produced by argon-arc welding using filler wire 1201 with scandium addition: *a*, *b* — distribution of dislocations and phase precipitates Al_2Cu and Al_3Zr (shown by arrows) in the bulk of grains (×20,000); *c* (×30,000) — segregation clusters and Al_2Cu and Al_3Sc phases of ultra fine sizes at dislocations and their clusters (shown by arrows); *d* (×30,000), *e* (×37,000) — phase formations at grain boundaries (shown by arrows); *f*, *g* — phase precipitates of the intragranular type (×20,000)

layers consisting of dense clusters of the Al–Li particles (Figure 3, *e*) can be seen at the grain boundaries. The above clusters are similar to phases formed in the case of filler wire containing no scandium.

With scandium additions, inclusions of the other type, i.e. phases Al_2Cu and Al_3Sc, characterised by a pronounced dark contrast (Figure 3, *c*–*e*), are formed in the zone of concentration of the Al–Li phases. Coarse phase precipitates (d > 2 μm) mostly of the intragranular type can also be seen. In some cases they are comparably homogeneous in composition (Figure 3, *f*), while in other cases they may consist of a mixture of the Li-containing phases of different sizes, including very fine ones ($d \cong 0.05$–0.10 μm) (Figure 3, *g*).

There are substantial differences also in the character of eutectic formations in the weld metal produced by adding scandium to the filler wire. As seen from Figure 4, in the case of adding scandium the boundary eutectic precipitates are characterised by heterogeneity of structure, morphology and, as noted above, chemical and phase compositions, i.e. along with dense, monolithic and massive formations of a composite structure (Figure 4, *a*, *b*) there are also the «loose» eutectics with fine inclusions of phases of a different contrast (Figure 4, *c*, *d*).

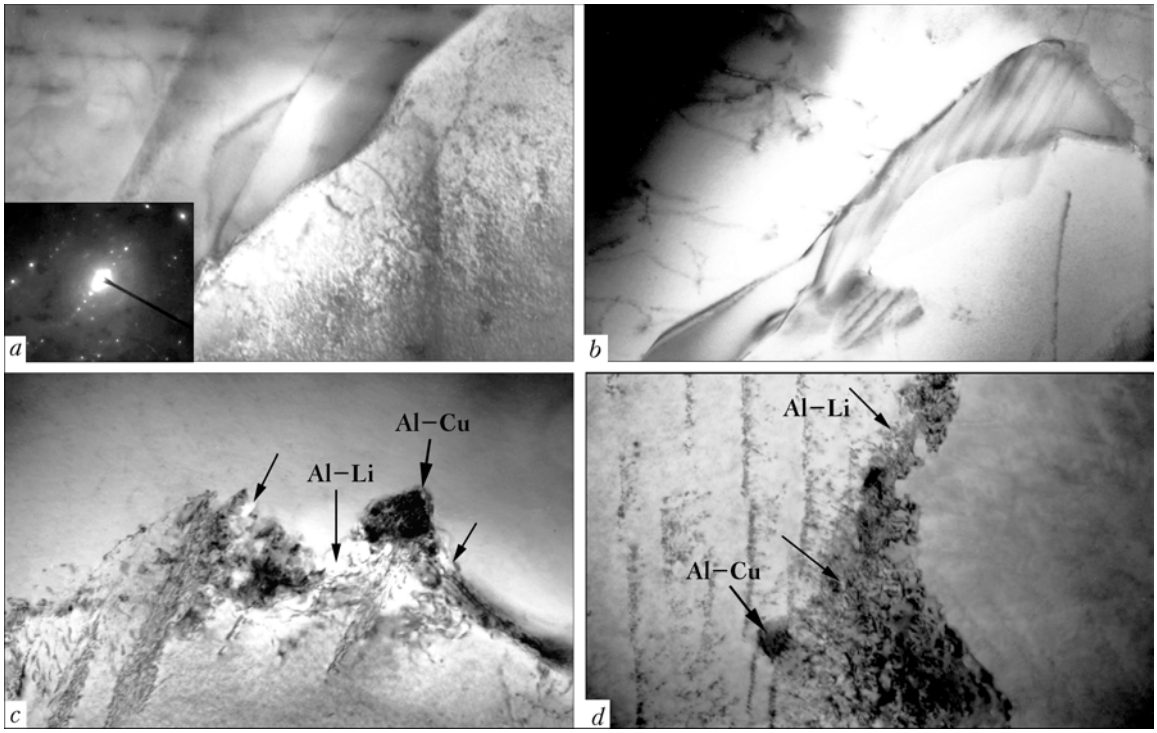

Figure 4. Microstructure of the weld metal on alloy 1460 produced by argon-arc welding using filler wire 1201 with addition of scandium: *a*, *b* — monolithic eutectics (×30,000); *c* (×30,000), *d* (×37,000) — loose eutectics in the form of clusters of phases of different sizes, mostly of the Al–Li and Al–Cu composition (shown by arrows)

Structure of the first type of the eutectics (consisting of dense, monolithic and massive phase formations) more than 1.5 μm thick is shown in Figure 4, *a*, *b*. Eutectic with a laminated structure, where the layers are about 0.03–0.10 μm thick, is well seen in Figure 4, *b*. Darker copper-rich layers of the eutectic alternate with Li-rich zones of a lighter contrast.

Structure of the dense eutectics having the Al_2Cu composition in their central part, enveloped with the Al–Li phase (of a lighter contrast), is also shown in Figure 5, *a*. It is noteworthy that the eutectics of this composite type are bordered on their contour with fine precipitates ($d \cong 0.01$–0.03 μm) containing scandium.

The second type of the eutectics having a loose structure is a cluster of fine (from 0.03–0.07 to 0.13 μm) Al–Cu and Al–Li phases (see Figure 4, *c*, *d*).

However, the most notable peculiarity of the weld metal in the case of using the Sc-containing filler wire is the formation of structures related to the processes of beginning of solid solution decomposition (see Figure 5). These processes are most pronounced in the zones with specific structural states, i.e. along the dislocation slip systems (Figure 5, *a*–*e*, *g*, *h*), in regions of grain and low-angle boundaries (Figure 5, *b*, *e*, *f*), and regions of concentration of the crystalline lattice defects. These zones, as a rule, are characterised by formation of special structures [11] of the Guinier-Preston (GP) type, having the form of dense segregation clusters at a high density of dislocation loops (Figure 5, *d*, *h*). It should be noted that fine scandium precipitates (Figure 5, *g*, *h*) are present in all the regions where solid solution decomposition takes place, which is proved by microdiffraction reflections of the examined regions.

As seen from the results of transmission electron microscopy examinations of fine structure, welding using filler wire with a 0.5 % Sc addition causes very important changes in the structure-phase condition of the weld metal, including refining of grain and subgrain (this corresponding to the obtained data [8, 9]), as well as increase in volume dislocation density, activation of the processes of solid solution decomposition and eutectic formation. This is accompanied by the formation of local segregations of chemical elements and ultra fine phases in regions of the grain boundaries along the individual dislocations and their clusters. The noted changes in structure and phase composition of the weld metal in the welding zone allow a scientific substantiation of positive effects associated with improvement of weldability and mechanical properties of welded joints on the advanced high-strength material for aerospace engineering application [12].

1. Bernshtejn, M.L. (1965) *Mechanisms of strengthening of solids*. Moscow: Metallurgiya.
2. Eshbi, I.F. (1972) About Orowan stress. In: *Physics of strength and ductility*. Moscow: Metallurgiya.
3. Honeycomb, R. (1972) *Plastic deformation of metals*. Moscow: Mir.
4. Kosik, J., Abson, D.J., Jonas, J.J. (1971) Strengthening effect of hotwork subgrains at room temperature. *J. Iron and Steel Inst.*, 209(**8**), 624–629.
5. Embury, J.D. (1982) Ductile fracture, strength of metals and alloys (ICSMA6). In: *Proc. of 6th Int. Conf.* (Melbourne, Aug. 16–20, 1982). Vol. 3. Melbourne.
6. Ivanova, V.S., Gordienko, L.K., Geminov, V.N. et al. (1965) *Role of dislocations in strengthening and fracture of metals*. Moscow: Nauka.
7. Gordienko, L.K. (1973) *Substructural strengthening of metals and alloys*. Moscow: Nauka.
8. Berezina, A.L., Kolobnev, N.I., Molebny, O.A. (2001) Effect of Sc and Zr on structure and properties of Al–Cu–Li

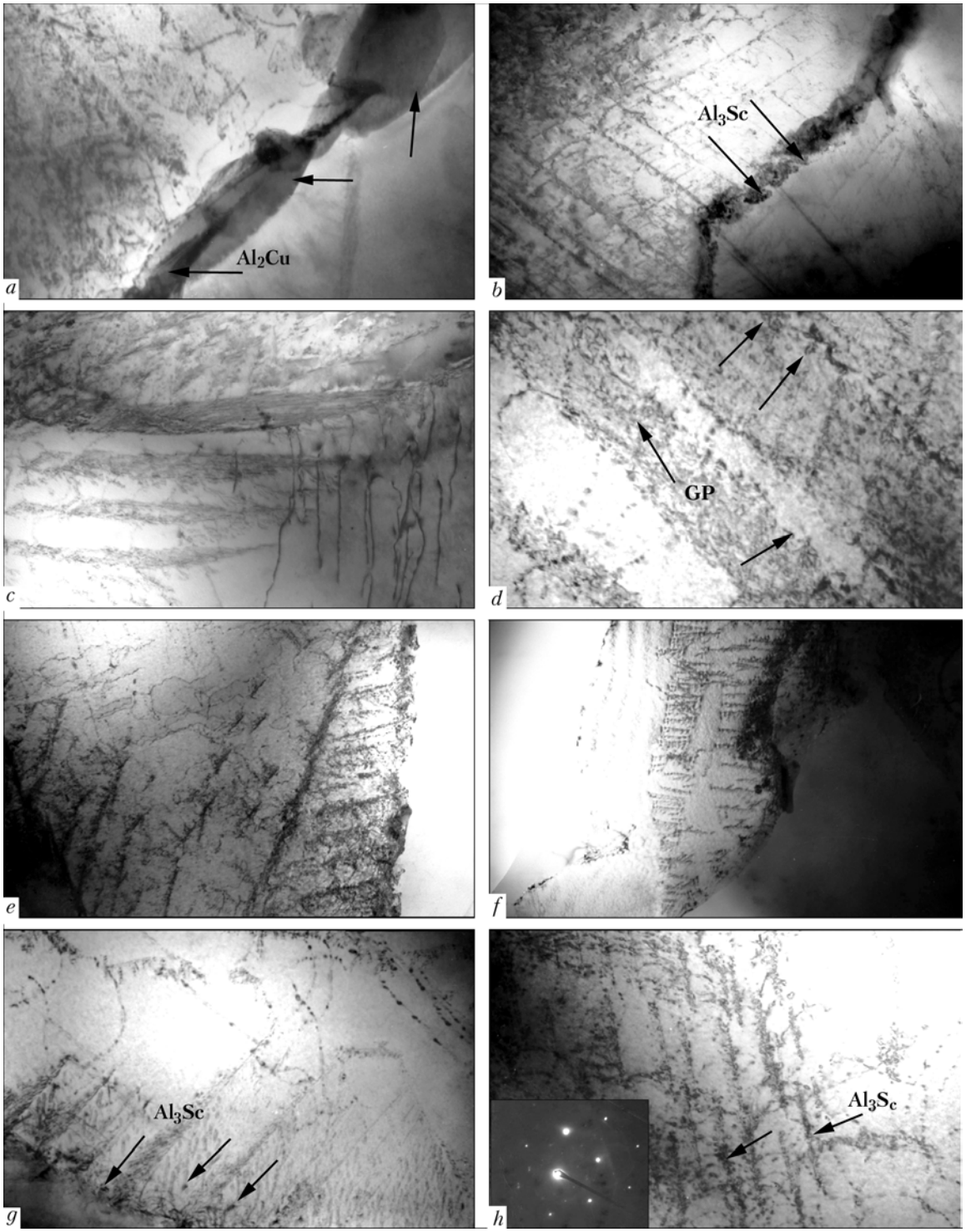

Figure 5. Grain-boundary precipitates and structural elements of decomposition of solid solution in the weld metal produced by argon-arc welding of alloy 1460 using filler wire 1201 + Sc: *a* (×37,000), *b* (×20,000) — segregation and phase precipitates in grain-boundary zones of the weld metal (phases Al_3Sc and Al_2Cu are shown by arrows); *c* (×20,000) — character of decomposition in the zones of propagation of slip systems; *d* (×50,000) — formation of structures of the GP zone type (shown by arrows); *e*, *f* — formation of sub-grains (×15,000); *g*, *h* — ultra fine precipitates of Al_3Sc phases (shown by arrows) at dislocation loops, individual dislocations and their clusters (×30,000)

alloys depending on copper concentration. *Metallofiz. Nov. Tekhnologii*, 23(**11**), 1531–1539.
9. Berezina, A.L., Shmidt, U., Monastyrskaya, T.A. et al. (2002) Structural transformations in rapidly quenched binary Al–Sc alloys. *Ibid.*, 24(**2**), 221–234.
10. Darovsky, Yu.F., Markashova, L.I., Abramov, N.P. et al. (1985) Method of preparation for electron microscopy analysis. *Avtomatich. Svarka*, **12**, 60.
11. Dumolt, S.D., Laflin, D.E., Williams, J.K. (1984) *Influence of welding on microstructure of heat-treated alloy 2219*. Kiev: Naukova Dumka.
12. Ishchenko, A.Ya. (2004) Peculiarities of application of high-strength aluminium alloys for welded structures. *The Paton Welding J.*, **9**, 15–25.

IMPROVEMENT OF WELD STRENGTH IN ARC WELDING OF Al–Cu ALLOYS WITH APPLICATION OF Sc-CONTAINING FILLERS

A.G. POKLYATSKY, A.V. LOZOVSKAYA, A.A. GRINYUK, M.R. YAVORSKAYA and **A.A. CHAJKA**
E.O. Paton Electric Welding Institute, NASU, Kiev, Ukraine

Comparative analysis of mechanical properties of deposited metal produced by using filler wires of Sv1201 type with different content of copper and scandium has been performed. It is shown that addition of 0.5 % Sc to welding wires creates prerequisites for an extra increase in tensile strength and proof stress of the welds. Methods are suggested to provide an extra increase of the strength of welded joints and weld metal directly during the welding process by passing current through a section of the filler and using postweld heat treatment by a special mode.

Keywords: arc welding, aluminium-copper alloys, scandium-containing fillers, welded joints, filler wire preheating, quenching, heat treatment, mechanical properties

Alloys 1201 (Al–6.3Cu–0.3Mn–0.06Ti–0.17Zr–0.1V) and 1460 (Al–3Cu–2Li–0.1Mg–0.12Ti–0.08Sc) are the most widely accepted of the high-strength Al–Cu alloys in various mechanical engineering industries for welded structure fabrication. After full heat treatment (quenching + artificial ageing) the sheet rolled stock of these alloys has rather high mechanical properties (Table 1). Their welding is performed using batch-produced Sv1201 wire, close to the respective base metal in its composition. However, the heat of arc welding leads to softening of these alloys, and the strength of welded joints, similar to the cast metal of welds, becomes much lower than that of the base metal [1].

One of the effective methods of strengthening aluminium alloy welds is application of Sc-alloyed wires in welding [2–5]. However, in the presence of copper in the weld pool, which comes from the base metal or filler wire, scandium behaviour remained unknown. At certain proportion of these elements in the alloy, copper can interact with scandium, significantly lowering the effectiveness of its application [6].

In this study evaluation of mechanical characteristics was performed for welded joints produced by arc welding of alloys 1201 and 1460, when using welding wires with different content of copper and scandium additives. Rationality of applying scandium in filler wires of Al–Cu system, containing from 3 to 6 % Cu, was evaluated first on cast metal, produced at three-layer deposition of beads on a 6 mm sheet of alloy 1201.

Deposition by non-consumable electrode argon-arc welding was conducted at the speed of 12 m / h in AS-TV-2M unit with power supply from MW-450 source. The first layer consisted of three welds made at 250 A current at the feed rate of 125 m / h with 1.6 mm filler wire. The second layer was made with two welds in the same modes, and the third ---- by one weld at 270 A current.

After making each weld, the plate cooled down to room temperature, and the metal surface was scraped bright mechanically before deposition of the next bead.

The tensile strength and ductility of the welds were evaluated at tension of round samples, cut out of the upper layers of the deposited metal to eliminate the influence of alloying elements of the substrate metal. Results of mechanical testing of samples cut out of the deposited metal in the longitudinal direction are given in Table 2.

Table 1. Mechanical properties of Al–Cu alloys

Alloy grade	Metal thickness, mm	Tensile strength σ_t, MPa	Proof stress $\sigma_{0.2}$, MPa	Relative elongation δ, %	Impact toughness a_n, J / cm^2	Bend angle α, deg
1201	6	436.2–435.1 / 435.7	353.8–353.4 / 353.6	9.6–9.5 / 9.6	8.9–8.6 / 8.8	30–28 / 29
1460	3	586.4–556.5 / 573.6	546.5–508.0 / 532.2	3.9–2.9 / 3.5	2.6–2.2 / 2.4	20–16 / 17
	6	514.4–509.3 / 511.7	467.7–460.1 / 463.8	4.6–4.4 / 4.5	4.3–3.7 / 4.0	29–26 / 28

Notes. 1. Samples for mechanical testing were cut out along the rolling direction. 2. Here and further on the numerator gives the maximum and minimum, and the denominator the average values by the results of testing 2–5 samples.

Table 2. Mechanical properties of deposited metal produced by TIG welding using filler wires with different content of copper and scandium

Content of alloying elements in the filler, %	As-welded		After artificial ageing (170 °C, 16 h)		After quenching in water (525 °C, 5 min) and artificial ageing (170 °C, 16 h)	
	Tensile strength σ_t, MPa	Proof stress $\sigma_{0.2}$, MPa	Tensile strength σ_t, MPa	Proof stress $\sigma_{0.2}$, MPa	Tensile strength σ_t, MPa	Proof stress $\sigma_{0.2}$, MPa
6Cu	258.5–231.8 / 245.5	174.4–165.2 / 171.2	300.3–264.1 / 281.3	252.7–238.4 / 245.8	315.1–311.2 / 314.6	275.1–268.7 / 272.6
6Cu–0.2Sc	264.6–251.6 / 258.1	175.9–173.7 / 174.8	288.9–281.7 / 285.3	249.8–247.4 / 248.6	326.3–314.4 / 320.4	279.6–274.8 / 277.2
6Cu–0.5Sc	299.7–287.8 / 289.4	281.8–247.9 / 260.9	319.8–304.1 / 314.0	262.2–258.6 / 261.6	344.5–342.6 / 343.3	286.4–277.4 / 280.7
5Cu–0.2Sc	212.5–186.5 / 199.5	147.6–143.1 / 145.4	256.7–224.1 / 240.4	223.4–220.7 / 222.1	310.3–309.9 / 310.2	272.3–246.9 / 259.6
5Cu–0.5Sc	254.8–242.5 / 248.7	171.3–168.1 / 169.7	272.1–269.8 / 271.0	246.3–243.6 / 244.2	--	--
3Cu–0.2Sc	197.3–178.9 / 188.1	125.4–118.0 / 121.7	223.1–212.0 / 217.6	167.3–165.8 / 166.6	268.0–257.8 / 262.9	212.5–207.5 / 210.0
3Cu–0.5Sc	231.8–220.8 / 226.3	157.6–152.3 / 155.0	263.5–254.8 / 259.2	219.6–207.3 / 214.0	278.9–275.1 / 277.0	235.2–232.7 / 234.0

Addition of 0.5 % Sc to Sv1201 filler allowed increasing the deposited metal ultimate strength by 18 %, and proof stress by 52 %. At subsequent artificial ageing of the samples the strength of the metal of welds deposited with this filler, also remains higher (by 12 %). Full postweld heat treatment of the welds, including their quenching in a special mode, and artificial ageing, allows preserving the strengthening effect, achieved due to the main alloying component, namely copper, and further increasing the strength due to scandium. When filler wires with a lower copper content were used, a directly proportional dependence between the ultimate strength and ductility, on the one hand, and scandium percentage in the filler, on the other hand, is also found. Thus, the obtained data are indicative of the rationality of applying the Sc-containing fillers in argon-arc welding of Al–Cu alloys, in which copper concentration varies in the range of 3–6 %.

To determine the influence of additives of 0.5 % Sc on the mechanical properties of the actual butt joints, 6 mm sheets of alloys 1201 and 1460 were joined by consumable-electrode (MIG) and nonconsumable electrode (TIG) argon-arc welding. Table 3 gives the results of mechanical testing of flat samples cut out of the produced joints.

When the nonconsumable electrode was used for welding 6 mm sheets, the filler wire composition did not have any significant influence on welded joint strength. Samples with a reinforcement failed at ten-

Table 3. Mechanical properties of welded joints of 6 mm sheets of alloys 1201 and 1460

Alloy grade	Filler grade	Welding process	Tensile strength σ_t, MPa		Impact toughness of weld metal a_n, J / cm^2
			Welded joint σ_t^w	Weld metal $\sigma_t^{w.m}$	
1201	Sv1201	TIG	243.8–237.4 / 240.6	238.0–234.2 / 236.1	12.2–11.8 / 12.0
	1201 + 0.5 % Sc		245.4–242.2 / 243.8	262.2–250.0 / 256.1	9.4–9.0 / 9.2
	Sv1201	MIG	269.4–263.0 / 266.2	262.8–257.8 / 260.3	18.4–18.0 / 18.2
	1201 + 0.5 % Sc		285.3–272.5 / 278.9	273.8–269.8 / 271.8	14.2–14.0 / 14.1
1460	Sv1201	TIG	279.4–270.4 / 274.9	251.2–244.4 / 247.8	14.6–14.2 / 14.4
	1201 + 0.5 % Sc		284.0–276.2 / 280.1	279.8–270.0 / 274.9	10.2–10.0 / 10.1
	Sv1201	MIG	292.2–286.6 / 289.4	289.3–283.9 / 286.6	17.0–16.4 / 16.8
	1201 + 0.5 % Sc		306.4–299.8 / 303.1	298.8–292.6 / 295.7	14.6–14.2 / 14.4

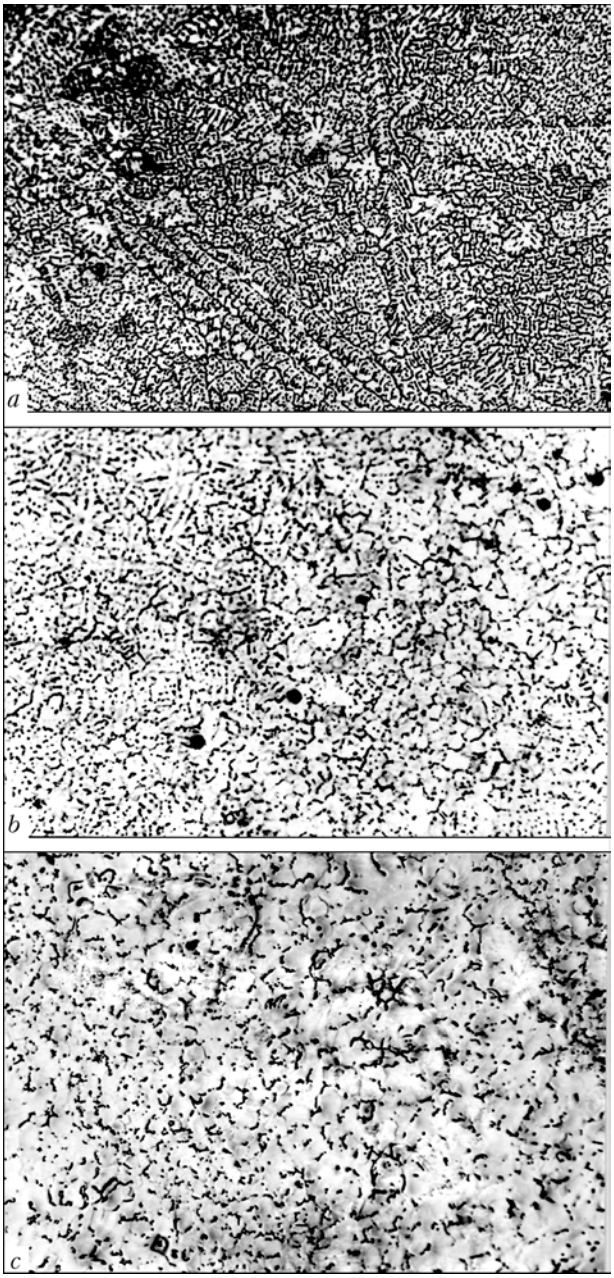

Microstructure of welds produced by TIG welding of 3 mm sheets of alloy 1460 with Sv1201 (*a*), 1201 + 0.5 % Sc (*b*) and heated 1201 + 0.5 % Sc (*c*) filler wire (×156)

sion in the zones of the weld fusion with the base metal, where its high overheating was noted. Decrease of welding heat input in TIG welding promotes a certain increase of the ultimate strength of the joints, in particular when Sc-containing wire is used.

At solidification of the weld pool metal, scandium promotes a greater dispersity of the residual phases, formation of a complex solid solution saturated with copper and scandium, and refinement of the weld structure as a result of subdendrite formation. Therefore, the strength of the metal of welds produced using such a wire, increases somewhat in welding both with the consumable and nonconsumable electrodes.

However, the strength coefficient of butt joints of alloys 1201 and 1460, produced by arc welding, does not exceed the values of 0.65 and 0.60, respectively, even with the use of wire of Sv1201 type alloyed with 0.5 % Sc. To increase the welded joint strength they are exposed to additional thermal impact. Low-temperature artificial ageing or high-temperature quenching with subsequent artificial ageing are usually used.

To some extent it was possible to perform the joint heat treatment directly during welding, by passing current through a section of the filler wire. Interaction of the electromagnetic fields induced around the arc discharge and the current-carrying filler, promotes a continuous change of the arc position in space [7, 8]. In combination with a change of heat balance of the weld pool, resulting from heated wire entering the pool, favourable conditions are in place for an effective thermal impact of the arc on the solidifying weld metal, this leading to a change of its structure (Figure).

In standard TIG welding of 1460 alloy using batch-produced filler wire Sv1201, the weld forms coarse directional crystallites. Addition of 0.5 % Sc to the filler wire promotes formation of a mixed dendrite and subdendrite structure. Heating of the filler wire fed into the weld pool allows producing the finest subdendrite structure of welds. This provides an increase of the strength of Sc-containing welds right after welding up to the level achieved on samples subjected to additional artificial ageing (Table 4).

Modes of joint strengthening after welding were selected so that both the mechanisms of metal strengthening as a result of precipitation of the particles of the main alloying elements and Al–Sc phases would be implemented simultaneously.

Investigations showed that at a short-time heating up to 550 °C, coherence of $ScAl_3$ phase with the matrix is probably not disturbed. Therefore, combining the operations of high-temperature short-time ageing to achieve precipitation of the Al–Sc phase and high-temperature recovery of the quenched state (with subsequent low-temperature ageing) for precipitation of the strengthening particles of the main alloying elements, allowed a considerable increase of the strength of weld metal and welded joint as a whole. Coefficient of strength of joints welded using Sc-containing wire rose up to 0.76.

Comparative analysis of the data obtained in welding with Sv1201 and 1201 + 0.5 % Sc wires, shows that the increase of strength (105.6 MPa) by approximately 46 % (49.1 MPa) achieved as a result of full heat treatment was due to scandium addition to the filler wire. In this case, impact toughness of weld metal is higher than that of the base metal.

To increase the strength of certain welded structures or individual weldments, postweld heat treatment can be additionally used, this treatment including a short-term high-temperature (550 °C) quenching and subsequent artificial ageing (130 °C, 20 h + 160 °C, 16 h).

Table 4. Mechanical properties of welded joints on 3 mm sheets of alloys 1460 produced by TIG welding

Condition of welded joint	Filler	Welded joint tensile strength σ_t^w, MPa	Weld metal tensile strength $\sigma_t^{w.m}$, MPa	Weld metal impact toughness a_n, J / cm^2	Welded joint bend angle α, deg
After regular argon-arc welding	Sv1201	313.0–306.0 / 307.2	258.6–243.7 / 251.4	18.5–18.1 / 18.3	180–163 / 174
	1201 + 0.5 % Sc	313.7–304.2 / 308.1	301.3–281.4 / 288.3	18.7–18.4 / 18.6	80–78 / 79
After welding with filler preheating	Sv1201	310.9–303.9 / 306.9	281.9–268.8 / 274.6	15.9–15.6 / 15.8	104–102 / 103
	1201 + 0.5 % Sc	334.3–329.1 / 331.2	316.2–292.4 / 304.3	13.7–13.3 / 13.5	93–92 / 93
After artificial ageing (130 °C, 20 h + 160 °C, 16 h)	Sv1201	--	296.3–286.9 / 290.3	13.2–12.0 / 12.7	42–37 / 40
	1201 + 0.5 % Sc	--	304.2–302.4 / 303.8	12.9–12.4 / 12.6	39–35 / 37
After heating up to 550 °C, instant cooling and subsequent artificial ageing (130 °C, 20 h + 160 °C, 16 h)	Sv1201	401.9–377.7 / 387.7	378.2–354.1 / 364.9	9.2–9.1 / 9.2	33–32 / 32
	1201 + 0.5 % Sc	440.2–433.4 / 436.8	397.0–390.5 / 393.5	5.5–5.1 / 5.3	21–16 / 19

CONCLUSIONS

1. Ultimate strength and proof stress of welds made by arc welding using Al–Cu wires is increased at scandium addition to their composition. At weld metal solidification a complex Cu-saturated solid solution of scandium in aluminium is formed, dispersity of residual phases becomes higher, and weld structure is refined as a result of formation of crystals of a subdendritic form.

2. Application of filler wire of Sv1201 type alloyed with 0.5 % Sc and heated by passing current in TIG welding of 1460 alloy allows the strength of the metal of welds and welded joints to be increased to a level, usually reached at their additional artificial ageing.

3. Developed modes of heat treatment of welded joints of alloy 1460 allow increasing the strength of welds and welded joints by combining the mechanisms of high-temperature recovery of the quenched state of the metal with dissolution of the strengthening phases formed by its main alloying elements, and high-temperature ageing with precipitation of $ScAl_3$ particles. Subsequent low-temperature ageing leads to precipitation of strengthening particles of the main alloying elements. Strength coefficient of welded joints of 1460 alloy 3 mm thick rises from 0.53 to 0.76, and the weld metal strength coefficient ---- from 0.43 to 0.69.

1. Lozovskaya, A.V., Chajka, A.A., Bondarev, A.A. et al. (2001) Softening of high-strength aluminium alloys in different fusion welding processes. *The Paton Welding J.*, **3**, 13–17.
2. Lukin, V.I. (1996) Sc as a promising alloying element for filler materials. *Svarochn. Proizvodstvo*, **6**, 13–14.
3. Elagin, V.I., Zakharov, V.V., Rostova, T.D. (1982) Future application of scandium additives to aluminium alloys. *Tsvet. Metally*, **12**, 96–99.
4. Ishchenko, A.Ya., Lozovskaya, A.V., Poklyatsky, A.G. et al. (1999) Structure and properties of joints produced in welding AMg6 alloy using filler wires with scandium. *Avtomatich. Svarka*, **4**, 19–25.
5. Ishchenko, A.Ya., Lozovskaya, A.V., Poklyatsky, A.G. et al. (2002) Increase in strength of welds in arc welding of alloy 1420 using Sc-containing fillers. *The Paton Welding J.*, **1**, 10–14.
6. Zakharov, V.V., Rostova, T.D. (1995) Scandium addition to aluminium copper-containing alloys. *Metallovedenie i Term. Obrab. Metallov*, **2**, 23–27.
7. Poklyatsky, A.G., Ishchenko, A.Ya., Grinyuk, A.A. et al. (2002) Non-consumable electrode argon-arc welding of aluminium alloys with arc oscillations. *The Paton Welding J.*, **2**, 18–22.
8. Poklyatsky, A.G., Lozovskaya, A.V., Grinyuk, A.A. (2002) Prevention of formation of oxide films in welds of Li-containing aluminium alloys. *Ibid.*, **12**, 39–42.

CURRENT TRENDS IN DEVELOPMENT OF TECHNOLOGICAL LASERS

V.P. GARASHCHUK and **V.D. SHELYAGIN**
E.O. Paton Electric Welding Institute, NASU, Kiev, Ukraine

Current trends in development of technological CO_2-lasers, optically excited sold-state lasers and semiconductor lasers are analysed on the basis of the information obtained at Fair «Laser-2005» and Essen Fair «Schweissen and Schneiden». Technological parameters of fibre and semiconductor lasers have been improved in the last years, while those of CO_2-lasers have remained almost unchanged. Two-coordinate scanning is additionally applied in technological systems based on the Cartesian manipulators. In welding technologies, the special consideration is given to combined welding methods, characterised by combined application of laser radiation and other heat sources, such as electric arc, non-coherent light sources, etc.

Keywords: technological lasers, CO_2-lasers, disk and fibre solid-state lasers, technological laser systems, combined welding methods

The XVII International Fair and International Congress «Laser 2005. World of Photonics» took place on 13–16 June 2005 in Munich, and the XVI International Fair «Schweissen and Schneiden» was held on 10–21 September 2005 in Essen, Germany.

Fair «Laser-2005» consisted of the following sections: lasers and optronics, optics, technologies for manufacture of optical parts, measuring and testing equipment, optical measuring systems, medical equipment, process equipment, and imaging. The Fair was accompanied by the XVII International Conference on Lasers and Electronics in Europe, as well as the International Professional Fair and Congress on Optical, Information and Communication Technologies «FiberComm».

Of the highest interest to the authors at the Fair was the technological laser equipment for thermal technologies of materials treatment: welding, cutting, heat treatment and cladding. 43 companies took part in these areas at the Fair, including 27 companies specialising in welding, 9 — in brazing and soldering, 26 — in cutting, and 19 — in surface treatment, more then half of them being permanent participants of the Fair.

Data on the world sales of laser equipment in 2004 were published in a special book [1]. The total volume of sales of laser systems for materials treatment in 2004 was 4.65 bln Euro. Out of this amount, 3.45 bln is the sum of sales of laser systems for macro treatment, including welding and cutting — 2.45 bln, marking — 650 mln, and 3D forming, perforation etc. — 350 mln Euro. The rest, i.e. 1.2 mln Euro, is the volume of sales of laser systems for micro treatment in semiconductor industry, production of electronic devices and chips, as well as eximer lasers for photolithography.

Distribution of technological laser systems in industries in terms of costs was as follows: automotive industry — 475, electrical engineering — 400, metal working in other industries — 1130, treatment of non-metals — 445, job shops — 950, electronics, semiconductors and production of displays — 1250 mln Euro.

The volume of sales in Europe was 34 % of the world sales, that in the North America and Japan was 22 % each, in East Asia — 19 %, and in other regions — 3 %. The main customer of laser equipment in Europe is Germany, the state of industrial development of which has a substantial effect on the market.

The world volume of sales of laser light sources in 2004 was 1.65 bln Euro. Among them, CO_2-lasers were sold for a sum of 660 mln, which constitutes 40 % of all sales, the more than 500 W CO_2-lasers being sold for an amount of almost 600 mln Euro. The amount of sales of solid-state lasers was 650 mln Euro (or 39 % of the total market). Eximer lasers were sold for a sum of 320 mln, and diode lasers during a short time reached a level of 20 mln Euro. Therefore, at present CO_2-lasers, judging from their sales, have lost the leading position they occupied from the middle of the 1970s. Further development of solid-state lasers will cause further pressing out of CO_2-laser. However, in the future they will be applied in large quantities as well.

Demand for lasers and laser systems used for materials treatment depends to a great degree upon the dynamics of industrial development. According to forecasts, in the next 10 years the annual growth of the world market of laser systems for materials treatment will constitute about 14 % or about 9.5 bln Euro, 6.1 and 3.4 bln being paid for laser systems for macro and micro technologies, respectively (unless no revolutionary changes in materials treatment methods take place in the forecast period).

Thermal laser technologies for materials treatment involve primarily three types of lasers: CO_2-lasers with diffusion (tube and slit types) and convective cooling (mostly with axial pumping), optically-excited solid-state lasers (rod, disk and fibre types), and diode (semiconductor) lasers [2].

Technological capabilities of lasers for cutting and welding are determined not only by the power of laser radiation, but also by beam transformation constant

Q (product of minimal transverse size of the focused beam by its convergence) [2]. In focusing of the beam the product of its minimal transverse size by the angle of its convergence is also equal to constant Q. Thus, the lower the Q value, the smaller the size of focusing of the laser beam and the smaller the convergence of the focused beam. Therefore, the lower the beam transformation constant, the higher the quality of the beam, as this provides a bigger depth of field at the same values of minimal section of the focused beam.

CO_2-lasers. No novelties have appeared in the field of CO_2-lasers. Not much improvement is seen in technological parameters of the tube-type diffusion- and convectively-cooled lasers, which seem to reach their ultimate values. It is possible that some new engineering designs will appear in the future. However, the main technological parameters of these lasers are predefined. The slit-type lasers intensively developed in the last decade were represented by the Rofin Sinar 3000 W laser with $Q < 4$ mm·mrad and beam parameters corresponding to single-mode generation. Similar laser was advertised (but not exhibited) by the St.-Petersburg Institute of Laser Physics, Russia. Most probably that this type of the lasers will compete with the single-mode tube-type ones.

Optically excited solid-state lasers. Technological parameters of the rod-type lasers have not changed during the last two years. Their maximal power is 4500 W and $Q = 25$ mm·mrad. Lasers with a power of less than 1000 W have a 2 times better beam transformation constant ($Q = 12$ mm·mrad).

Meanwhile, technological parameters of the disk lasers have been improved. Company TRUMPF advertised its 250–4000 W disk lasers with $Q = 8$ mm·mrad for the highest-power lasers and $Q = 4$ mm·mrad for lasers with a power of up to 500 W. Hence, increase in the laser radiation power is accompanied by deterioration of the quality of the laser beam (as Q increases). To compare, at the Fair of 2003 this Company exhibited this type of the lasers with a power of no more than 1000 W and $Q = 6$ mm·mrad.

In the field of fibre lasers, the most productive company is IPG Laser GmbH (Russia, Germany, USA). The 300 W laser module with $Q = 0.4$ mm·mrad being exhibited at the Fair of 2003, the same module exhibited at the Fair of 2005 had a power of 1000 W and the same Q value, corresponding to single-mode generation, i.e. the maximum possible one. Lasers with a many kilowatt power are made of separate single-mode units, the output ends of the fibres of which are arranged in parallel to each other, thus forming a multi-channel laser beam. Its transformation constant is approximately a square root times higher than that of the used output fibres. The fibre lasers use optical fibres doped with ytterbium, having a generated wavelength of 1.07–1.12 μm. Diode lasers are used to excite them. Available is a series of standard industrial lasers (with a power of 100, 200, 500, 1000, 2000, 5000, 10000, 20000 and 50000 W), having a 25 % efficiency. Such values of power were achieved only in CO_2-lasers with a much lower beam quality. The 20 kW laser, measuring approximately $800 \times 800 \times 1500$ mm, without a cooling unit and power supply was exhibited at the Fair.

Within a short period of time IPF managed to develop the highest-power solid-state laser, whereas it took almost 20 years to develop the rod-type solid-state lasers with a power 4500 W. It is likely that the use of the principle of a fibre-optic laser will help to eliminate many problems, which lasers of the other design fail to solve. The IPG lasers feature a high beam quality, which allows using them for cutting, welding, drilling, micro treatment, thermal printing and engraving. The Company also built the fibre-optic lasers with a very high beam quality for medical applications. Their active medium is doped with thulium, having a generated wavelength of 1.75–2.20 μm.

Diode (semiconductor) lasers. Much success has been achieved in the field of diode (semiconductor) lasers ---- during a period of two years their power was increased more than 1.5 times. Data on technological parameters of the LASERLINE direct-action lasers with the radiation delivered via optic fibres, which were exhibited at the 2003 and 2005 Fairs, are given in Tables 1 and 2.

The achieved light power densities allow using them for welding, brazing, cladding and heat treatment. Because of high values of the beam constant, these lasers cannot be applied for high-quality cutting of heavy metal sections, although sheets about 1 mm thick can be cut quite well (the same applies to welding with deep penetration). The record high efficiency of such lasers poses a challenge to developers to achieve not only high power values, but also the possibility of focusing the laser beam to smaller sizes at low convergence of the focused beam, i.e. low values of the beam constant, which creates conditions for their unlimited applications in the materials treatment technologies.

Companies that develop technological lasers pay much attention to automation of welding, cutting and marking processes. Companies REIS and KUKA exhibited their 3D robotic systems for performing welding and cutting operations (in particular, for automo-

Table 1. Comparison of technological parameters of direct-action semiconductor lasers

Beam transformation constant, mm·mrad	Minimal size of light spot in lens focusing ($F = 100$ mm), mm	Maximal laser power, W		Density of light power in focused beam $\cdot 10^{-6}$, W / cm^2
		2003	2005	
40×40	0.4×0.4	600	1500	0.94
40×60	0.4×0.6	900	2000	0.84
60×100	0.6×1.0	1600	3500	0.58
60×300	0.6×3.0	6000	10000	0.55

Table 2. Comparison of technological parameters of semiconductor lasers with delivery of radiation via optic fibre

Beam transformation constant, mm·mrad	Diameter of optic fibre with numerical aperture A_N = 0.2 μm	Minimal size of light spot in lens focusing (F = 100 mm), mm	Maximal laser power, W		Density of light power in focused beam $\cdot 10^{-6}$, W / cm^2
			2003	2005	
40	400	0.4	0.85	1.4	1.11
60	600	0.6	1.30	3.0	1.06
100	1000	1.0	4.00	6.0	0.76
150	1500	1.5	4.00	6.0	0.34

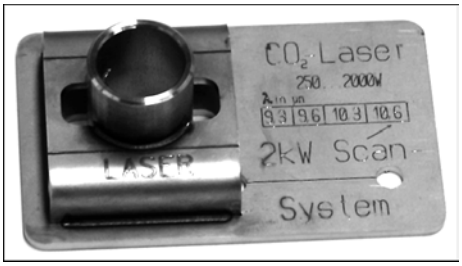

Sample made and marked with one set-up

tive industry). In the majority of cases laser radiation is delivered to the final control element of the robot via an optic fibre, where the beam inevitably loses its power, especially at the input and output. Moreover, delivery of the beam via an optic fibre causes some deterioration of its quality. Compactness and light weight of the diode laser heads allowed REIS to mount them on final control elements of the anthropomorphous robot, thus avoiding the above losses and distortions of the beam.

Two-coordinate scanning is indicated for welding, cutting and marking on a plane. This problem is solved using not only Cartesian manipulators, but also scanners with a plane scanning performed with two mirrors oscillating in mutually perpendicular planes. Scanners can be used as part of any process equipment with any lasers. For example, LASERLINE employs them with semiconductor lasers, and Plant FEHA ---- with CO_2-lasers. The Figure shows a plate with a clip welded to it, and a ring with inscriptions welded into the clip. All these operations were made in one set-up of the preliminarily mechanically assembled structure, that took 1 min. One of the developers of the scanners is Company SCANLAB.

Scanners providing scanning on a plane with a diameter of not more than 500 mm were exhibited at fairs in the previous years. At the XVI Fair in Essen that took place in September 2005, Company TRUMPF demonstrated its laser system TrumaScan L4000 equipped with the 6 kW CO_2-laser, where the scanner processed a field of 1500 mm in diameter. If it is required by production, several scanners can be installed, or one scanner can be moved within the 2400 mm limits. The working volume of the system is $1500 \times 2400 \times 500$ mm. The scanner provides displacement of the focused beam over the surface of a workpiece at a velocity of 4 m / s, which is a hard problem for mechanical displacement of the focusing head.

Company FEHA is specialising in development and mass production of CO_2-lasers, which can generate wavelengths of 9.3, 9.6, 10.3, 10.6 and 11.2 μm, this allowing using them for welding and cutting of not only metals but also plastics. In treatment of plastics, the most suitable wavelength is selected for a given operation. For example, polypropylene has the highest transparency at a wavelength of 9.3 μm, a bit lower transparency at a wavelength of 10.6 μm, whereas at a wavelength of 10.3 μm it is absolutely non-transparent. Hence, it is most efficient to cut polypropylene with the radiation of this wavelength. The technology for making permanent overlap joints in plastics by penetration welding has been developed during the last years. The point of the method is that the upper plate of plastics is transparent for this radiation, while the lower plate absorbs it. Thus, it is heated and heats the lower surface of the upper plate. A permanent joint is formed in subsequent pressing and cooling. With this welding method the lower plate can be metal. The lasers made by Plant FEHA are applied to produce joints in different plastics by penetration welding.

Among the technological developments on welding of metals, noteworthy are the combined methods developed also by the E.O. Paton Electric Welding Institute [3]. These methods use laser radiation together with the consumable- or nonconsumable-electrode electric arc, as well as light-beam heaters. The methods are implemented using the specially developed focusing heads with wire feed mechanisms, arc electrodes and light-beam heaters mounted on them. Companies PRECITEC and HIGHYAG, specialising in manufacture of focusing heads, occupy a marked position in this field. Thus, PRECITEC produces the focusing heads for overlap welding with pressing the plates welded on one or two sides using rotating rollers, which are employed in automotive industry for the manufacture of car bodies.

Various components for lasers and process fixtures manufactured by different companies were also exhibited at the Fair, including, first of all, optical equipment (lenses, windows, mirrors), power meters, optic fibres, scanners, focusing heads for welding and cutting, compressors for fast-flowing CO_2-lasers, coolers for active laser media, air purifiers, etc.

1. (2005) *World of laser technology. Core of photonics*. 7th ed. Frankfurt am Main: VDMA.
2. Garashchuk, V.P. (2005) *Principles of laser physics. Lasers for thermal technologies*: Manual. Kiev: PWI.
3. Shelyagin, V.D., Krivtsun, I.V., Borisov, Yu.S. et al. (2005) Laser-arc and laser-plasma welding and coating technologies. *The Paton Welding J.*, **8**, 44–49.

METHODS TO LOWER THE HYDROGEN CONTENT IN METAL OF WELDED JOINTS OF LOW-ALLOYED STEELS IN SUBMERGED-ARC WELDING

V.V. GOLOVKO
E.O. Paton Electric Welding Institute, NASU, Kiev, Ukraine

The paper gives the results of thermodynamic calculations of probable metallurgical reactions in submerged-arc welding using agglomerated fluxes, which promote lowering of partial pressure of hydrogen within the arcing zone and suppressing the diffusivity of hydrogen in the weld. They are in good agreement with experimental data. It is concluded that the use of fused intermediate products is advantageous for production of welding fluxes, in order to decrease the hydrogen content of weld metal.

Keywords: arc welding, low-alloyed steel, welded joints, hydrogen in welds, flux, metallurgical processes

Cold crack prevention remains an urgent problem in welding thick low-alloyed steels. Currently available methods usually envisage heating of the edges being welded or application of special welding consumables of austenitic class. In a number of cases, however, application of heating is not rational, and quite often it is even impossible. Therefore, attention is focused on application of special consumables, providing a low content of hydrogen in the welds due to their metallurgical activity.

Three main metallurgical methods are currently known to lower the hydrogen content in the low-alloyed weld metal:

- hydrogen binding into stable gaseous compounds, that are insoluble in liquid metal;
- arc atmosphere dilution by gases, which do not dissolve in weld pool metal;
- hydrogen binding into hydrides, resistant to high temperatures.

The first of the above directions in welding process metallurgy is often implemented using the reactions of formation of silicon tetrafluoride as an intermediate step in hydrogen binding into hydrogen fluoride, the solubility of which in liquid steel is much lower than that of atomic hydrogen. Reaction of the following type is one of the most probable ones:

$$2CaF_2 + 3SiO_2 = 2CaSiO_3 + SiF_4\uparrow. \quad (1)$$

Volatile silicon tetrafluoride interacts with hydrogen or water vapour in the gaseous medium by the following reactions:

$$SiF_4 + 4H \Leftrightarrow Si + 4HF, \quad (2)$$

$$SiF_4 + 2H_2O \Leftrightarrow Si\hat{I}_2 + 4HF. \quad (3)$$

In addition, reactions of direct interaction of calcium fluoride with hydrogen or water vapour in the gaseous medium can take place:

$$CaF_{2(g)} + 2\acute{I} \Leftrightarrow 2HF + Ca_{(g)}, \quad (4)$$

$$CaF_{2(g)} + \acute{I}_2\hat{I}_{(g)} \Leftrightarrow 2HF + Ca\hat{I}. \quad (5)$$

For thermodynamic evaluation of the probability of these reactions running, let us use an approximate calculation of free energy by the known formula

$$\Delta G^0_T = \Delta H^0_{298} - T\Delta S^0_{298},$$

where ΔH^0_{298} and ΔS^0_{298} are the algebraic sums of standard heat contents of reaction products and standard enthropies taken with the plus sign, and initial substances with the minus sign, respectively.

The considered formula does not take into account the enthalpy of the phase and polymorphous transformations, while providing a qualitative evaluation of the possibility of running of certain reactions. Reaction (1), which was studied in [1], depending on the temperature interval, proceeds with varying intensity. In terms of weld metal saturation with hydrogen, hydrogen concentration on the boundary with the molten metal is the most significant parameter. Therefore, proceeding from the data of [2], let us select average weld pool temperature (1770 ± 100 °C) as the design quantity. Then, free energy can be found for the above reactions:

$$\Delta G^0_1 = -3375 \text{ kJ}; \quad \Delta G^0_2 = -342.5 \text{ kJ};$$

$$\Delta G^0_3 = -3561.5 \text{ kJ}; \quad \Delta G^0_4 = +442.5 \text{ kJ};$$

$$\Delta G^0_5 = -64 \text{ kJ}.$$

It is seen that the reaction of silicon tetrafluoride formation requires quite large amounts of CaF_2 and SiO_2. The formed SiF_4 will bind hydrogen in the most effective manner in keeping with reactions (3) and (5), whereas development of reaction (4) is improbable at these temperatures.

Charge components, due to which reactions (1)–(5) proceed, usually are fluorspar concentrate and quartz sand. Higher requirements to the level of cold- and crack resistance of the metal of welds of high-strength low-alloyed (HSLA) steels can only be met

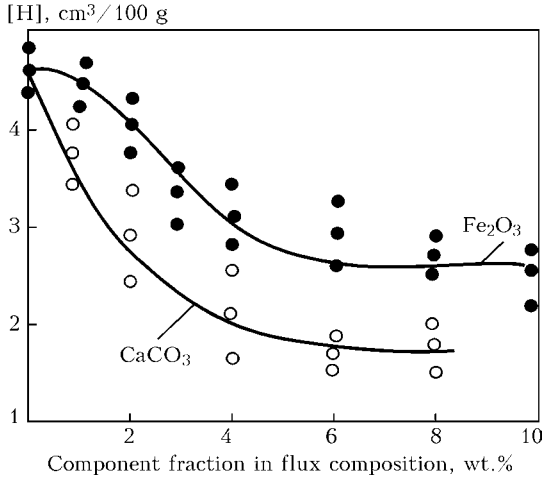

Figure 1. Influence of marble and iron-ore concentrate in agglomerated flux composition on hydrogen content in weld metal

at a low content of phosphorus in them [3]. In SAW it is impossible to noticeably lower phosphorus concentration in the weld metal as a result of metallurgical reactions, so that high requirements are made to the content of the latter in the welding consumables. From this viewpoint, there are certain limitations for application of fluorspar concentrate, which may contain up to 0.15 % P according to DSTU 4421, in fluxes for welding HSLA steels.

Another important requirement to the quality of weld metal is its content of non-metallic inclusions. Special research [4, 5] showed that oxygen content of 0.02–0.04 % is optimum for HSLA steel welds, while the main bulk of non-metallic inclusions should be made up of titanium oxides and manganese alumosilicates [6, 7]. Achieving such a composition of inclusions requires taking special measures on suppression of Si-reduction process. One of these measures consists in lowering the content of free silica in the composition of welding fluxes. The limited amount of silicon dioxide, which is required to provide the welding-technological properties of the flux, is added in the form of complex silicates of calcium or manganese.

Thus, limitations in the use of fluorspar concentrate and silica in fluxes designed for welding HSLA steels, do not allow taking full advantage of the method of hydrogen binding into gaseous hydrides to lower the diffusive hydrogen content in the weld metal. Practical application of both the fused and agglomerated fluxes confirms such a conclusion [8].

The second possible method for lowering the hydrogen content in the weld metal, is use of components in the welding consumables composition, which are capable of diluting the arc atmosphere by gases, having a lower solubility in liquid steel (CO_2, CO and OH^-). However, in addition to lowering the hydrogen partial pressure as a result of dilution of the atmosphere in the arcing zone, CO_2 can also enter into the following reaction with hydrogen:

$$CO_2 + 2H = CO + HO^-, \quad (6)$$

$$2CO_2 \Leftrightarrow 2CO + O_2, \quad (7)$$

$$O + H = HO^-. \quad (8)$$

More over, the above higher oxides of metals at their addition to the composition of welding consumables decompose under the influence of the welding arc heat with evolution of oxygen which also interacts with hydrogen.

Using the above procedure, let us calculate the free energy for reactions (6)–(8):

$$\Delta G_6^0 = +360 \text{ kJ}; \ \Delta G_7^0 = -925 \text{ kJ}; \ \Delta G_8^0 = -240 \text{ kJ}.$$

Obtained data show that only the reactions of carbon dioxide dissociation (7) and atomic hydrogen oxidation (8) may develop in this temperature interval, whereas proceeding of reaction (6) is impossible in terms of energy. Therefore, in order to lower the hydrogen partial pressure in the welding arc atmosphere, it is rational to use carbonates in the flux composition. Addition of compounds which decompose in heating with oxygen evolution, will allow lowering the partial pressure of hydrogen, but running of reactions between oxygen and hydrogen with formation of OH^- ion in the gaseous medium is improbable in this case.

To study the possibility of lowering the diffusive hydrogen content in the weld metal as a result of arc atmosphere dilution, test fluxes were made, the composition of which included additives of iron-ore concentrate (Fe_2O_3) or marble ($CaCO_3$) (Figure 1). The flux base was the slag system of MgO–Al_2O_3–SiO_2–CaF_2. diffusive hydrogen content in the metal was determined by the procedure described in DSTU 17745. At the same time, metal samples were taken and results were obtained by a procedure specified by GOST 23338. Both of these methods demonstrated a good agreement of the results.

The above data show that addition of 4 % marble to the flux charge allows lowering the diffusive hydrogen content to 2 cm^3 per 100 g of weld metal. Influence of iron-ore concentrate on this process is much less effective, which is in agreement with the performed theoretical estimates. Lowering of hydrogen partial pressure in the welding arc atmosphere occurs due to evolution of oxygen (when higher iron oxides are added) or carbon dioxide (when carbonate is added) as a result of the reaction of additive component dissociation. The content of oxygen and non-metallic inclusions in the deposited metal is increased. In the case of addition of 4 % iron-ore concentrate, oxygen content in the deposited metal is equal to 0.056 %, and that of non-metallic inclusions is 0.44 %. At addition of 4 % marble to the flux, oxygen content in the deposited metal is equal to 0.038 %, and that of non-metallic inclusions –– to 0.35 %. Obtained results suggest that it is not rational to introduce iron-ore concentrate additives into the flux composition, as this leads to higher contamination of weld metal with non-metallic inclusions. Content of the latter in welds made with fluxes containing marble additives is a little lower, but even it is higher than 0.25 % value admissible in such cases. In addition,

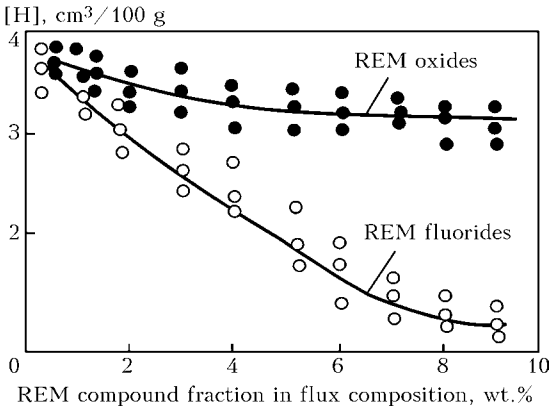

Figure 2. Influence of REM compounds in the agglomerated flux composition on hydrogen content in the weld metal

presence of marble additives in the flux charge impairs the flux welding-technological properties.

Proceeding from the above considerations, the possibility of applying a third method to lower the content of diffusive hydrogen in weld metal was studied. With this purpose, components (Ti, Sr, REM) were added to the flux, promoting hydrate formation, both in the weld pool metal, and in the weld metal during its cooling:

$$\alpha\text{-Ti} + H_2 = TiH_2, \quad (9)$$

$$Sr_{(s)} + H_2 = SrH_2. \quad (10)$$

Let us calculate the value of free energy of reactions (9) and (10) for the temperature range of existence of a two-phase region of solidifying weld metal of low-alloyed steels:

$$\Delta G_9^0 = -77.5 \text{ kJ}; \quad \Delta G_{10}^0 = -46 \text{ kJ}$$

Calculation shows that addition of titanium compounds to the flux composition is the most effective measure in terms of lowering the hydrogen content in the weld metal. In view of the fact that at high temperatures characteristic for existence of liquid metal in the weld pool, the alloying elements participating in reactions (9) and (10) have a high affinity to oxygen and nitrogen, the additives used were not only master alloys and ferroalloys, but also oxides and fluorides of metals.

Addition of titanium, aluminium and boron oxides to the flux composition did not influence the content of diffusive hydrogen, but at addition of 8 % of REM oxides to the charge it was possible to lower the content of diffusible hydrogen in the weld metal to 3.2–3.5 cm^3 / 100 g. Use of REM fluorides turned out to be much more effective from this point of view. At addition of 8 % of such a component, diffusive hydrogen content decreased to 1.3–1.5 cm^3 / 100 g of weld metal (Figure 2). Unfortunately, it turned out to be impossible to make full use of the obtained effect, as REM fluorides are highly toxic, and their application in welding consumable manufacture makes the technological process much more complicated.

Ferrotitanium, ferroboron and a complex modifier (AKTse-0) containing 15 % REM, 10 % Al, 15 % Ca,

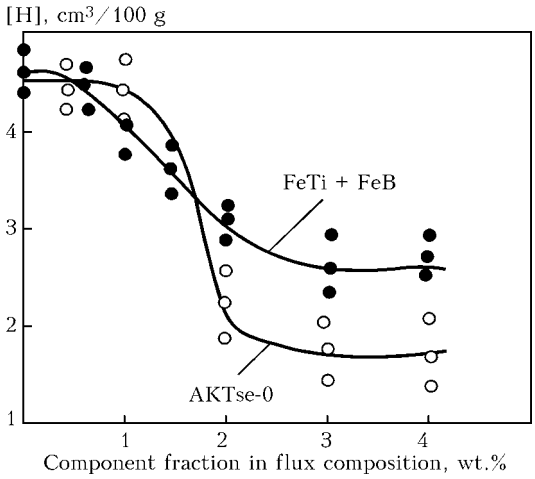

Figure 3. Influence of ferrotitanium and boron, as well as AKTse-0 master alloy in agglomerated flux composition on hydrogen content in weld metal

the rest being Fe, were used as metal additives in the flux composition. Research results, shown in Figure 3, indicate that addition of 3 % of complex modifier to the flux composition allowed lowering the diffusive hydrogen content in the weld metal to 1.5–1.8 cm^3 / 100 g. It should be noted that the residual hydrogen content in the weld metal in this case increased up to the level of 0.0003 %. Use of ferrotitanium and ferroboron as additives yielded the most pronounced effect at their simultaneous addition to the flux composition. At 2.5 % ferrotitanium and 0.5 % ferroboron in the flux, the amount of diffusive hydrogen in the deposited metal was on the level of 2.5 cm^3 / 100 g.

Thus, either a complex modifier, used in production of special steel grades, or ferrotitanium in combination with ferroboron, can be used as additives to the flux for lowering the diffusible hydrogen content in the metal of HSLA steel welds. The first variant envisages application of a rather expensive and deficit component ---- a complex modifier, promoting a higher content of residual hydrogen in the weld metal, while the other does not allow lowering the diffusive hydrogen content below 2.5 cm^3 / 100 g of weld metal.

Technologies of agglomerated flux manufacture envisage component addition to the flux composition without high-temperature treatment or melting, so that moisture content in the initial components is very important for fluxes of this type. The basic initial components of the fluxes of MgO–Al_2O_3–SiO_2–CaF_2 system are fired magnesite, electrically fused corundum, quartz sand and fluorspar concentrate. Moisture

Table 1. Moisture content in agglomerated flux components, cm^3 per 100 g of component

Component	As-delivered	After heat treatment at 900 °Ñ
Corundum	92	13
Quartz sand	240	15
Fluorspar	340	15
Margnesite	6300	1080

Table 2. Composition of test samples of synthetic slags, wt.%

Slag designation	SiO_2	Fe_2O_3	Al_2O_3	CaO	MgO	MnO	CaF_2	S	P
ShSM	27.52	3.45	16.96	7.66	38.79	1.23	3.67	0.038	0.024
ShSS	26.00	1.75	20.07	6.44	41.02	1.10	3.40	0.019	0.012

content in these components in as-delivered condition and after heat treatment at the temperature of 900 °C was determined by the method of chromatographic analysis (Table 1).

As shown by the above data, one of the main components of agglomerated fluxes of a high basicity (magnesite) includes a large quantity of moisture, which cannot be completely removed even at its high temperature heat treatment. Such a phenomenon is attributable to the fact that fired magnesite actively absorbs moisture from ambient air with formation of $Mg(OH)_2$, capable of retaining moisture at high temperatures. In addition, magnesite has in its composition a certain part of free calcium oxide that also is active moisture absorbent.

The most radical method to lower moisture content in the agglomerated flux components is using components after the melting operation. Test samples of synthetic slags, the composition of which is given in Table 2, were melted for this purpose.

ShSM slag after melting was granulated by the «wet» method, i.e. into water, and ShSS slag ---- by the «dry» method on a steel plate. By the results of chromatographic analysis it was found that ShSM and ShSS slags contain 303 and 241 cm^3 / 100 g of slag. Synthetic slags were used to make test batches of agglomerated fluxes, the composition of which included 78–82 % of synthetic slags. Analysis of the samples of metal deposited using these fluxes, showed that they contain 1.3–1.5 cm^3 H per 100 g of deposited metal. The rationality of constructing the slag-forming part of agglomerated fluxes on the basis of synthetic slags with a high content of magnesium and aluminium oxides was thus confirmed.

In conclusion it should be noted that the service conditions of HSLA steel welded joints require further improvement of their brittle fracture resistance, which is related, primarily, to lowering of hydrogen content in the weld metal. There exist several variants of lowering the hydrogen content in the weld metal, based on metallurgical characteristics of welding fluxes, each of which has its limitations. The most promising is the comprehensive approach, in which the charge materials used are the fused slag intermediate products with lower moisture content in combination with components promoting a lowering of hydrogen partial pressure on the metal–slag interface and diffusive hydrogen content in the weld metal.

1. Kuzmenko, V.G. (1980) Specifics of reaction of fluorite and silica interaction at the temperature of 800–1900 °C. *Avtomatich. Svarka,* **6**, 33–35.
2. Frumin, I.I., Pokhodnya, I.K. (1955) Study of mean temperature of weld pool. *Ibid.*, **4**, 13–20.
3. Pokhodnya, I.K., Vojtkevich, V.G., Alekseev, A.A. et al. (1992) Influence of phosphorus on impact toughness and chemical microheterogeneity of weld metal. *Ibid.*, **2**, 3–7.
4. Widgery, D.J. (1976) Deoxidization practice for mild steel weld metal. *Welding J.*, **3**, 57–68.
5. North, T.H., Bell, H.B., Koukabi, A. et al. (1979) Notch toughness of low oxygen content submerged arc deposits. *Ibid.*, **12**, 343–354.
6. Liu, S., Olson, D.L. (1986) The role of inclusions in controlling HSLA steel weld microstructures. *Ibid.*, **6**, 139–149.
7. Horii, Y., Ichikawa, K., Ohkita, S. et al. (1995) Chemical composition and crystal structure of oxide inclusions promoting acicular ferrite transformation in low-alloy submerged arc weld metal. *Quart. J. JWS*, 13(**4**), 500–507.
8. Davidson, J.L. (1998) Advances in hydrogen management: the science based design of low hydrogen consumables for the future. *Australian Welding J.*, **43**, 33–39.

SANITARIAN-HYGIENIC CHARACTERISTICS OF WELDING FLUXES WITH LOCALLY CHANGED CHEMICAL COMPOSITION OF GRAINS

V.G. KUZMENKO[1] and **V.I. GUZEJ**[2]
[1]E.O. Paton Electric Welding Institute, NASU, Kiev, Ukraine
[2]Kiev City State Administration, Kiev, Ukraine

Intensity if formation of welding aerosol and its composition in submerged arc welding using fused flux AN-60 containing fluoride added by different methods, e.g. by adding fluoride raw materials to the charge followed by its melting in furnace, or by heat treatment in the fluorine-containing gases, namely products of decomposition of ammonium fluoride NH_4F, are studied.

K e y w o r d s : electric arc welding, welding fluxes, fluorination treatment, welding aerosols, sanitarian-hygienic characteristics

Electric welding arc used in different technologies ensures significant productivity of the process of the base and a filler metal melting and high level of operation characteristics of a weld. However, it causes problem of working and natural environment protection against harmful emissions [1] ---- welding aerosols, which include solid and gaseous components, whereby practically all slag components that participate in a welding process get in smaller or greater amounts into air of the working area. The only electric arc process, in which trapping of welding aerosols takes place, is submerged arc welding. If the process proceeds normally, the flux completely shields against arc light radiation and significantly reduces, but at the same time changes character of emission formation in welding. In high-temperature area of the welding pool, in which takes place melting of the base and filler metals and the flux, the following zones may be singled out proceeding from peculiarities of welding aerosol emission (Figure 1): generation (inter-electrode gap *1*); concentration of aerosols (near-arc space *2*); filtration of aerosols (solid flux layer *3*).

On one hand, presence of flux in high-temperature zone of the pool enables increase of amount and change of properties of aerosols in zone *1*, and on the other hand, flux in zone *3* of the upper cold layer ensures cooling and trapping of aerosols during filtration in inter-grain space. Fluorine, which enters into composition of welding consumables, may exert significant influence on electric conductivity of arc gap and state of the arc as a whole, depending upon the degree of plasma ionization. As far as this element has the highest potential of ionization (in comparison with other elements), increase of fluorine content in welding arc causes increase of its electric resistance, change of which, in its turn, affects size, shape, and temperature of the welding arc. According to [2], reduction of CaF_2 content in flux causes increase of the arc length, which is proved by increase of its gap interval l_a. According to [3, 4], increase of content of fluorine and halogenides in the arc zone causes reduction of l_a and diameter of the column, and temperature increase of the latter.

Contribution of fluxes into formation of aerosols in welding is determined by their chemical composition and physical properties, whereby in the arc zone components with low boiling point and high pressure of vapor are evaporated first of all from the flux, especially those having significant positive deviation from the Raoult's law. In addition, composition of welding aerosols depends upon formation of gaseous products of interaction, in particular fluorides, occurrence of which is connected with chemical reaction, which proceeds between calcium fluoride CaF_2 and oxides in high-temperature zone of the pool. These fluorides include, first of all, silicon tetrafluoride SiF_4, which forms as a result of CaF_2 interaction with a respective oxide.

Amount of formed welding aerosol and its composition are affected by the character of arc burning, which, in its turn, depends upon flux composition. Depending upon composition of the flux and, therefore, composition of the gas-vapor phase, in which arc burns, state of the latter may change. So, presence of components with high ionization potential in the arc will cause reduction of its length and diameter of the column and increase of its temperature. Components with low ionization potential exert opposite effect,

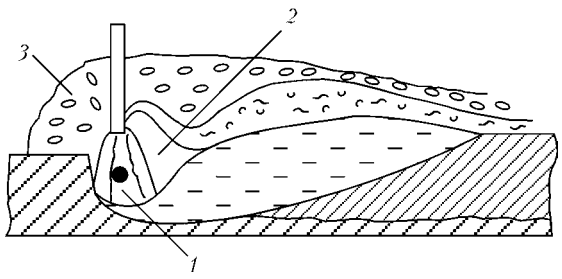

Figure 1. Scheme of zone of formation and trapping of aerosols in high-temperature area of welding pool in SAW (for designations see the text)

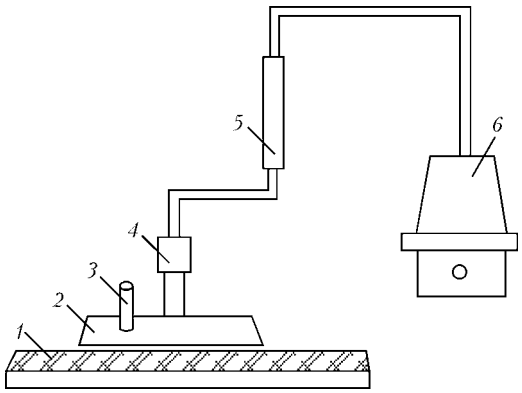

Figure 2. Scheme of unit for trapping aerosols in SAW: *1* — flux; *2* — cap; *3* — tip of welding machine; *4* — cartridge with filter; *5* — rotameter; *6* — vacuum cleaner

whereby depending upon state of the arc intensity of aerosol formation in welding increases or reduces.

Earlier [5, 6] we studied propensity to hydration of fluxes, which contain increased concentration of fluorine in surface layer of grains, and their ability to ensure resistance of the weld metal against formation of porosity from rust in welding. As showed results of studies, such fluxes have 2–3 times lower propensity to absorption of moisture from air and ensure significantly higher resistance of the weld metal to pore formation in comparison with standard fluxes with uniform distribution of fluorine within a grain volume, whereby these parameters are ensured at fluorine contents (recalculated into CaF_2) within 0.5–1.5 %. Due to lower (in comparison with standard fluxes) general content of fluorine in surface-fluorinated fluxes, their application may, presumably, improve sanitarian-hygienic characteristics of fluorinated fluxes.

Influence of fluorinated fluxes on sanitarian-hygienic characteristics of welding process were studied on experimental unit designated for trapping aerosols in SAW (Figure 2). In this unit air with welding aerosol was pumped through a special filter, in which solid particles were trapped. Amount of aerosol accumulated in the filter was determined by its weighing

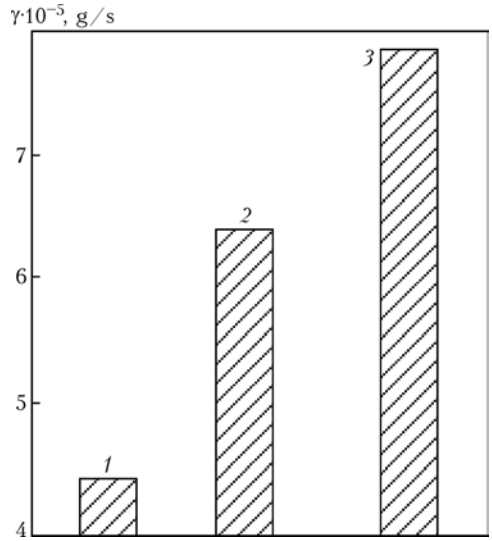

Figure 3. Intensity γ of aerosol solid component precipitation in SAW using flux AN-60 fluorinated by 0.5 (*1*) and 1.0 (*2*) wt.% NH_4F, and standard flux AN-60 (*3*)

Chemical composition of studied fluxes of AN-60 type, wt.%

Content of NH_4F in mixture with non-fluoride flux in fluorination thermal treatment, wt.%	MnO	SiO_2	CaF_2	CaO	Fe_2O_3
0	36.5	45.3	–	8.9	0.28
0.5	36.7	45.0	0.48	8.2	0.23
1.0	36.9	45.3	0.84	7.9	0.32

before and after exposure. Deposition was performed in the experiments under the following conditions: 600–620 A DCRP; 37 V arc voltage; deposition rate of 32 m / h; 50 V open-circuit voltage of the transformer; electrode extention of 70 mm; height of the flux layer filling was 40 mm. In the study standard flux AN-60 and two non-fluoride manganese-silicate fluxes were used, composition of which was close to the composition of the flux of indicated grade (Table), but calcinated at temperature 500 °C in a closed vessel in the mixture containing 0.5 and 1.0 wt.% salt of ammonium fluoride NH_4F. Chemical compositions of the initial and fluorinated fluxes are given in the Table.

Data on intensity of the welding aerosol solid component release, depending upon type of a flux, are given in Figure 3. One can see from the Figure that its amount is 12–37 % lower when fluorinated fluxes are used, than in case of using standard AN-60 flux, and reduces even more by means of NH_4F content reduction. Chemical composition of solid component of the aerosol is also established, and content of manganese, silicon and soluble and insoluble fluorine compounds in it is determined as well (Figures 4 and 5). Chemical composition of solid component of the weld-

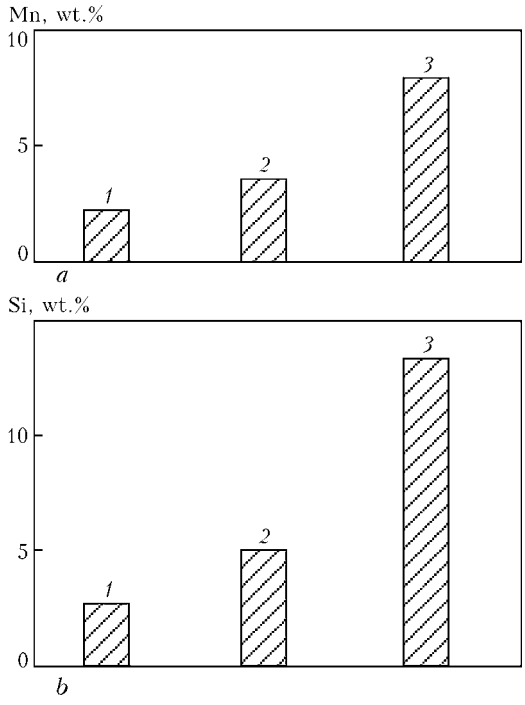

Figure 4. Content of manganese (*a*) and silicon (*b*) in solid component of welding aerosol formed in SAW with different types of fluxes (*1–3* are same as in Figure 3)

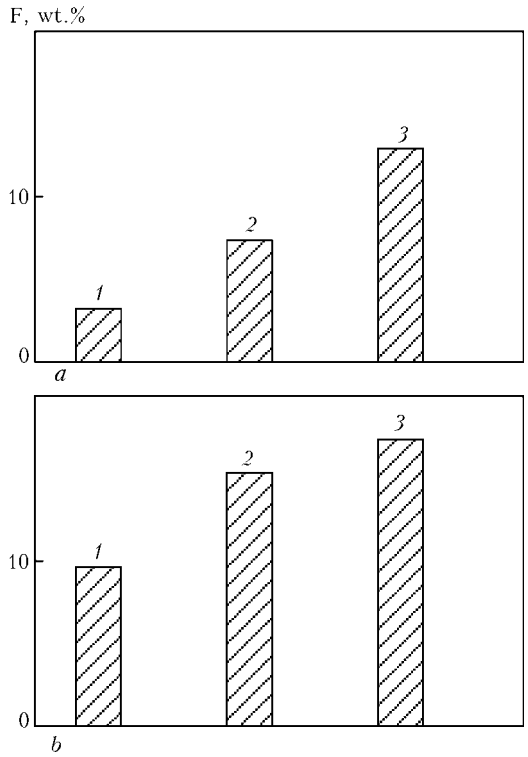

Figure 5. Fluorine content in soluble (*a*) and insoluble (*b*) compounds in welding aerosol formed in SAW (*1–3* are same as in Figure 3)

ing aerosol in case of SAW using fluorinated fluxes differs from that in case of using flux AN-60 by reduced content of the components: manganese ---- by 56–75 %, silicon ---- by 62–80 %, insoluble fluorides -----by 40–75 %, and soluble fluorides ---- by 10–50 %.

For determining the reason of such improvement of sanitarian-hygienic characteristics of fluorinated fluxes l_a was measured in case of using non-fluoride fluxes of AN-60 and AN-348-A types, which underwent heat treatment in mixture with 0.1, 0.2, 0.4, 0.6 and 1.5 wt.% NH_4F at the temperature 500 °C. The same parameter was measured in standard fluxes AN-60 and AN-348-A. Results of studies are given in Figure 6. Breaking length of arc gap in volume of fluorinated fluxes reduces by means of NH_4F content, used for their treatment, increase and achieves level of standard fluxes: for pumice-like flux of AN-60 type at 1.7 % of mentioned salt, and glassy flux of AN-348-A type at 0.9 % NH_4F, which in recalculation into CaF_2 makes up ≈ 1.3 and 0.7 wt.%, respectively.

So, local character of fluorine location on surface of grains causes essential improvement of sanitarian-hygienic characteristics of the flux in comparison with

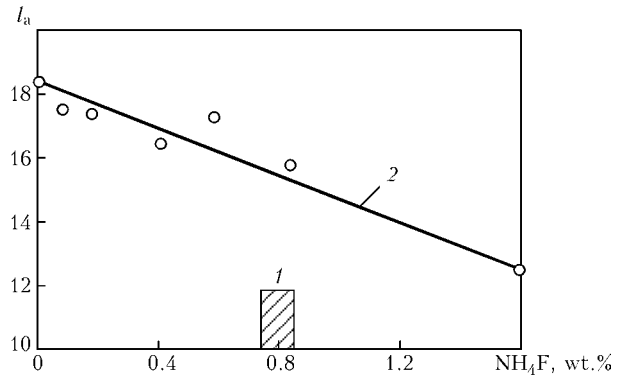

Figure 6. Change of arc gap length l_a during excitation and extinction of arc in volume of fluorinated flux of AN-60 type (for standard flux AN-60 l_a = 12 mm)

its uniform distribution in volume of grains of standard fluxes, first of all due to reduction of general content of fluorine and, evidently, due to reduction of arc temperature.

CONCLUSIONS

1. Sanitarian-hygienic studies of initial non-fluoride fluxes of manganese-silicate type, which underwent fluorination treatment, showed that in case of their use reduction of solid component content of welding aerosol by 12–37 %, manganese by 56–75 %, silicon by 62–80 %, insoluble fluorides by 40–75 %, and soluble fluorides by 10–50 % (in comparison with standard fluxes) takes place.

2. Results of studies of the length of arc gap of fluxes with fluorine, which was locally distributed on surface of grains, produced using fluorination treatment, showed that essential improvement of sanitarian-hygienic characteristics of a welding process takes place as a result of reduction of general content of fluorine and change of the arc burning parameters.

1. Migaj, K.V. (1975) *Hygiene and safety of labor in electric welding jobs in shipbuilding*. Leningrad: Sudostroenie.
2. Kirdo, I.V., Podgaetsky, V.V. (1949) Influence of flux on porosity of automatic welding joint caused by rust. *Trudy po Avtomat. Svarke pod Flyusom*, **6**, 36–62.
3. Lapin, I.A., Turkin, P.S., Samsonov, V.I. (1978) Influence of fluorite on structure of arc burning in air atmosphere. *Svarochn. Proizvodstvo*, **4**, 1–2.
4. Shevchenko, G.D., Turkin, P.S., Lapin, M.L. et al. (1974) Influence of fluorite on temperature of welding arc. *Ibid.*, **11**, 3–4.
5. Kuzmenko, V.G., Guzej, V.I. (2004) Hydration of fluxes with a locally-changed chemical composition of grains. *The Paton Welding J.*, **6**, 41–43.
6. Kuzmenko, V.G., Guzej, V.I. (2005) Pore formation in weld metal in submerged arc welding with surface saturation of grains with fluorine. *Ibid.*, **2**, 14–17.

PRODUCTION AND APPLICATION OF FLUX-CORED WIRE IN UKRAINE

R. ROSERT[1] and **A. ALIMOV**[2]
[1]Altleiningen-Drahtzug, Germany
[2]Donetsk, Ukraine

New state Ukraine appeared on the European map in 1649, however, its independence was short. The civil of war of 1654 tore the country apart. After collapse of tsarism Ukraine again gained its independence for a very short period of time from 1918 till 1922. Before its independence in 1991 Ukraine was among 15 Soviet socialist republics.

Ukraine is rich in mineral resources. These are the deposits of oil and lime in the Donets Basin (Donbass), deposits of iron ore in the south, manganese ore in Nikopol, mineral salts and gas in Carpathians and near Kharkov and Poltava. There is an oil deposit in the south-eastern part of Kiev oblast covering 20 % of the total Ukrainian consumption. Ore mining and processing, coal mining, aircraft and automobile engineering, electronics, nuclear industry, cement production, chemical, textile and food industries are the key sectors of economy in the country.

Growth of GDP is provided mainly by such industries as processing, food and light industry, as well as machine-building and trade. It is worth mentioning aviation industry such as construction of aircrafts of An-140 and An-70 types. Appropriate infrastructure such as city and railway transport is available. Germany is the second biggest trade partner to Ukraine after Russia.

Steel industry is the most important area for application of welding equipment in Ukraine. The steel market collapsed after 1992. By 2003 the market of rolled steel shrank down to almost 3 mln t (10 % of 1992 level). From time to time demand for steel grows in machine-building and construction. About 90 % of rolled steel articles were exported mostly to Asia (mainly these were ingots, semi-finished items and plates). Ukrainian steel industry could not compete with the neighboring Eastern European countries. High utilization of production facilities for pipe steel proved that nominal production capacities were not decreased. In the sphere of rolled stock production the standby capacities reached almost 8 mln t [1]. Ukraine is the seventh world producer of pipe steel. With the world production being 1,055 mln t, the share of Ukraine in 2004 was about 3.66 %. Figure 1 shows a comparison of Ukraine with Germany and Russia.

In 2005 production of pipe steel again increased. Increase of steel production is accompanied with modernization and reconstruction of production facilities. New equipment is installed, thus resulting in growth of quality. Application of welding filler alloys is closely related to the production of pipe steel. For example, in 1990–2003 the consumption of filler materials decreased due to run-down of pipe steel production.

Welding consumables. After 2003 a growth in welding production was observed. Figure 2 shows the quantity of different filler materials produced in the territory of Ukraine in 2003.

A share of manual electrodes in the production is the largest. From 2002 to 2003 their total quantity increased by 7.6 % with the highest growth (25 %) of special electrodes. In recent years a lot of small enterprises for production of electrodes came into being. This led, first, to high competition in this sphere and, second, to the absence of inspection and control at these enterprises. This means that many of such enterprises cannot be certified. In this case the consumer has to control the quality.

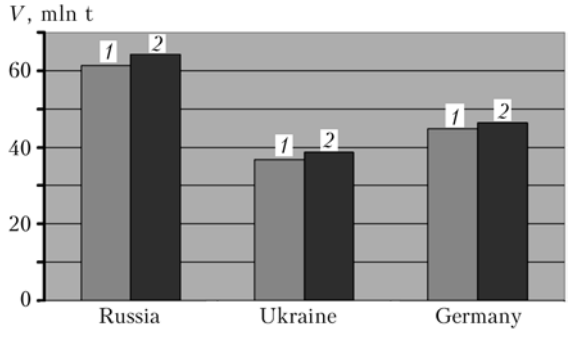

Figure 1. Production of pipe steel *V* in Ukraine in comparison with Germany and Russia in 2003 (*1*) and 2004 (*2*)

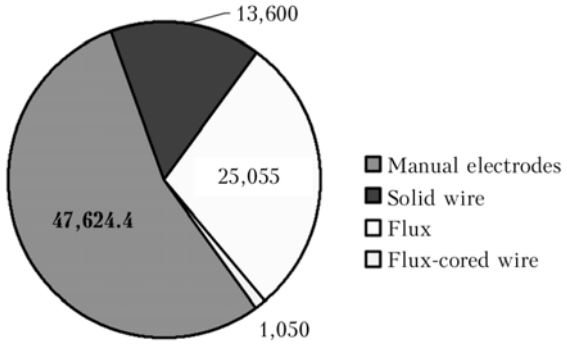

Figure 2. Production of filler materials, *t*, in Ukraine in 2003 [2]

This situation is evidently temporal because in the future the market will demand high-quality electrodes. Old electrode producers are equipped with the required equipment for production control and have laboratories with well-trained staff. Production program of large enterprises in most cases include solid wire. Growth in production of solid wire in 2003 was 4.9 % in comparison with 2002. It is noteworthy that out of 13000 t of wire about 54.5 % falls on wire 0.8–1.4 mm in diameter. A share of welding flux is relatively high and is 25055 t / year. Mainly fused fluxes are produced in Ukraine and their largest share is exported to Russia. Production of welding fluxes in Russia decreased in 2003 by 42 %. A share of flux-cored wire for welding and surfacing was in Ukraine in 2003 at least 1.3 %.

Flux-cored wire. Application of machine gas-shielded welding with solid and flux-cored wire is on the high level in the developed industrial countries. Application of manual solid wire welding is decreasing. Use of flux-cored wire welding grows in the countries with high-developed ship-building, for example, in the South Korea and Japan. According to [3] Japan consumed 90500 t of flux-cored wire in 2001. This is 29.38 % of the total consumption of filler materials and 75 % as compared to solid wire for gas-shielded welding (119800 t). For comparison, a share of flux-cored wire in total quantity of wires was in Europe in 2000 only about 9 %. In Ukraine production of flux-cored wire was on the low level before 2003 amounting to 1050 t. From this quantity 271 t was provided for welding and 779 t for surfacing.

Undoubtedly, in the nearest future this situation will change in favor of forthcoming mechanization and automation of production. Development of machine-building, ship-building, construction engineering, oil production and refinery and other branches of industry, as well as growth of salary, in Ukraine require new solutions in modernization of production and increase of output capacity.

In the former USSR flux-cored wire was produced since 1960. The E.O. Paton Electric Welding Institute (Kiev), then a leading institute of welding equipment in the USSR, played a key role in development and application of flux-cored wire.

At that time more than 10000 employees worked at PWI including its pilot production. PWI worked at practically all directions of welding equipment and related technologies. Many methods for production of flux-cored wire of different types and chemical composition received international patents. Numerous licenses were sold in such countries as China, USA, France, Japan, Hungary, Bulgaria and others. In [4] there is a review of specifications and technological peculiarities of flux-cored wires as of the technical level of the 1980s. Diameter of the produced flux-cored wires were mostly ranging within 1.1–6.0 mm. Corresponding state standards [5, 6] on classification and control of the flux-cored wires are effective today. After collapse of economical system in the 1990s the production of flux-cored wire terminated. During some time period it was produced on old obsolete equipment using the old compounding. There were no new developments in place and the production went down. The available production capacities were operational only for about 10 %. However, there were a number of proposals on restoration, improvement and production of flux-cored wire.

With the aim of integration to the world community Ukraine is creating the market economy. The goal is to become the WTO members and eventually the EU member [7]. In this connection the producers of filler materials are involved into a number of developments in the sphere of flux-cored wire production of 1.2 up to 2.0 mm in diameter for welding regarding the European and world standards, for example EN 758. Rutile flux-cored wires with fast-solidifying slag and wires with metallic powder for machine and robotic welding are developed. Specific attention in the course of development is paid to good technological properties, low sputtering and small release of harmful fumes.

A number of self-shielding flux-cored electrode wires with fluoric-basic type of slag is developed for welding. In connection with their adapted characteristic it became possible to decrease the silicon and aluminium content in the molten deposited metal so that the minimal impact toughness 47 J is achieved at the low temperature (down to –40 °C) [8]. In this case one should not forget about flux-cored wire with a doubled shell (Figure 3, *a*).

Flux-cored wire with a doubled shell belongs to the flux-cored wire of closed profile produced from strip. Its design is such that all components of the metallic powder are in the inner shell, while gas- and slag-forming components are in the outer shell. Therefore, it is possible to provide in welding an effective protection without external supply of shielding gas. Even though according to the authors this form is especially good for self-shielding flux-cored wire, it has not gained a wide application for two reasons, first, high production cost due to complex section of the wire and, second, it is no possible to produce wire 1.2 mm in diameter.

In the sphere of surfacing it is worth noting a specialized form of the flux-cored wire developed at PWI (Figure 3, *b*). These are flux-cored strips that have a closed profile and in contrast to seamless flux-cored strips are produced from two solid strips. Size in the range of (10–18) × (3–4) mm is mainly used

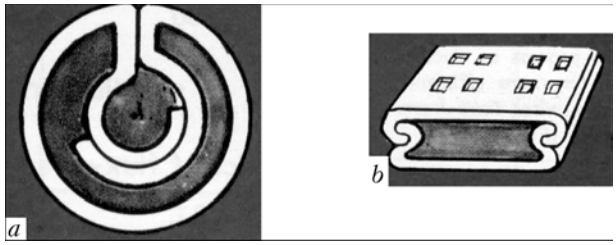

Figure 3. Cross-section of doubled-shell flux-cored wire (*a*) and flux-cored strip (*b*)

Figure 4. Shop for production of flux-cored wire in Dnepropetrovsk

for surfacing of large areas. These flux-cored strips may have powder filling density up to 80 % providing a high range of alloying. Material of the shell may be on the basis of iron, nickel and cobalt. Self-shielding flux-cored wires and flux-cored wire for submerged-arc welding and electroslag surfacing are also created.

Flux-cored wire has been produced in Ukraine since 1960. First the flux-cored wire of AN1 grade for welding of non-alloyed steel structures was produced at PWI pilot plant. First production shop was opened in the mid-1960s in Dnepropetrovsk. Until 1990 there were four enterprises that produced flux-cored wire in the territory of Ukraine: two of them in Kiev and two in Dnepropetrovsk.

Now flux-cored wire and strip is produced at six Ukrainian enterprises. The audit of these enterprises is carried out by the UkrSEPROS certification body. In [9] there is an actual report on the flux-cored wires certified by UkrSERPOS with indication of the certification validity. Two largest producers of flux-cored wire in Ukraine are certified according to the ISO 9001: 2000 standard. Eight foreign enterprises also have UkrSEPROS certificates for their flux-cored wire.

At present Ukraine is producing seamless flux-cored wire and flux-cored wire of closed profile [10] on the basis of iron in compliance with the effective European standards [11, 12]. Figure 4 shows a shop for production of flux-cored wire in Dnepropetrovsk. Staff of the enterprise is highly qualified. Technology is under ongoing improvement and equipment under modernization to increase productivity. Systems of quality control are integrated to provide a maximally possible level of quality and its control.

Examples of flux-cored wire application. Volumes of the available Ukrainian tolerances for flux-cored wire testify to the fact that Ukrainian economy in the sphere of application of flux-cored wire may be considered a market one both nationally and internationally. Before making a decision on what is appropriate to use: flux-cored wire, solid wire or manual electrodes, it is necessary to carry out a cost study regarding the regional labor payment. In terms of application the following tendencies are considered:

- it is necessary to note a maximal growth in the sphere of rutile flux-cored wires with fast solidifying slag;
- development of high- and higher-strength steels is a reason for growing demand for the flux-cored wires of corresponding strength, which would guarantee smaller content of hydrogen in the deposited metal;
- in automatic welding the application of high-productive methods prevail, for example, flux-cored multiwire welding;
- application of alloys with increased wear resistance for increasing service life of components in the metallurgical, coal mining and metal mining industry and thus for decreasing the costs.

Gas-shielded and submerged-arc welding, and electroslag surfacing may be mainly considered as welding methods, where flux-cored wire and strip are employed. There are some examples of applying flux-cored wire in Ukraine.

At present flux-cored wire is mostly applied in ship-building for welding and repair of wearing parts at the metallurgical enterprises. There are 20 ship-building enterprises and shipyards in Ukraine located along the Black Sea cost and Dnieper river bank.

Figure 5. Aircraft carrier «Admiral Gorshkov»

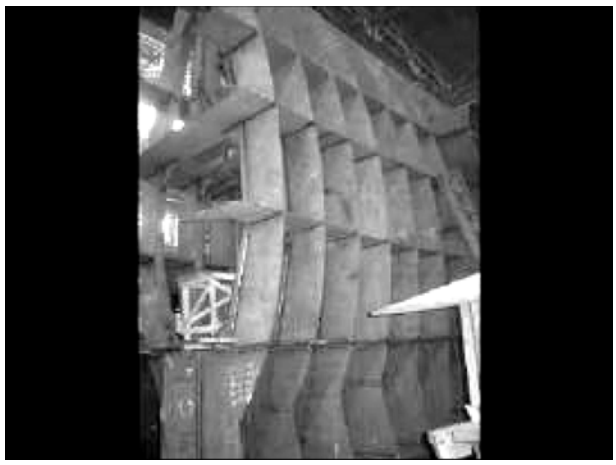

Figure 6. Fragment welded with rutile flux-cored wire (ASME 5.20 E71-T1)

Figure 7. Nikolaev shipyard dry dock

Enterprises in the Nikolaev oblast have more than a century traditions in ship-building. Application of flux-cored wire achieved a high level. Many highly qualified welders are working at these enterprises. Some of them after reduction of the number of orders for construction of new ships are working abroad. This is related to the fact that after independence Ukraine lost many orders on construction of mainly military ships from Russia.

For this year the capital repair of aircraft carrier «Admiral Gorshkov» (Figure 5) is planned. Repair technology with application of high-strength flux-cored wires is developed. After capital repair it is planned to sell the aircraft carrier to India. A fragment welded with flux-cored wire at the shipyard in Nikolaev in 2005 is shown in Figure 6. Figure 7 shows one of the dry docks of Nikolaev shipyard.

Production of large-diameter pipes, construction of cranes and vessels are other spheres of flux-cored wire application. Figure 8 shows also an example of electroslag surfacing with flux-cored wire of closed profile. Surfacing productivity is from 25 to 30 kg / h. It is used for surfacing of continuous casting rolls, blast furnace gas collector bells or worn-out panels.

CONCLUSIONS

- Ukraine has traditions for producing flux-cored wires since 1960;
- after a period of stagnation one could observe starting from 2003 growth of the volumes of flux-cored wire Ukraine;
- flux-cored wire is applied in many branches of industry for welding and surfacing;

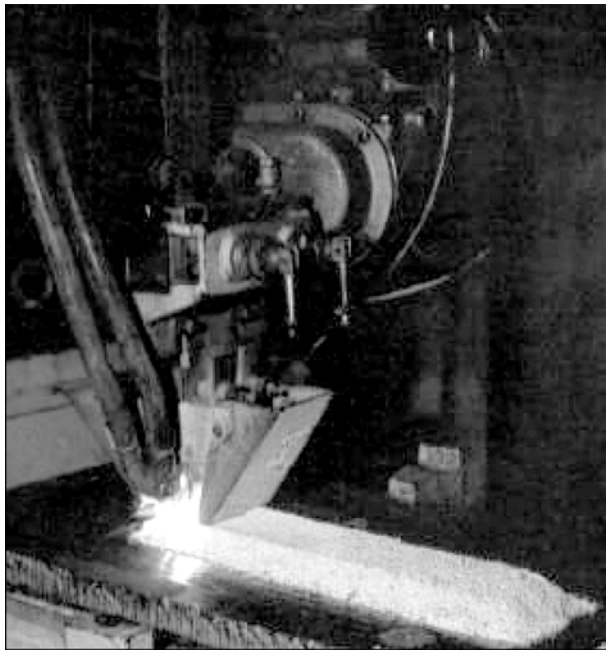

Figure 8. Closed-profile flux-cored wire electroslag surfacing at PWI pilot plant

- Ukrainian enterprises producing flux-cored wire are in the ongoing process of modernization of their equipment, increase of productivity and optimization of the quality control system;
- new spheres for application of the flux-cored wires are opened and new compoundings are being developed.

1. (2004) *Study of the state-of-the art of steel industry in Ukraine*.
2. Ignatchenko, P.V. et al. (2003) *About some tendencies of development of welding filler materials in Ukraine*.
3. Pokhodnya, I.K. (2005) *Welding filler materials: state-of-the-art and tendencies of development*. Kiev: PWI.
4. Pokhodnya, I.K. (1980) *Flux-cored wire for arc welding*. Kiev: Naukova Dumka.
5. *GOST 26101–84*: Flux-cored wire for surfacing.
6. *GOST 26271–84*: Flux-cored wire for joint welding.
7. Timmermann, H. (2003) *The EU and new neighbores: Ukraine and Belarus. Science and policy institution.*
8. Shlepakov, V.N., Naumejko, S.M. (2005) Self-shielded flux-cored wires for welding low-alloy steels. *The Paton Welding J.*, **4**, 28–30.
9. Protsenko, N.A. (2005) Manufacturing of welding filler materials — state-of-the-art on 01.01.2005. *Avtomatich. Svarka*, **4**, 47–52.
10. (2004) Flux-cored wires for welding and surfacing. In: *Principles and terminology M 0941-1*. Issue 3. Duesseldorf.
11. *EN 758–97*: Flux-cored wires for arc welding with and without shielding gas for non-alloy and fine-grained steels.
12. *EN 12535–99*: Flux-cored wires for MIG welding of high-strength steels.

SURFACING CONSUMABLES FOR HARDENING OF PARTS OPERATING UNDER IMPACT-ABRASIVE WEAR CONDITIONS

A.N. BALIN, A.V. BEREZOVSKY, A.A. VISHNEVSKY and **B.A. KULISHENKO**
Plant for Welding Consumables, Berezovsky, Russia

Data are given on flux-cored wires and electrodes used as surfacing consumables for hardening of parts operating under impact-abrasive wear conditions.

Keywords: arc surfacing, flux-cored wire, covered electrodes, impact-abrasive wear, hardening of parts

The Plant for Welding Consumables manufactures a number of in-house materials, in addition to the known grades of surfacing consumables (Table 1), for hardening of parts operating under impact-abrasive wear conditions.

Flux-cored wire of the PP-Np-60Kh12D5R2T grade is used to advantage for hard-facing of parts of mining equipment operating under abrasive wear conditions with substantial impact loads (excavating machine bucket teeth and shells, drainage buckets, ripper bits). Service life of parts hard-faced with this wire extends 2.5–3 times compared with untreated ones, and 1.5–1.8 times compared with use of the known PP-200Kh15S1GRT grade wire. A new sparsely-alloyed PP-Np-200Kh8T2R wire is applied for hard-facing of parts operating under conditions of abrasive wear and frequent impact loads (components of dredging pumps, crushing and milling equipment). Service life of components hard-faced with this wire, which are parts of the equipment in operation at the Nevinansky mine (Sverdlovsk District), extends 2–4 times, compared with the untreated ones (steel 110G13).

The Plant has mastered manufacture of small-diameter wires (2 mm) for hard-facing of parts of a small thickness, which are subjected to abrasive wear in operation (fan baffles, brick press components, etc.).

Manufactured are wires for hard-facing of parts subjected in operation to cavitation-corrosion and corrosion-abrasive wear (components of oil-and-gas stop valves, water gates, etc.). Wires PP-ZSM-101, PP-ZSM-110, PP-ZSM-112, etc. have proved advantageous for these service conditions.

Electrodes ZSM-6 (E-150Kh8T2R) have been developed and are mass produced for hard-facing of parts operating under abrasive and impact-abrasive wear conditions. As-deposited metal produced by using these electrodes has structure consisting of the austenitic-martensitic matrix, primary carbides and carboborides of chromium and titanium (about 20–25 %). Metastable austenite transforms into martensite under the effect of impact loads, which provides very high

Table 1. Chemical composition and hardness of deposited metal

Flux-cored wire grade	Content of elements in deposited metal, wt.%										Hardness of deposited metal HRC_e
	C	Cr	Mn	Si	Mo	Cu (Nb, N)	B	Ti	S	P	
PP-ZSM-101	0.10	17.0	1.0	5.0	–	–	–	0.5	≤ 0.04	≤ 0.04	29–36
PP-ZSM-104	0.60	12.0	0.5	0.5	0.5	5.3	1.3	1.4	≤ 0.03	≤ 0.04	58–62
PP-ZSM-110	0.20	9.0	9.0	0.3	–	–	–	0.5	≤ 0.04	≤ 0.04	22–45
PP-ZSM-111	1.50	8.0	–	–	–	–	0.8	1.8	≤ 0.03	≤ 0.04	45–62
PP-ZSM-112	0.11	14.0	0.5	0.3	–	–	–	0.5	≤ 0.04	≤ 0.04	39–48
PP-ZSM-125	2.00	15.0	1.1	1.5	–	–	0.7	0.5	≤ 0.04	≤ 0.04	47.5–59.0
PP-ZSM-150	1.50	15.0	–	0.5	–	–	2.5	2.0	≤ 0.03	≤ 0.04	58–68
PP-ZSM-151	2.50	10.0	–	2.0	–	7Nb	–	–	≤ 0.04	≤ 0.04	51.5–59.0
PP-ZSM-155	0.15	14.0	1.5	0.5	1.0	–	–	–	≤ 0.03	≤ 0.03	40–48
PP-ZSM-170	0.80	20.0	–	–	–	–	3.0	0.6	≤ 0.04	≤ 0.04	59–68
OZN-6	0.90	4.4	2.6	3.7	–	–	1.0	–	≤ 0.035	≤ 0.04	≥ 55
OZN-7	0.70	4.6	4.1	3.2	–	0.15N	1.1	–	≤ 0.035	≤ 0.04	≥ 56
ZSM-6	1.30	8.0	–	≤ 1.0	–	–	0.3	2.2	≤ 0.035	≤ 0.04	≥ 50

resistance to abrasive wear. Wear resistance in tests to friction on a fixed abrasive is 5–7 times higher than for steel 110G13. The presence of 50–70 % austenite in the initial structure allows the deposited metal to resist impact loads.

The technology for manufacture of the above surfacing consumables should provide certain chemical composition of the deposited metal, particularly the carbon content. Carbon transfers to the deposited metal in the form of graphite from high-carbon ferrochromium. Adding of crushed electrodes (milled graphite) to the charge of flux-cored wires and electrode coverings fails to ensure a consistent content of carbon in the deposited metal. Therefore, in development of charge and covering mass composition, it is advisable to minimise the graphite content.

The Klyuchevsky Factory for Ferroalloys produces high-carbon ferrochromium of the FKh60U9, FKh55U10 and FKh55U12 grades according to TU 14-141-02–96 and TU 14-141-37–00. However, to form a batch of ferrochromium, the Factory applies a composite method, consisting in using two ferroalloys (with low and high carbon content). Chemical composition indicated in the certificate is calculated as an average weighted one of two ferroalloys. Therefore, each pack (barrel) contains two materials not mixed with each other. This circumstance makes the production process much more complicated, as it involves an extra operation for thoroughly mixing the content of each separate barrel. The drawback of ferroalloys FKh60U9, FKh55U10 and FKh55U12 is their high content of phosphorus and silicon. At present, the Plant receives carbon chromium of the Kh75B grade (Table 2) from the Klyuchevsky Factory. The use of the latter in surfacing consumables provides a more consistent chemical composition of the deposited metal in terms of the carbon and chromium content, and allows the fill factor of flux-cored wires and weight factor of the electrode coverings to be decreased.

Table 2. Chemical composition of carbon chromium of Kh75B grade (TU 14-5-124–81), wt.%

Batch No.	Cr	C	Si	Al	Cu	S	P
K 11	82.5	10.2	1.15	1.38	0.022	0.07	0.047
K 19	83.0	10.2	1.13	0.72	0.023	0.05	0.045
K 20	79.7	10.2	1.20	3.11	0.023	0.05	0.045

TECHNOLOGY FOR FRICTION STIR CLADDING OF COPPER AND ITS ALLOYS

The E.O. Paton Electric Welding Institute developed the technology for friction stir cladding of copper and its alloys. The point of the process is as follows. A workpiece and filler metal in the form of a plate are fixed using clamps. A rotating tool is brought into contact with the filler plate to a finger stop. Heat needed to plasticise the filler metal and part of the workpiece metal is generated due to friction of the tool. The overlap bead is formed in movement of the tool. Workpieces are clad by successive deposition of such beads with overlapping.

Experimental unit based on a vertical-type machine tool with a drive power of 10 kW allows deposition of a copper layer up to 1 mm thick.

Available are various designs of the tools with a different ratio of sizes and shapes of their components, which have sufficient safety factor to ensure a long-time performance under high mechanical and thermal loading conditions.

The equipment is simple in design and maintenance. The floor area needed to locate the main equipment is 50 m².

The range of main parameters, i.e. cladding speed and rotation frequency of the tool, ensuring quality formation of the deposited layer was identified.

Fragment of plate of copper continuous casting machine mould after cladding

Results of chemical analysis of the deposited layer and base metal proved their identity and absence of oxygen enrichment of the deposited layer.

Application. Repair and restoration of sizes of metallurgical and heat engineering facilities and transportation vehicles.

Contacts: Prof. Zhadkevich M.L.
E-mail: office@paton.kiev.ua

REACTIVITY OF FERROALLOYS IN LIQUID GLASS*

N.V. SKORINA and **A.E. MARCHENKO**
E.O. Paton Electric Welding Institute, NASU, Kiev, Ukraine

The results of investigation into reactivity of fine ferroalloys (ferrosilicium FS-45, ferromanganese, ferrosilicomanganese, etc.) used in production of electrodes as weld metal deoxidizers and alloying elements of the weld metal, are presented. Individual batches of ferrosilicium FS-45 were revealed to have an extremely high reactivity. It was suggested that such high reactivity might be associated with peculiarities of the production technology, which could either deteriorate homogeneity of ferrosilicium ingots or cause formation of particularly reactive structural components.

Keywords: production of electrodes, electrode compound, liquid glass, ferroalloys, reactivity, gas emission, passivation

In the process of manufacturing and processing electrode compounds grains of their ferroalloy and metal powdered components interact with liquid glass (a binder), whereby the process is accompanied by emission of heat and gas. This causes gradual thickening of the coating mixture up to complete loss of plasticity by it, increase of thickness non-uniformity, swelling of the coating, formation of pores and cracks in it, and significant reduction of the coating strength after heat treatment of electrodes.

Actually, mentioned interaction processes are chemical reactions between active metals (silicon, manganese, manganese carbide, etc.) and alkaline ROH (where R is Na and / or K) formed as a result of liquid glass hydrolysis, or water:

$$Si + 2ROH + H_2O = R_2SiO_3 + 2H_2\uparrow; \quad (1)$$

$$Mn + 2H_2O = Mn(OH)_2 + H_2\uparrow; \quad (2)$$

$$Mn_3C + 6H_2O = 3Mn(OH)_2 + CH_4\uparrow + H_2\uparrow; \quad (3)$$

$$2Al + 2ROH + 2H_2O = 2RAlO_2 + 3H_2\uparrow; \quad (4)$$

$$Mg + 2H_2O = Mg(OH)_2 + H_2\uparrow. \quad (5)$$

Technologists have to take into account from the very beginning of commercial manufacturing of coated electrodes difficulties connected with proceeding of chemical reactions in electrode compounds (1)–(3). By now on the basis of results of the studies and accumulated experience these difficulties are overcome by passivation of the surface of active powder particles, i.e. by creation of strong oxide film on it.

Nevertheless, a number of enterprises, which manufacture coated welding electrodes, faced mentioned problem in various years of the last decade. Application of certain traditional technological methods of ferrosilicium powder passivation did not bring positive results. In certain cases it turned out that they cause opposite effect, in particular, intensify chemical interaction of ferrosilicium powder with liquid glass, thus provoking malfunctions in the technology of electrode manufacturing.

In this work results of studies, carried out in PWI in cooperation with leading electrode manufacturing enterprises of Ukraine and RF, are presented. They illustrate peculiarities of chemical interaction with liquid glass of ferroalloy and metal powders, which are widely used in manufacturing of electrodes. Samples were studied, which were taken from commercial product lots, manufactured by Zaporozhie (ZFP), Nickopol (NFP), Novokuztentsk ferroalloy plants and Chelyabinsk Electrometallurgical Works, which demonstrated in the process of commercial use different degree of reactivity. At the same time efficiency of their activity suppression using known technological methods was checked. Reactivity of ferroalloys and metal powders was checked by the volume V of gas (method of volume equalization), which is released within the time of interaction of 1 g ferroalloy powder, sieved through the mesh of 160 μm size, with 170 g sodium-potassium liquid glass, having density 1400 kg / m^3 and viscosity 50–70 mPa·s. Modulus of liquid glass was 2.9–3.0 units and the reaction zone temperature was 70 °C. Weight of powders with very low reactivity was increased up to 3 g (results obtained were also reduced to 1 g of ferroalloy powder). Reaction observation usually lasted for 1.5 h.

In Figures 1–3 reactivity of ferrosilicium powders of FS-45 type (47 lots), ferrosilicomanganese (131 lots), low-carbon and carbon ferromanganese (34 and 10 lots, respectively), and metal manganese (11 lots)

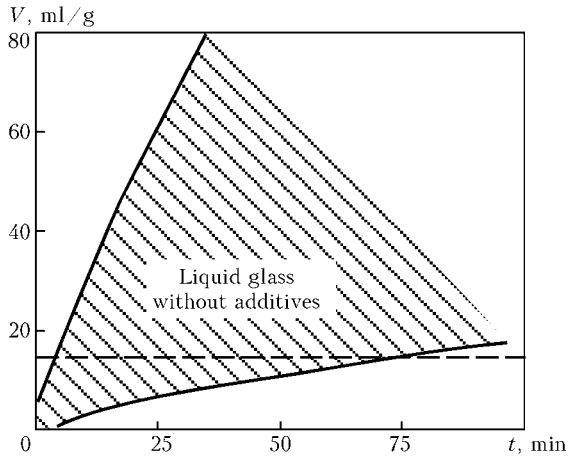

Figure 1. Kinetics of gas release in interaction of ferrosilicium powder of FS-45 grade with liquid glass

*This material was presented in the form of a report at the 2nd scientific-practical workshop «Arc welding. Materials and quality» (Magnitogorsk, Sept. 26–30, 2005).

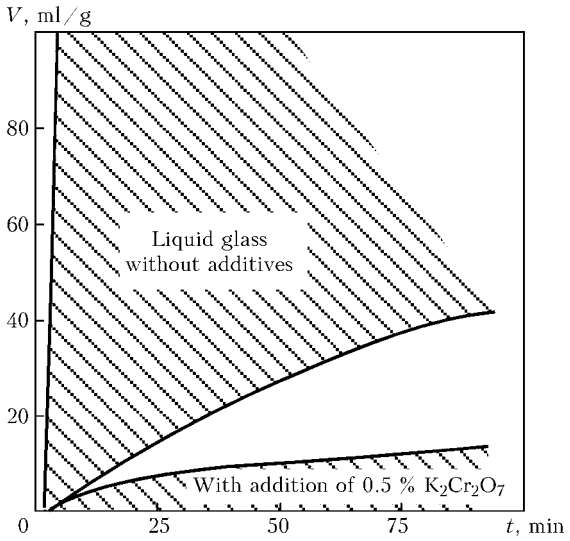

Figure 2. Kinetics of gas release in interaction of ferrosilicomanganese (wt.%: 0.2–1.5C, 62–71Mn, 15–29Si) powder with liquid glass

is shown. The results obtained prove that technologists may face rather high reactivity of ferrosilicium and ferrosilicomanganese in liquid glass environment. Volume of gas released within 90 min, during which the reaction of ferroalloy powders with liquid glass proceeds, significantly exceeds critical volume 15 ml / g (dashed line in Figure 1). Despite the fact that chemical composition of studied ferroalloys remained within the limits regulated by the state standard, degree of their reactivity significantly differed from each other

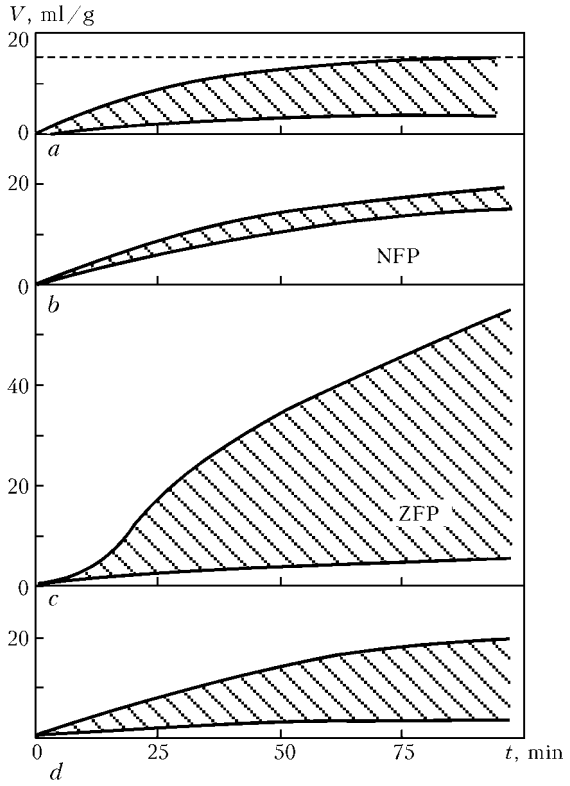

Figure 3. Kinetics of gas release in interaction of ferromanganese powder (*a–c*) and metal manganese (*d*) with liquid glass (wt.%): *a* — medium-carbon (0.8–2C, 1.1–2.9Cr, 86–93.2Mn); *b*, *c* — high-carbon ferromanganese (*b* — 6.4–6.5C, 77.1–78Mn, 1.1–1.4Si, 0.18–0.5P; *c* — 6.1–6.4C, 77.6–81.1Mn, 2.6–3.5Si, 0.25P); *d* — metal manganese (0.10–0.16C, 95.7–97.7Mn, 0.6–0.8Si, 0.05–0.07P)

(see shaded areas). Reactivity of ferrosilicomanganese may be even higher than that of standard ferrosilicium, although concentration of silicon in ferrosilicomanganese is significantly lower, whereby unambiguous connection between change of content of ferroalloy components and their reactivity in liquid glass was not detected. However, it was established that by means of silicon content increase in ferrosilicium and ferrosilicomanganese within grade allowance their reactivity in many cases increases. Addition of $K_2Cr_2O_7$ (potassium bichromate) into liquid glass suppresses reaction of ferrosilicomanganese interaction with it. It will be further said about efficiency of this method in relation to ferrosilicium.

Medium-carbon and carbon ferromanganese manufactured at NFP and metal manganese are characterized by low reactivity in liquid glass. These ferroalloys don't need passivation. At the same time in-

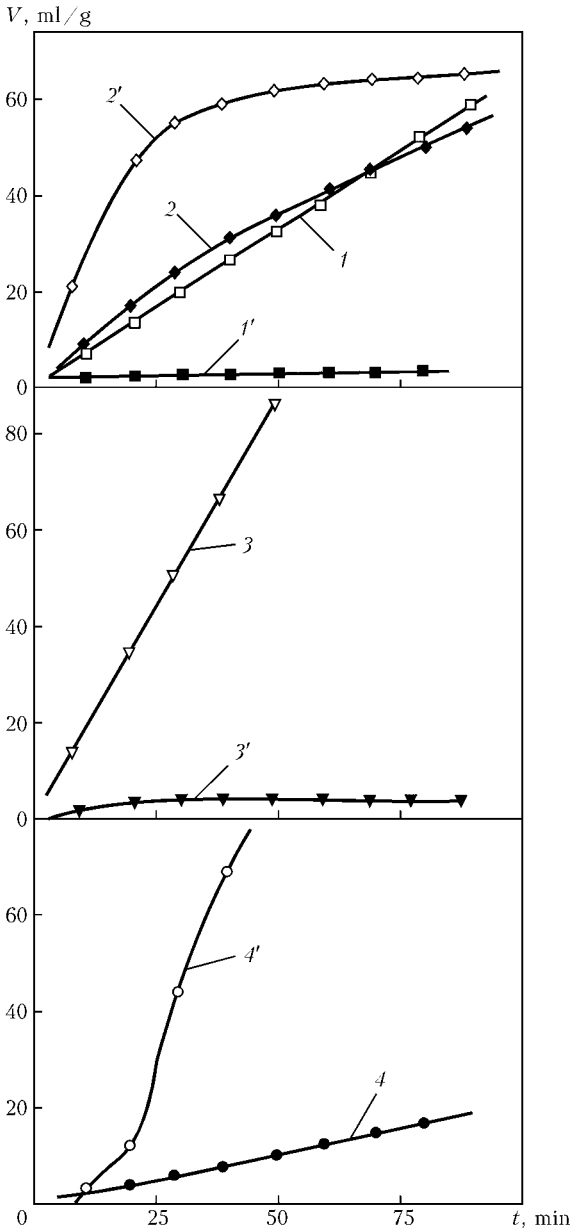

Figure 4. Influence of potassium bichromate addition (0.5 %) into liquid glass on kinetics of gas release (different lots of ferrosilicium FS-45 were studied): *1–4* — liquid glass without additive; *1′–4′* — same with addition of potassium bichromate

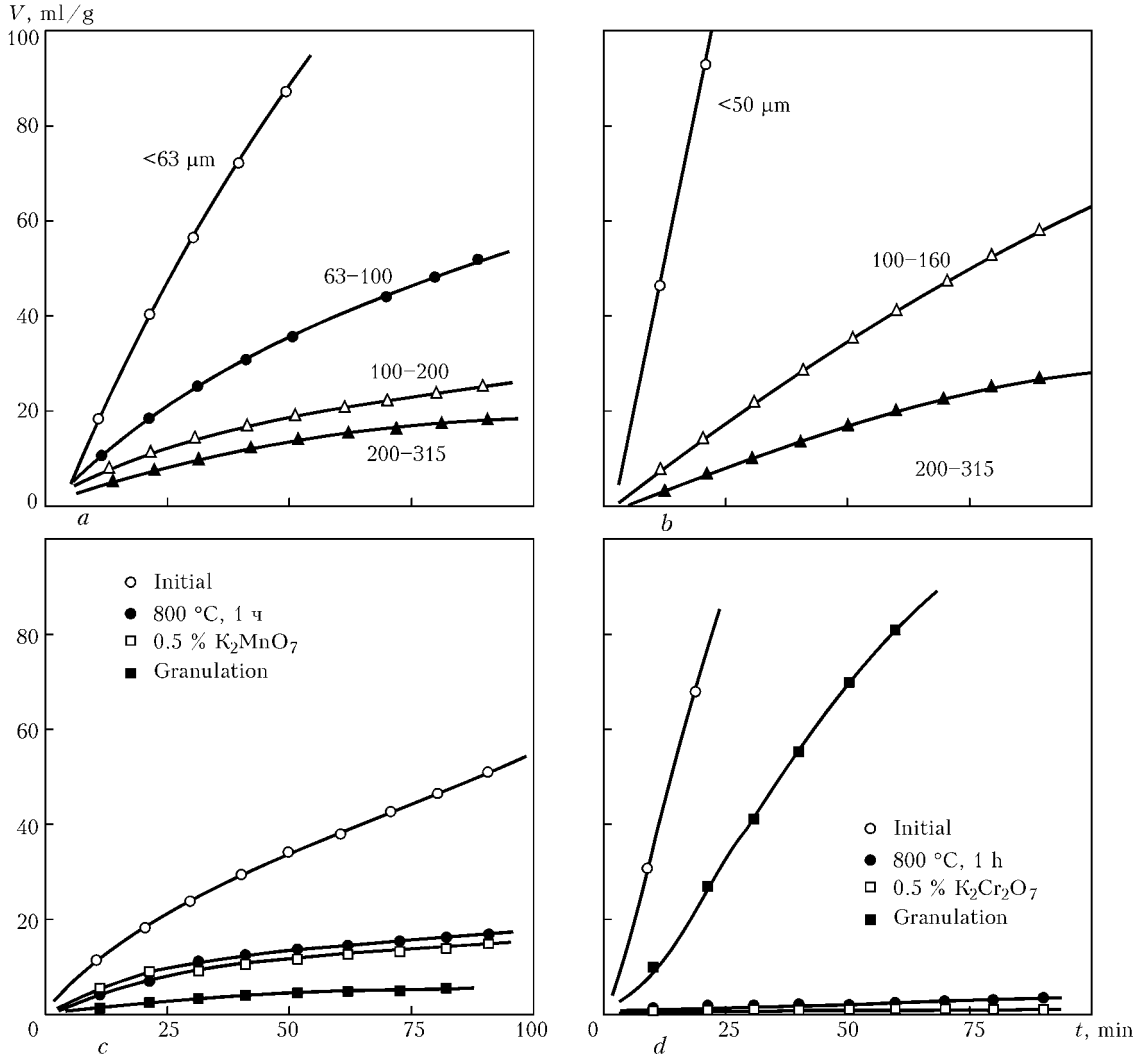

Figure 5. Influence of grain dispersity, achieved by different methods of reactivity suppression of ferrosilicium FS-45 (*a*, *b*) and ferrosilicomanganese (*c*, *d*) powders, on kinetics of gas release during their interaction with liquid glass

creased reactivity of carbon ferromanganese supplied by ZFP was noted, which may be explained by higher content of silicon in it.

Aluminium powders of PA-3 grade and aluminium-magnesium powders of PAM-4 grade are characteristic of rather low reactivity in liquid glass environment (4), (5). Additives of potassium bichromate into liquid glass suppress their activity even more, especially it relates to the powder of PAM-4 grade. Magnesium powder is characteristic of high activity, but in this case potassium bichromate is rather efficient passivation additive too. In principle, ready for delivery powders of all named types don't need additional passivation.

Passivation effect caused by interaction of potassium bichromate, added into liquid glass, with ferrosilicium is of ambiguous character. It is noted that there are lots of ferrosilicium, activity of which, as it was expected, is suppressed in case of addition of potassium bichromate into liquid glass (compare curves *1* and *1′*, *3* and *3′* in Figure 4). At the same time activity of other lots of mentioned ferroalloy significantly increases under influence of the same additives (compare curves *2* and *2′*, *4* and *4′*). Unfavorable influence of potassium bichromate additives was also observed in study of ferrosilicium, silicon content in which approaches 52 %, and standard ferrosilicium of FS-65 grade. One may assume that state-of-the-art technologies of FS-45 grade ferrosilicium production enable inhomogeneous distribution of silicon and impurities in ingots or cause formation of especially active structural components.

Reactivity of ferrosilicium powder may be reduced by using powders with low content of fine fractions (63 μm and less), passivation heating (800 °C for 1 h), adding 0.5 % saturated water solution of potassium permanganate in mixture or by pulverizing (granulating) a melt by water jet (Figure 5). The latter method is the most efficient.

Reactivity of ferrosilicomanganese powder also reduces when content of fine-grain fractions in the powder reduces (but degree of the reactivity reduction is less than in case of ferrosilicium), potassium bichromate is added into liquid glass (this technology should not be used because of environmental reasons) or solution of potassium permanganate is added into the mixture, and passivation heating at 800 °C is used. Technology of ferrosilicomanganese granulation by water jet does not ensure necessary technological effect (see Figure 5) and because of this reason is not recommended for use.